Chair of Applied Geophysics

Master's Thesis

Deconvolution of seismic data from mine production blasts

November 2018

Franziska Patrizia Reiner, BSc

Affidavit

I declare that I have authored this thesis independently, that I have not used other than the declared sources/resources, and that I have explicitly indicated all material which has been quoted either literally or by content from the sources used. The text document uploaded to MUonline is identical to the present masters thesis.

Date

Signature

Danksagung

An erster Stelle möchte ich mich ganz herzlich bei Univ.-Prof. Dipl.-Geophys. Dr.rer.nat. Florian Bleibinhaus bedanken, der diese Arbeit erst ermöglicht und sich während der Erstellung dieser Arbeit immer Zeit für Diskussionen genommen hat.

Weiters gilt mein Dank dem ganzen Geophysik Institut, insbesondere Dipl.-Ing. Cornelia Tauchner und Dipl.-Ing. Jens Zeiss, da sie immer ein offenes Ohr für mich hatten und mir wertvolle Tipps mitgeben konnten.

Danke auch an meine Freunde und Studienkollegen, ohne die Leoben ein sehr trostloser Ort geworden wäre.

Ein großes Dankeschön an meine wunderbare Familie, die mich in jeglicher Hinsicht im Laufe des Studiums unterstützt hat und immer für mich da ist.

Zu guter Letzt gilt mein Dank meinem großartigen Freund, auf dessen emotionale Unterstützung ich immer zählen kann, der mich anspornt und meine größte Motivation hinter allem ist. Danke für alles!

Abstract

This study is about the deconvolution of production blasts in a mine. The data for this study was recorded by an array of 124 seismic stations recording continuously during three weeks in November 2016 at Mt. Erzberg mine, Austria. In that time, 10 production blasts were recorded, ranging from 2-6 t explosives in 5-28 boreholes, each. Single blasts were detonated with a nominal delay time of 33-42 ms, however, the actual delay is poorly controlled and can deviate several ms. This results in a complex, unknown source-time function of up to 0.6 s length. First, all traces were aligned at the P-arrival and stacked to obtain a mastertrace for each shotpoint. Then, the Wiener Shaping Filter method was used to obtain a filter which was applied to each seismic section. This worked relatively well for some shots and the S-wave could be detected for shotpoint 27 for example.
In a second step, attempts were made to separate each source-time-function into an average wavelet of a single blast and the blast sequence, respectively. This did not work, suggesting that the individual blasts might not be similar enough, at least not considering the full bandwidth.

Im Rahmen dieser Masterarbeit wurde eine Dekonvolution an Produktionssprengungen in einem aktiven Bergbau durchgeführt. Die Daten für diese Studie wurden im November 2016 während einer dreiwöchigen Messkampagne im Steirischen Erzberg von 124 Stationen kontinuierlich aufgezeichnet. In dieser Zeit wurden 10 Produktionssprengungen erfasst, die 2-6 t Sprengstoff in jeweils 5-28 Bohrlöchern umfassten. Jedes einzelne Bohrloch wurde mit einer nominalen Verzögerungszeit von 33-42 ms detoniert, jedoch ist die tatsächliche Verzögerung unbekannt und kann mehrere ms abweichen. Daraus ergibt sich eine komplexe, unbekannte Quellfuntktion von bis zu 0,6 s Länge.
Zuerst wurden alle Spuren nach dem Ersteinsatz ausgerichtet und gestapelt, um eine Masterspur für jeden Schusspunkt zu erhalten. Anschließend wurde mit der Wiener Shaping Filter-Methode ein Filter generiert, der auf jede Masterspur und jedes Seismogram angewendet wurde. Dies erzielte bei einigen Schüssen relativ gute Ergebnisse und die S-Welle konnte z.B. für Schusspunkt 27 detektiert werden.
In einem zweiten Schritt wurde versucht, jede Masterspur in ein durchschnittliches Quellsignal einer einzelnen Detonation zu zerlegen. Dies funktionierte nicht, was darauf hindeutet, dass die einzelnen Quellsignale jeder Detonation möglicherweise nicht ähnlich genug sind, zumindest nicht unter Berücksichtigung der gesamten Bandbreite.

Contents

List of Figures

List of Tables

Chapter 1

Introduction

The optimum Wiener Filter Theory is a deconvolution method, providing techniques like Spiking Deconvolution and the Wiener Shaping Filter. Both are time-domain methods, which should remove the source signal contained in the seismic trace. To understand deconvolution properly, the convolutional model has to be considered first. The convolutional model describes the seismogram as the result of convolving the reflection series, produced by various layers of rocks, with the seismic wavelet, which comprises signals from the source. Deconvolution is the inverse process of convolution. It removes the source-time-function from the seismogram to reconstruct the earth's impulse response.

The softwares ProMAX and Seismic Unix were utilised to test the Spiking Deconvolution method and the Wiener Shaping Filter. Synthetic wavelets, earth's impulse response series and seismograms were generated to perform some tests beforehand. Via those tests, the methods could be optimised and it could be decided which method would work properly on the real data.

The real dataset was recorded in November 2016 in the course of the *SLIM* (Sustainable Low Impact Mining) project at Mt. Erzberg mine, which is located next to Eisenerz. SLIM focuses on characterising the test site to minimise vibrations initiated through production blastings. Measurements were performed during 4 weeks in November 2016. 10 production shots and 21 seismic shots were collected using 124 3-component geophones. This work focuses on data recorded during production blasting operations (Fig 1.1). The vertical component of the data from shotpoint 22 (SYBO 298) was primarily used and some methods were also performed on the vertical component of the data from shotpoint 27 and 28. The results of the other nine shotpoints (23 - 31) can be found in the appendix. A different amount of boreholes had to be drilled for each productionshotpoint. Shotpoint 22, for example, contained 11 boreholes, detonated with +/- 33 ms delay between each drill hole. The other shotpoints were made up of 5 to 28 drill holes and the designated delay time between each detonation ranged from 33 to 42 ms. However, the real delay times vary by an unknown amount (probably more than 10 ms) due to technical constraints of the ignition system.

In this study, the two deconvolution methods mentioned above are used to deconvolve the traces in the seismic section. The aim is to unfold the traces so that other phases become visible, especially the signal of the S-wave, since P- and S-wave velocity models serve as starting models for further investigations. Another goal is the deconvolution of the stacked trace to characterise the wavelet of a single shot since the source signals should resemble each other. As the individual blasts might not be similar enough and the real delay time between each single shot is unknown and hence the exact impulse sequence is unknown, deconvolution was quite complicated. The deconvolution performances of the synthetic data are discussed in Chapter 3. The analysis of the real data sets, with a short introduction to *SLIM* and the test site Mt. Erzberg mine beforehand, can be found throughout the Chapters 4, 5 and 6.

Figure 1.1: Example of a production detonation at Mt. Erzberg mine (*http://www.vaerzberg.at/, retrieved August 19, 2018*)

Chapter 2

Introduction to Deconvolution

2.1 The Convolutional Model

To describe deconvolution a short explanation to convolution is necessary beforehand. Seismic recordings can be defined using the convolutional model and the mathematical formulation regarding this principle is given in equation 2.1.

$$x(t) = w(t) * e(t) = \int_0^t w(\tau)e(t-\tau)d\tau \tag{2.1}$$

where

$x(t)$ = recorded seismogram

$w(t)$ = seismic source wavelet

$e(t)$ = earth's impulse response

Mathematically, convolution of two functions can be described as the integral over their product, whereby one of the two functions got reversed in time. The seismogram $x(t)$ is the outcome of this convolutional proces. Figure 2.1 illustrates the equivalence to equation 2.1 whereby an impulse response is convolved with a source wavelet to produce a noise-free seismogram, which is combined with some noise to obtain the final seismogram [Yilmaz, 1987].

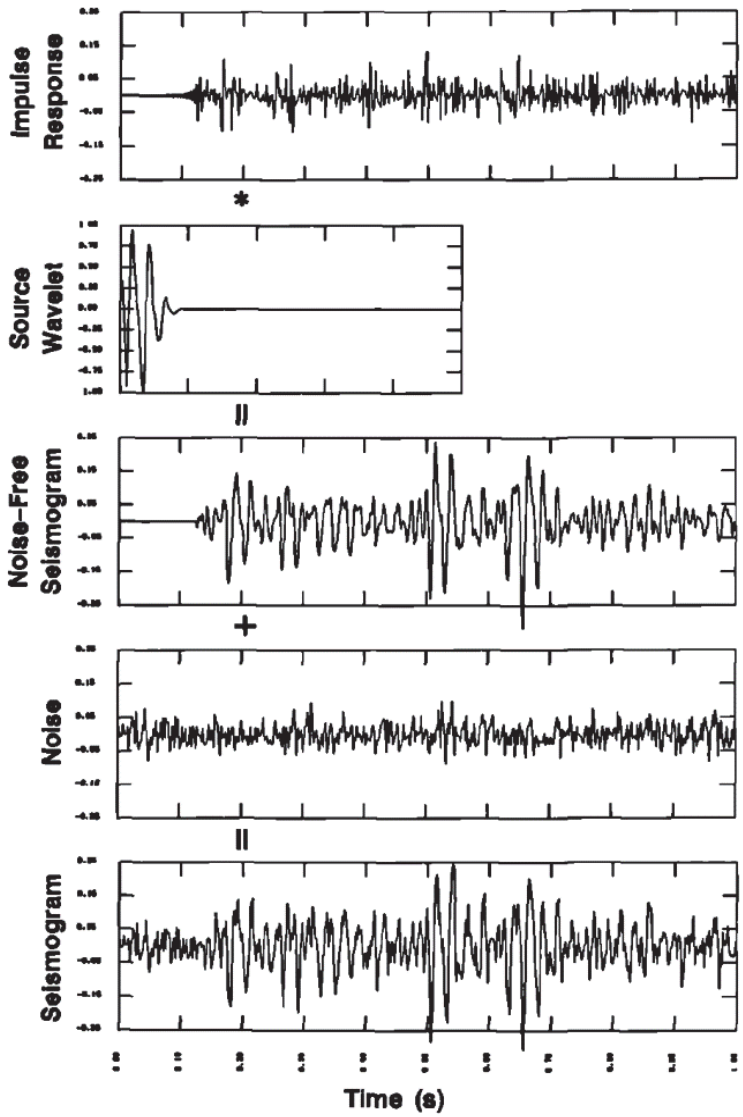

Figure 2.1: The convolutional model showing an impulse response, convolved with a source wavelet and overlaid by some noise to produce a seismogram
[Yilmaz, 1987]

2.2 Deconvolution

The inverse process of convolution is called deconvolution. Deconvolution tries to recover the earth's impulse response through removing the source wavelet from the recorded seismogram (Fig 2.2). Through deconvolution by spectral division noise signals at high frequencies are produced in the amplitude spectrum, because absent frequencies get boosted. To ensure stability and remove small values from the input amplitude spectrum one can add a so-called water-level w.

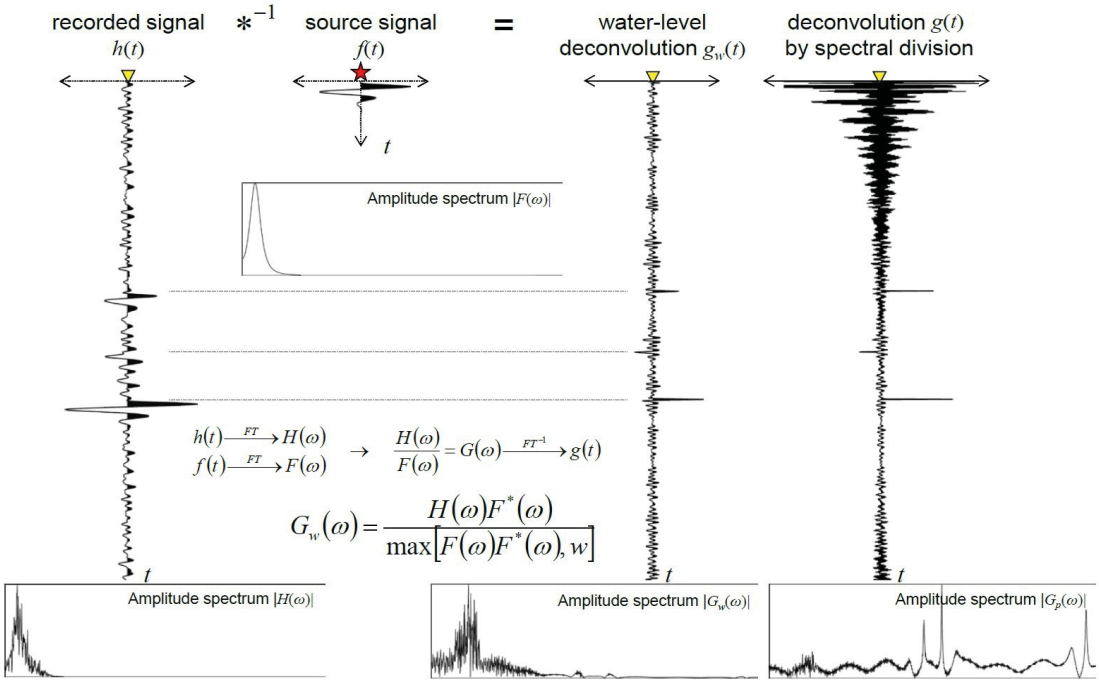

Figure 2.2: The principle process of deconvolution encompasses the reconstruction of the earth's impulse response through removing the source wavelet from the recorded signal and adding an amount of water level w to stabilise the result (see *Bleibinhaus F. (2016) Reflection Seismology lecture notes*)

The deconvolutional process compresses the wavelet which leads to an improve of the resolution and reconstructs the reflectivity series. Moreover, deconvolution of a recorded seismic trace can be used to eliminate the impulse series and recover the unknown source wavelet. Looking at equation 2.1 leads to the perception that only the seimogram x(t) is known and the two other components (neglecting the ambient noise) are unknown. So in an usual case the wavelet is unknown and the deconvolutional problem can be stated as statistical. One statistical method would be the optimum Wiener Filter Theory. In special cases, though, the wavelet is known and the problem would be called deterministic, in which the filter would be obtained for example through least-squares inverse filtering [Yilmaz, 1987] or water-level deconvolution.

2.3 Optimum Wiener Filter

Algorithms based on this optimum Wiener Filter Theory are called Wiener-Levinson algorithms, which include methods like Spiking Deconvolution and the Wiener Shaping Filter. They are performed on time domain seismograms and the principle workflow is the same for both methods. The procedure of generating the optimum filter coefficients include the autocorrelation of the input seismogram and the crosscorrelation of the input with the desired output (Fig 2.3).

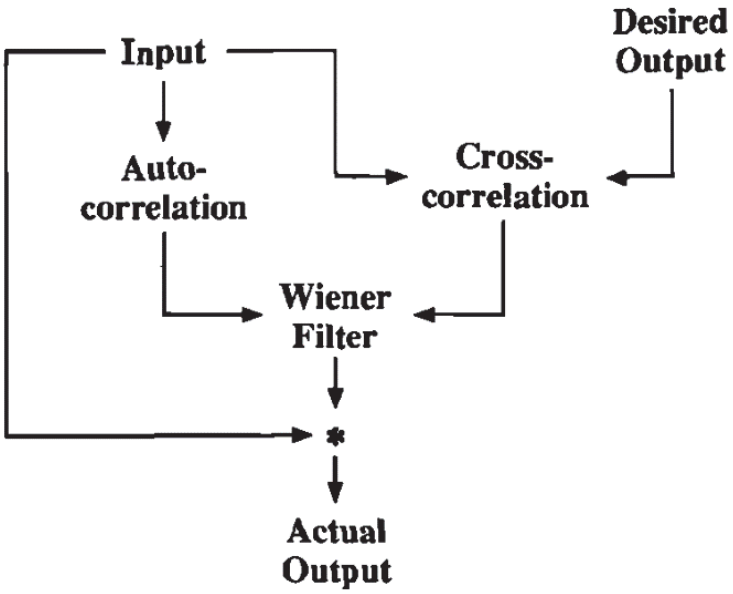

Figure 2.3: The workflow of generating a Wiener Filter and application [Yilmaz, 1987]

The Wiener filter coefficients are then convolved with the input to obtain the deconvolved trace or actual output. The matrix equation (eq 2.2) can be seen as the correspondent mathematical representation of Figure 2.3.

$$\underbrace{\begin{bmatrix} r_0 & r_1 & r_2 & \dots & r_{n-1} \\ r_1 & r_0 & r_1 & \dots & r_{n-2} \\ \vdots & \vdots & \vdots & \ddots & \vdots \\ r_{n-1} & r_{n-2} & r_{n-3} & \ddots & r_0 \end{bmatrix}}_{autocorrelation\ \ matrix\ \ R} \quad \underbrace{\begin{bmatrix} f_0 \\ f_1 \\ \vdots \\ f_{n-1} \end{bmatrix}}_{filter\ \ coefficients\ \ F} = \underbrace{\begin{bmatrix} g_0 \\ g_1 \\ \vdots \\ g_{n-1} \end{bmatrix}}_{crosscorrelation\ \ matrix\ \ G} \tag{2.2}$$

The matrix on the left handside (r_i, with i=0,1,2,3....,n-1) represents the autocorrelation of the input seismogram. This matrix is a symmetrical Toeplitz matrix and therefore the Levinson recursion can be considered for solving it [Claerbout, 1985]. The vector matrix on the right handside (g_i, with i=0,1,2,3....,n-1) represents the crosscorrelation of the desired output with the input seismogram. The vector in the middle contains the desired

optimum Wiener filter coefficients (f_i, with i=0,1,2,3....,n-1) which can be derived from the two matrices R and G applying the above mentioned Levinson algorithm. According to [Robinson and Treitel, 1980], the Wiener filter is "optimum" when the error, containing the squared residuals between actual y_t and the desired output d_t, is minimum (eq 2.3).

$$L = \sum_t (d_t - y_t)^2 \tag{2.3}$$

As shown in Figure 2.3 the actual output results from the convolution of the filter with the input:

$$y_t = f_t * x_t \tag{2.4}$$

Inserting equation 2.4 into equation 2.3 and expanding the squared expressions leads to:

$$L = \sum_t d_t^2 - 2\sum_t d_t \sum_\tau f_\tau x_{t-\tau} + \sum_t (\sum_\tau f_\tau x_{t-\tau})^2 \tag{2.5}$$

When L is a minimum, the derivative is zero ($\frac{\partial L}{\partial f_i} = 0$) with i=0,1,2,3,...,(n-1) and it follows:

$$\frac{\partial L}{\partial f_i} = -2\sum_t d_t x_{t-i} + 2\sum_t (\sum_\tau f_\tau x_{t-\tau}) x_{t-i} = 0 \tag{2.6}$$

or

$$\sum_\tau f_\tau \sum_t x_{t-\tau} x_{t-i} = \sum_t d_t x_{t-i} \tag{2.7}$$

After setting

$$\sum_t x_{t-\tau} x_{t-i} = r_{i-\tau} \tag{2.8}$$

and

$$\sum_t d_t x_{t-i} = g_i, \tag{2.9}$$

g_i can be written as:

$$\sum_t f_\tau r_{i-\tau} = g_i \quad \text{with} \quad i = 0, 1, 2, ..., (n-1) \tag{2.10}$$

This equation can also be brought in matrix form (eq 2.2). The least-squares error can be computed now by using following relationships:

$$\sum_t x_t x_{t-\tau} = r_\tau \tag{2.11}$$

and

$$\sum_t d_t x_{t-\tau} = g_\tau \tag{2.12}$$

and by inserting them into equation 2.5:

$$L_{min} = \sum_t d_t^2 - 2\sum_\tau f_\tau g_\tau + \sum_\tau f_\tau \sum_i f_i \sum_t x_{t-\tau} x_{t-i} \tag{2.13}$$

Using the expression shown in equation 2.10, L_{min} finally becomes

$$L_{min} = \sum_t d_t^2 - \sum_\tau f_\tau g_\tau. \tag{2.14}$$

The difference between Spiking Deconvolution and the Wiener Shaping Filter now rests in the choice of the desired output forms. After Yilmaz (1987) [Yilmaz, 1987] it can be selected between five different form types:

Type 1 = Zero-lag spike

Type 2 = Spike at arbitrary lag

Type 3 = Time-advanced form of input series

Type 4 = Zero-phase wavelet

Type 5 = Any desired arbitrary shape

If type 1 is desired the Wiener filter can be referred to as the least-squares inverse filter. The process discussed in this section is therefore mathematically identical to the least-squares inverse filtering. Except for the former, the input would be the recorded seismogram and for the latter, computations would be performed with the known source wavelet.

2.3.1 Spiking Deconvolution

Spiking deconvolution is used when the desired output should be a type 1. The general form of the matrix equation shown in equation 2.2 is modified and a specialised form is adopted (eq 2.15). The column matrix on the right, representing the crosscorrelation, was normalised by $1/g_i$ and indicates now the matrix of a zero-lag spike. Hereby the filter

coefficients f_i are written as a_i.

$$\underbrace{\begin{bmatrix} r_0 & r_1 & r_2 & \dots & r_{n-1} \\ r_1 & r_0 & r_1 & \dots & r_{n-2} \\ \vdots & \vdots & \vdots & \ddots & \vdots \\ r_{n-1} & r_{n-2} & r_{n-3} & \ddots & r_0 \end{bmatrix}}_{R} \underbrace{\begin{bmatrix} a_0 \\ a_1 \\ \vdots \\ a_{n-1} \end{bmatrix}}_{A} = \underbrace{\begin{bmatrix} 1 \\ 0 \\ \vdots \\ 0 \end{bmatrix}}_{spike} \tag{2.15}$$

In practice it is important that the seismogram is made up of a minimum-phase wavelet otherwise the output would not be a zero-lag spike. It can be concluded that spiking deconvolution is only valid, if the input wavelet is minimum-phase [Yilmaz, 1987].

2.3.2 Wiener Shaping Filter

Compressing the wavelet to a zero-lag spike is not always the best choice. An alternative process that leads to type 5 desired output would be wavelet shaping. The filter that generates any arbitrary shaped output is the so-called Wiener Shaping Filter. An example of using the Wiener Shaping Filter is given in Figure 2.4.
In this example, it is obvious that a zero-lag spike (Fig 2.4a) as desired output (1) is not a good choice, when the input (0) is mixed phase. The actual output (3) exhibits noisy spikes, and not one single spike at time zero. It is clearly visible that the actual output results in an almost perfect spike with more delay in time (Fig 2.4b-h). The best result is obtained with a 60 ms delay of the desired output (Fig 2.4e).
The shape of the actual output depends not only on the privileged type of output but also on the selection of the wavelet. If the input is minimum-phase a zero-lag spike is desired, but when the input is mixed-phase a nonzero delayed spike is preferred. In the case of a maximum-phase wavelet the desired output should have a delay equal to the length of that wavelet.
If one chooses the Wiener Shaping Filter as deconvolution process, the desired output can have any optional shape, but one has to think about the shape of the input first and adapt the desired output to that. On the other hand, if one chooses the Spiking Deconvolution method, the desired output is always a type 1 zero-lag spike, but this is only effectual if the input is a minimum-phase wavelet [Yilmaz, 1987]. With regard to this study, a zero-lag spike should be achieved using both, the Shaping Filter and the Spiking Deconvolution method. This means that in both cases one actually speaks of a spiking deconvolution, because the wavelet should be compressed to a zero-lag spike. Nevertheless, I distinguish between these two methods because, as explained in the next part, two different software packages were used.

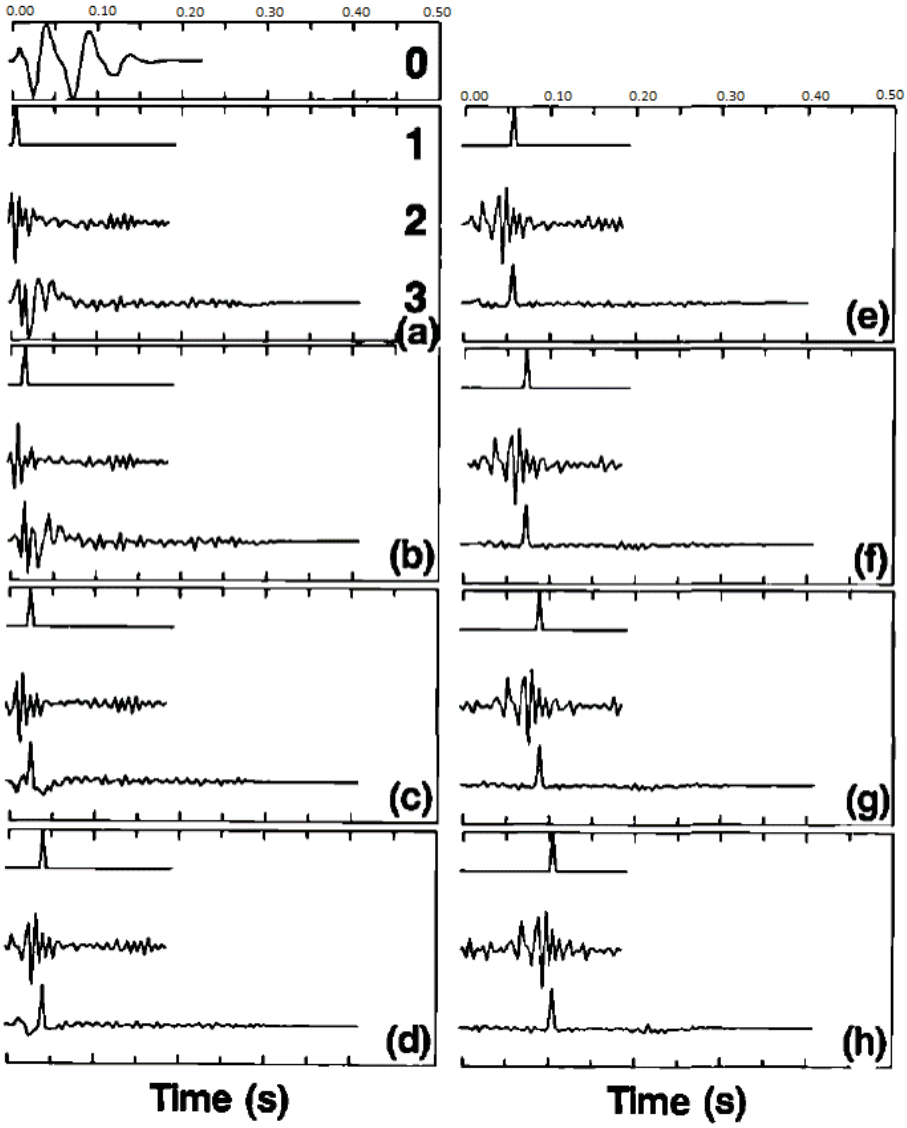

Figure 2.4: Application of the Wiener shaping filter on (0) a mixed-phase input wavelet, with (1) desired output, (2) shaping filter operator and (3) actual output
[Yilmaz, 1987]

2.4 Software packages utilised for the two selected deconvolution methods

The methods discussed in subsections 2.3.1 and 2.3.2 were tested with two different software packages. Seismic Unix (SU) was used on the one hand, SeisSpace ProMAX software family on the other. With the first one the Wiener Shaping Filter was generated and with the latter a Spiking Deconvolution was performed.

Seismic Unix is a free software package for unix-based systems which is world-wide applied for seismic data processing and research reasons. It was developed by Jack K. Cohen and Shuki Ronen in the late 1980s at the Colorado School of Mines (CSM) in cooperation with the Center for Wave Phenomena (CWP). SU is utilised by a wide range of geophysicists, seismologists, environmental engineers, software developers and others, mainly by academics and researchers but also by major companies. Since it is free of cost, one has unrestricted access to all codes, which are extended in an interval of 3 to 6 months. Furthermore, the unix-based system provides flexibility with all unix-like operating systems and it is possible to extend the functionality of a SU package with a shell script. The data format used in SU is obviously a SU data format, but it consists of SEG-Y traces. Therefore the SEG-Y data format is simply converted to SU data format.
The command used to establish a shaping filter is called *sushape*. The *sushape* routine was written by Jack Cohen and later on John Stockwell added some further options. The required parameters encompass the vector (w) of the input or the file (wfile) comprising the input wavelet and the vetor (d) or file (dfile) comprising the desired output. The command for shaping a minimum-phase wavelet to a type 1 desired spike would look like this for example:
"sushape < minimum-phase.su wfile=minimum-phase.su d=1,0,0,... > shaped-data.su"
Further options include the possibility to display the shaping filter by saving it as an ascii file and converting it to SU format [John W. Stockwell and Cohen, 2008].

The ProMAX family is composed of different processing systems such as ProMAX 2D, ProMAX 3D, ProMAX 4D and ProMAX VSP. This product line was sophisticated by Advance Geophysical Corporation, a Landmark Graphics Company, in 1995. ProMAX, as well as SU, is a seismic processing software based on unix operating systems (see *Advance Geophysical Corporation (1995) ProMAX Reference Manual: Volume 1*). SeisSpace is a later on developed interface used within ProMAX to execute jobs. It can be stated as an advanced developement of the previous interface. This kind of software family is not accessible for free and therefor more often used in major companies. Compared to SU the interface is made up of four basic sections. The most important section is the flow editor where one can build its flow using the appropriate modules from the ProMAX processes list. The processes list encompasses main processes such as "Data Input/Output", "Geometry/Headers", "Amplitude/Editing" and much more and beside all of this main sections, some subsections are available. A wide range of formats, including the standard

SEG-Y data format, are supported.
As mentioned above ProMAX was chosen to fulfill a spiking deconvolution. The spiking deconvolution operator applied to the input data is based on the Wiener-Levinson, least square algorithm and therefore the type which can be selected among three others is called Traditional Wiener-Levinson *spiking deconvolution*.
Important parameters used during this kind of deconvolution are the deconvolution operator length, the operator white noise level and the window rejection factor. The operator length, provided in ms, specifies the autocorrelation window length will be used and normally corresponds to half of the wavelet length when choosing a window rejection factor equal to 2. An appropriate operator length is chosen, when autocorrelation of the input seismogram and the autocorrelation of the wavelet are similar. If the wavelet is unknown the operator length is much harder to define [Yilmaz, 1987]. The window rejection factor is the factor by which to multiply the operator length and the result will be compared to the length of the data trace. The white noise level, provided in percent, defines the noise level added to the output. The factor is normally set to 0.1. The output can be selected from three options: autocorrelation output, filter operator output and normal deconvolution output, at which the latter shows the deconvolved trace (see *Landmark Graphics Corporation (2007) SeisSpace Seismic Processing and Analysis Training Manual: Volume 1*).

A short comparison of the two software packages regarding the deconvolution problem is given in table 2.1.

Table 2.1: Comparison of SU and ProMAX software packages in relation to deconvolution

Seismic Unix	**ProMAX**
+ open source (modifications in code possible)	+ graphical interface
+ expandable with shell scripts	+ clearly arranged workflows
+ mathematical background of most algorithms is published	- manual does not provide detail information on the implemented methods and the mathematical framework
+ shaping filter command quite well explained	- no command line
- no interactive graphical interface	- more difficult to handle with no a-priori knowledge

Chapter 3

Synthetic data

3.1 Introduction to wavelets

To recap the difference between the three mentioned wavelets in subsection 2.3.2, Figure 3.1 is used. A minimum-phase wavelet is called minimum, because its energy buildup has its maximum at the front. A mixed-phase wavelet has its energy gathered in the middle and for a maximum-phase wavelet energy is maximally end-loaded [Yilmaz, 1987].
Wavelets, in general, have an impermanent waveform with a finite duration (definition after [Yilmaz, 1987]). Moreover a minimum-phase wavelet has its onset at zero, which means that it is zero before t=0 s. Such a wavelet is also called causal. A perfect seismic source would be a spike, because at each frequency maximum amplitudes can be found. In most real cases the source waveform is minimum-phase or the source waveform is converted to minimum-phase [Sunjay, 2010]. According to [Robinson, 1966] it has to be differed between minimum-phase and minimum delay, whereby the latter is referred to time domain. All in all it is meant the same, but to understand the term minimum-phase it is better defined by minimum delay. A minimum delay (or minimum-phase) wavelet has the least energy delay and vice versa. A minimum-phase wavelet can be assumed as well in this research, at least for the wavelet that only includes a single shot, since dynamite was used as source, which leads to maximum energy at the beginning. The generated synthetic wavelets, discussed in the next section, are therefore minimum-phase.

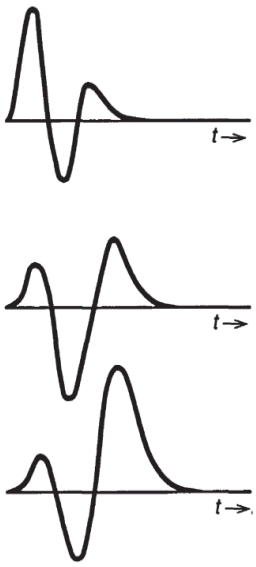

Figure 3.1: Minimum-phase (top), mixed-phase (middle) and maximum-phase (end) wavelet
[Yilmaz, 1987]

3.2 Synthetic wavelets and seismograms for deconvolution tests

In order to test how deconvolution affects the existing real data set, a synthetic data set was created. At first only simple wavelets were produced to test the methods and to find out if ProMAX could achieve better results than Seismic Unix. A flowchart of generated data and deconvolved results is given in appendix A.

Wavelets for test 1
The first established source wavelet is the so called Kuepper wavelet [Kuepper, 1958]. It was built with SU according to equation 3.1.

$$w(t) = A_0[\sin(m\Pi ft) - \frac{m}{m+2}\sin((m+2)\Pi ft)] \tag{3.1}$$

where

$w(t)$ = source wavelet

A_0 = amplitude

m = amount of extrema

f = frequency

t = time

The equation is based on Mueller [Mueller, 1970] and Fuchs & Mueller [Fuchs and Mueller, 1971] and modified for this purpose. Hereby A_0 is 1 and for m 2 is chosen.

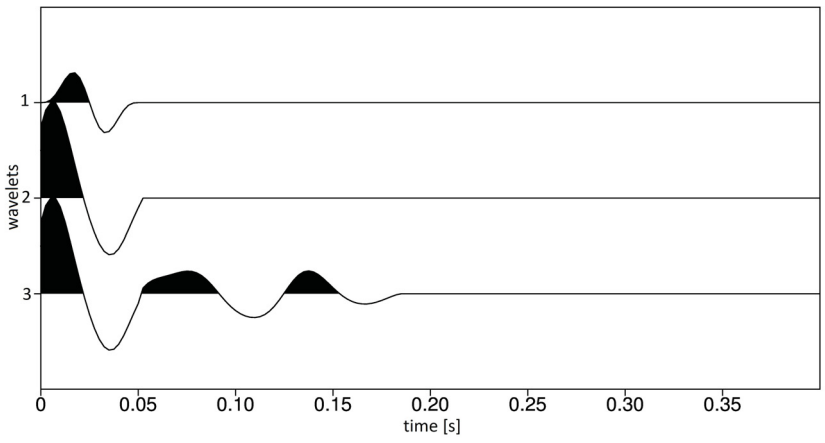

Figure 3.2: Generated synthetic wavelets using SU whereby 1 is generated first using equation 3.1 and 2 and 3 are modified afterwards

The output is displayed in Figure 3.2, where number 1 shows a 20 Hz, 0.05 s long Kuepper

wavelet with two lobes. The first deconvolution tests were performed with this wavelet, but the results were not that well. Therefore the other two wavelets were generated whereby number 2 and 3 resemble more minimum-phase wavelets as the energy delay is minimum for both. All three wavelets were resampled to a sample interval of 2500 μs. For further tests, synthetic seismograms, following the principle of the convolution model given in Figure 2.1, were established.

Seismogram for test 2

The first modelled seismogram is based on a convolution of wavelet 3 with a synthetically created earth's impulse response series (Fig 3.3).

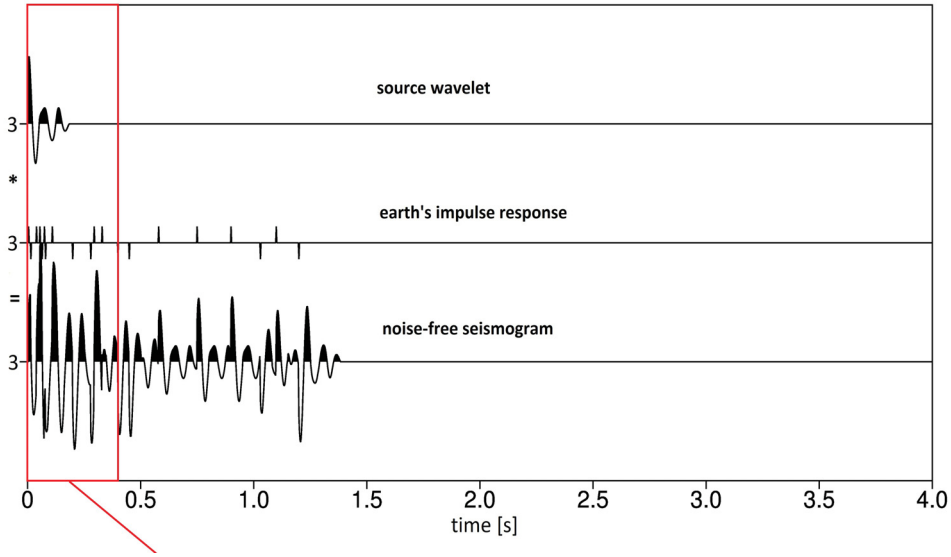

(a)

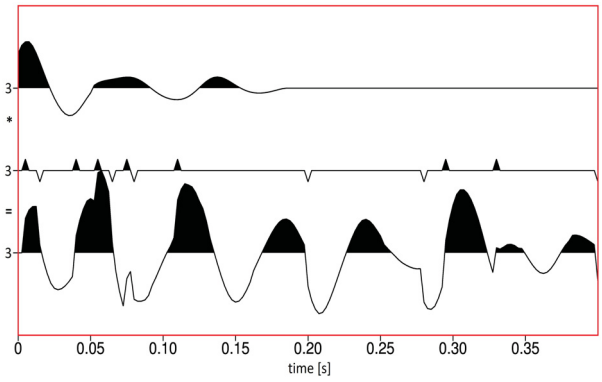

(b)

Figure 3.3: Synthetic seismogram whereby wavelet 3 is convolved with synthetic spike series 3 and output seismogram 3 is created (a) showing whole trace length & (b) showing first 0.4 s

The spike series was chosen arbitrarily and positive and negative spikes were deliberately. The second tests were performed using seismogram 3.

Seismograms for test 3
The third modelled seismogram is much more complex as the characteristic of it should resemble reality, which means that the seismogram is composed of a source wavelet convolved with the impulses produced through the source itself and furthermore convolved with impulse responses belonging to the subsurface. Therefore the fifth and final synthetic seismogram 5 (Fig 3.4b) is composed of seismogram 4, which is the output of the convolution of the minimum-phase wavelet 3 with spiking series 3i (three spikes for simulating three shots at intervals of 33 ms), convolved with a synthetic earth's impulse response 4. Seismogram 5 and Seismogram 4 were utilised for conducting the third tests.

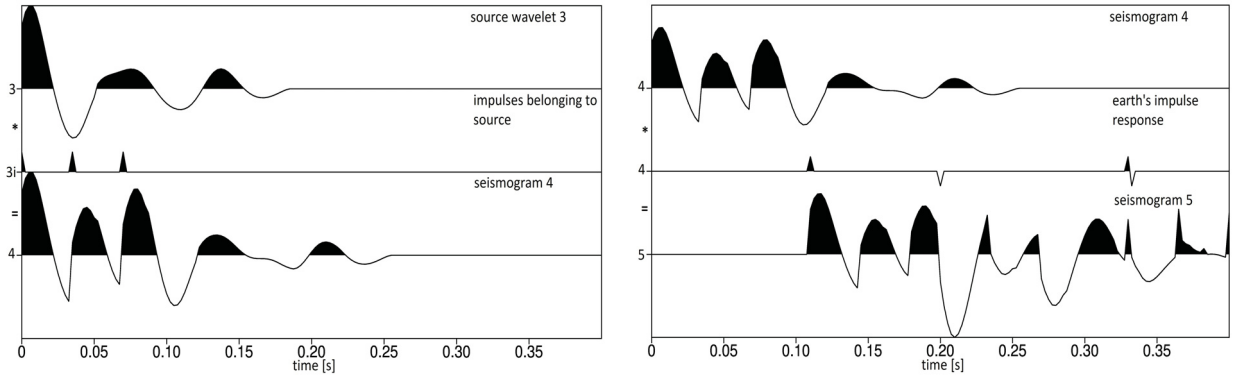

(a) (b)

Figure 3.4: (a) Convolution process using minimum-phase wavelet 3 which is convolved with spike series 3i simulating shot signals and producing output seismogram 4 (b) seismogram 4 is convolved with the synthetic earth's impulse response 4 to obtain final seismogram output 5

3.3 Testing deconvolution methods on generated synthetic wavelets - test 1

3.3.1 Using Wiener Shaping Filter method

Test 1 was performed using wavelets 1, 2 and 3 (Fig 3.2). First, the Kuepper was taken and the SU command *sushape* was applied. The whole trace encompasses 4 s and applying the shaping filter directly moves the output spike to the middle (2 s). As output shape a type 1 was desired, because the Kuepper wavelet was assumed to be a minimum-phase wavelet, but the maximum energy onset of the wavelet is observed at t=0.0025 s and not at t=0 s as expected. The deconvolved output displays a noisy spike with several sidelobes

and the main peak shows a minimum deviation from t=0. (Fig 3.5a).

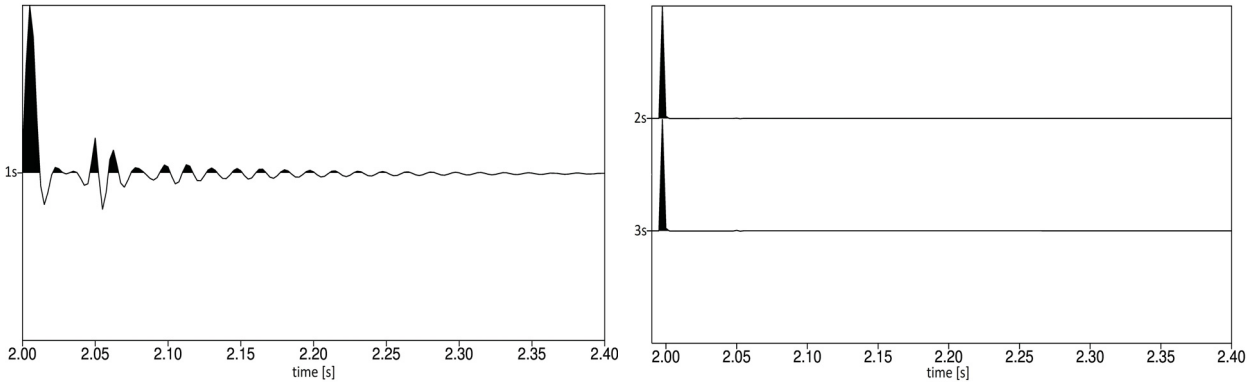

(a) (b)

Figure 3.5: Deconvolved outputs of (a) wavelet 1 & (b) wavelets 2 and 3 using the sushape command in SU

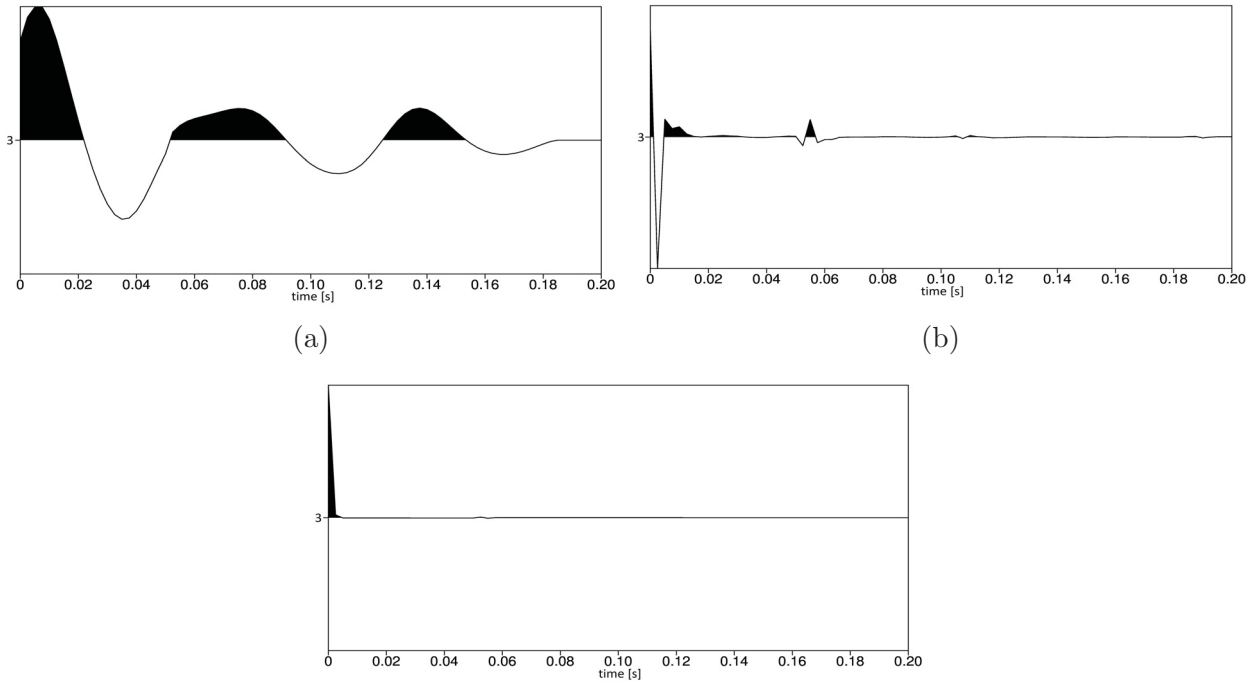

(a) (b)

(c)

Figure 3.6: Deconvolution process using (a) minimum-phase wavelet 3 which is convolved with (b) filter 3 to obtain (c) zero-lag spike output 3

The deconvolved outputs for wavelets 2 and 3 do not show any significant sidelobes. It can be said that a zero-lag spike is obtained for both wavelets (Fig 3.5b). Beside the possibility of applying the shaping filter directly within the routine, it is also possible to

save the shaping filter as output. The *sushape* routine was therefore applied again, but this time the filter is chosen as output. Generated filter 3 is displayed in Figure 3.6b. Following the flowchart in Figure 2.3, the filter is convolved with the input. An example of a deconvolved trace is given in Figure 3.6c, where wavelet 3 was convolved with filter 3 beforehand to receive the actual output. The actual output is consistent with the desired zero-lag spike. The entire trace length encompasses again 4 s but only the first 0.2 s are displayed.

3.3.2 Using Spiking Deconvolution

Spiking deconvolution should compress the wavelet to a zero-lag spike. Although the traditional Wiener-Levinson spiking deconvolution is selected and different operator lengths are tested, the outputs contain sidelobes which encompass $\frac{1}{4}$ of the height from the main peak (Fig 3.7b).

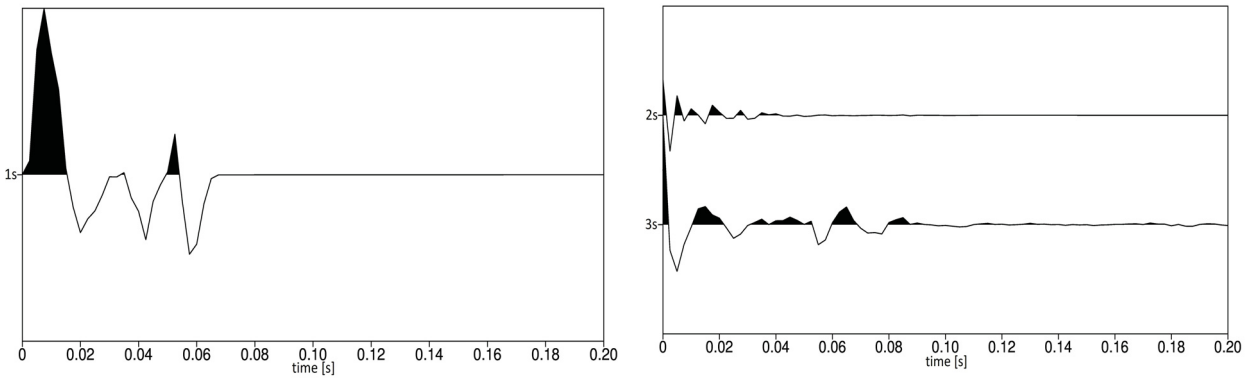

(a) (b)

Figure 3.7: Deconvolved outputs of (a) wavelet 1 & (b) wavelets 2 and 3 using spiking deconvolution with maximum operator length of 21.5 ms for wavelet 1 & 38 ms and 91.5 ms for wavelets 2 and 3

The deconvolved output of wavelet 1 (Fig 3.7a) can be compared to the output of wavelet 1 using the SU routines (Fig 3.5a). As explained before, the output can not be a zero-lag spike because the Kuepper is not perfectly minimum-phase since the energy onset is not exactly at t=0 s. This is why the spike deviates from the zero point here as well. Nevertheless the output of wavelet 2 and 3 should be a zero-lag spike as visible in Figure 3.5b as well, but ProMAX is not capable of compressing the wavelet to a spike without some artefact remains. The output of both wavelets is noisy and there are some erroneous small-amplitude spikes visible after t=0 s (Fig 3.7b). A maximum operator length using the window rejection factor of 2 is chosen for all three wavelets. After Yilmaz (1987) [Yilmaz, 1987] a longer operator should whiten the spectrum further. In Figure 3.8a and 3.8b the amplitude spectrum of wavelet 3 and the amplitude spectrum of a single spike is

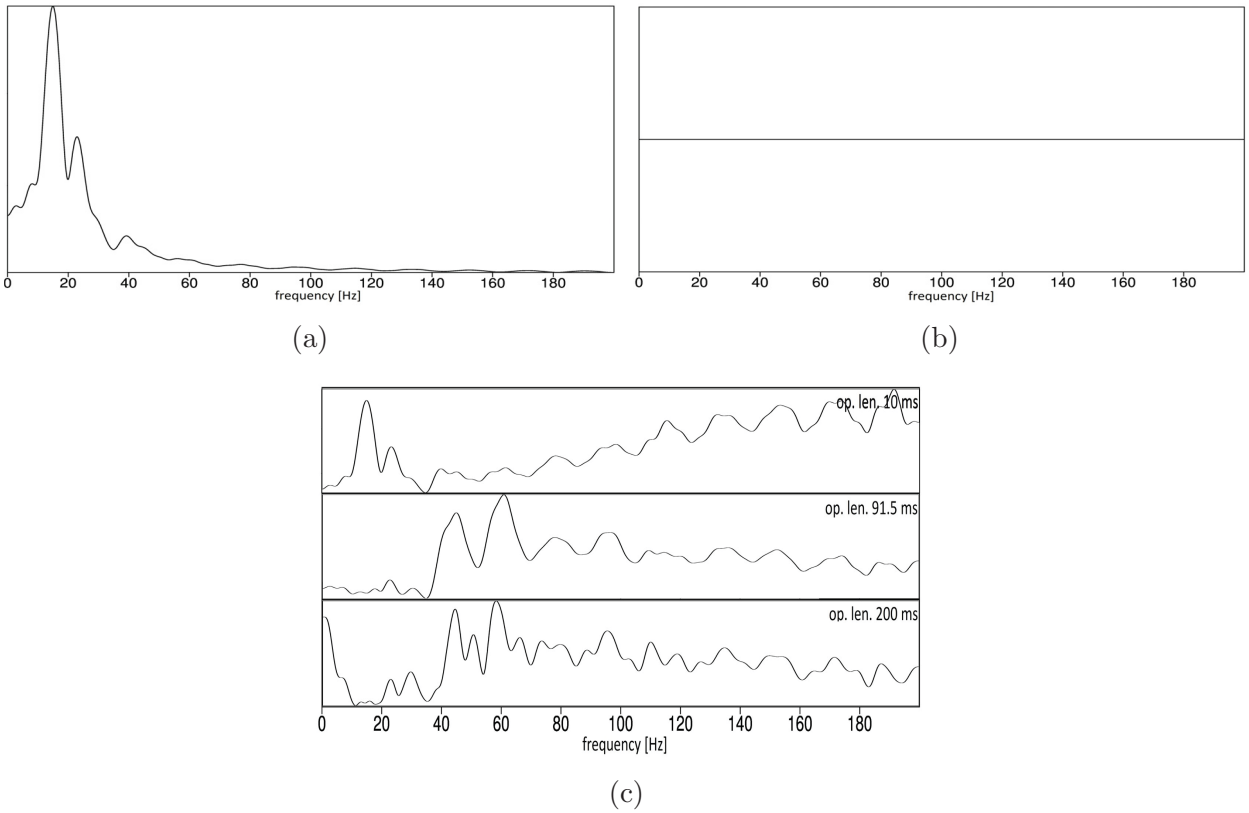

Figure 3.8: Amplitude spectra of (a) minimum-phase wavelet 3, (b) a zero-lag spike and (c) the spikes obtained using different operator lengths, whereby the amplitude spectrum in the middle is the one belonging to the spike output 3 in figure 3.7b

shown. Furthermore the amplitude spectrum of the deconvolved output of wavelet 3 for three different operator lengths is given (Fig 3.8c). Considering the amplitude spectrum it is difficult to decide which operator length is the best choice, but it is notable that with an operator length of 10 ms the amplitude spectrum of the wavelet is still maintained at the beginning. The spike output showed also more sidelobes compared to the following and therefore the 10 ms operator is not the right choice. Comparing the middle and last plot, the amplitude spectrum seems to be smoother using the maximum operator length 91.5 ms and the deconvolution output for this lengths resembled more a spike than using longer operator lengths and a window rejection factor 0. Although no spike output and thus a white spectrum could be achieved, the choice is made on the 91.5 ms operator because an output was generated, where less noisy spikes were produced.

3.3.3 Resume

To sum up, Seismic Unix works well for minimum-phase wavelets. In contrast to ProMAX, the algorithms of Seismic Unix are known, which lead to better results. The results,

using ProMAX and the selected spiking deconvolution method, are not that satisfying for wavelets 2 and 3, because it is not possible to collapse the energy of a minimum-phase wavelet to a clear spike without noise. The output of wavelet 1 in contrast can be compared to the output of wavelet 1 using SU. In both cases a zero-lag spike could not be obtained.

3.4 Testing deconvolution methods on generated synthetic seismograms - test 2

3.4.1 Using Wiener Shaping Filter method

The deconvolution steps are the same as mentioned in section 3.3. The filter shown in Figure 3.6b is chosen and convolved with the obtained seismogram 3 of Figure 3.3. The goal of deconvolving the synthetic seismogram is to get rid of the source wavelet to reconstruct the earth's impulse response. The original reflectivity series and the one obtained after deconvolution are displayed in Figure 3.9. In the first 0.4 s, the 12 spikes appearing in this section are reconstructed showing just a few low-amplitude sidelobes (Fig 3.9b).

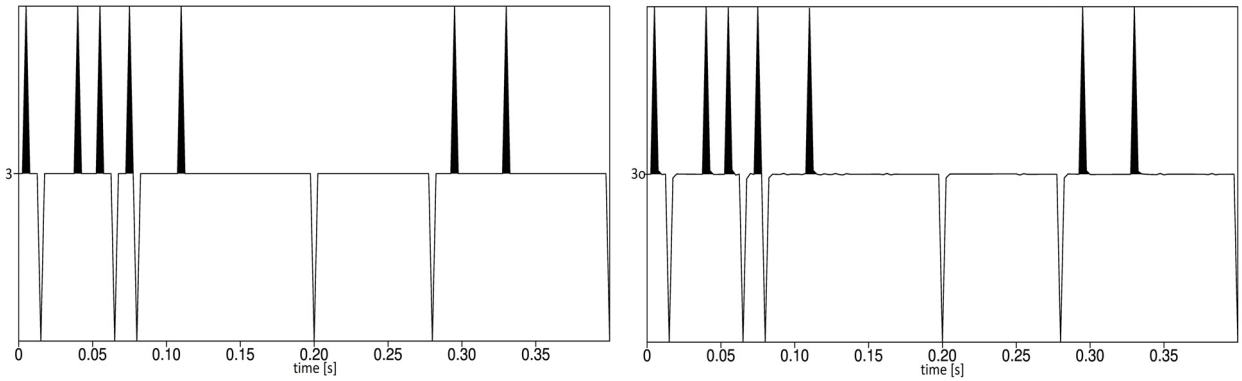

(a) (b)

Figure 3.9: (a) Reflectivity series 3 used for generating seismogram 3 and (b) result 3o after deconvolving seismogram 3 to reconstruct the spikes using the Wiener shaping filter method

3.4.2 Using Spiking Deconvolution

ProMAX' deconvolution method is tested again and this time the reflectivity series is reconstructed more precisely than the spike using this software before. The reflectivity series is not perfectly recuperate but compared to the original section the spikes that correspond

to the reflections are reproduced with some success. Different operator lengths are tested here again and operator lengths smaller than 150 ms are neglected. The best result is obtained with a minimum operator length of 150 ms (Fig 3.10b) because the autocorrelation of the input seismogram does not resemble the autocorrelation of the wavelet beyond and below this length. For comparison reasons the output with maximum operator length (685 ms) and window rejection factor of 2 is shown as well (Fig 3.10a).

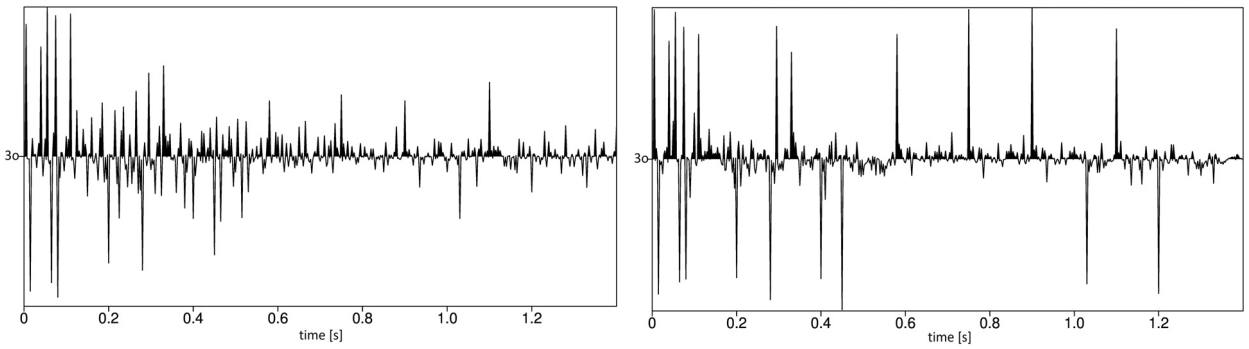

(a) (b)

Figure 3.10: Resulting reflectivity series after deconvolving seismogram 3 via the spiking deconvolution method using (a) a maximum operator length of 685 ms and (b) a minimum operator length of 150 ms

This plot indicates a lot of noisy spikes and the main spikes are basically reproduced with lower amplitudes. Looking at Figure 3.10b the improvement of the deconvolution choosing a shorter operator can be seen. The figure below is showing the autocorrelation of the original wavelet 3 and the autocorrelation of the deconvolved seismogram for different operator lengths. The autocorrelogram of the seismogram indicates the autocorrelogram of the source wavelet only in the first 15 seconds that is why the 150 ms operator worked best (Fig 3.11c).

3.4.3 Resume

Seimic Unix is working perfectly of course because the shaping filter is established from the known wavelet. However, it should be mentioned that this is not possible with the real data because the wavelet is not known and a filter can only be created from the available seismogram. The attempt to generate a filter from the synthetic seismogram does not succeed, though. ProMAX, compared to Seismic Unix, only receives the seismogram as input parameter. This means ProMAX must generate a filter operator from the available seismogram. Therefore, the output can be considered very good this time and the reflectivity function is reproduced although the filter is established from the seismogram.

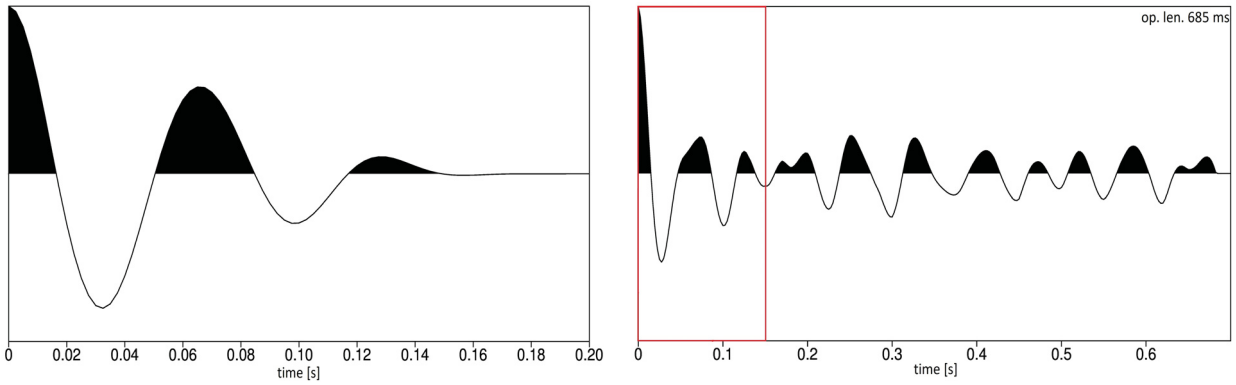

(a) (b)

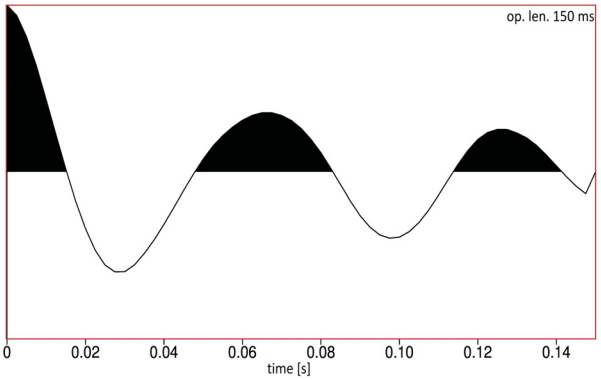

(c)

Figure 3.11: Autocorrelograms of (a) minimum-phase wavelet 3, (b) deconvolved seismogram 3 using operator length 685 ms and (c) using operator length 150 ms, whereby the red square indicates the first 15 s in which the autocorrelogram of original source wavelet is represented

3.5 Testing deconvolution methods on generated synthetic seismograms - test 3

3.5.1 Using Wiener Shaping Filter method

As described beforehand seismogram 5 is used for the third test because it should resemble the complex structure of a real seismogram, recorded during blasting operations. The complex synthetic seismogram here is convolved with filter 3 and the outcome is the deconvolved trace showing the impulse responses from earth convolved with the impulses belonging to the source. As mentioned, filter 3 is used again, because it was not possible to create a filter from the input seismogram 5. Moreover, the threefold replication of the earth's reflectivity is reconstructed (Fig 3.12b) of course and not a single spike.

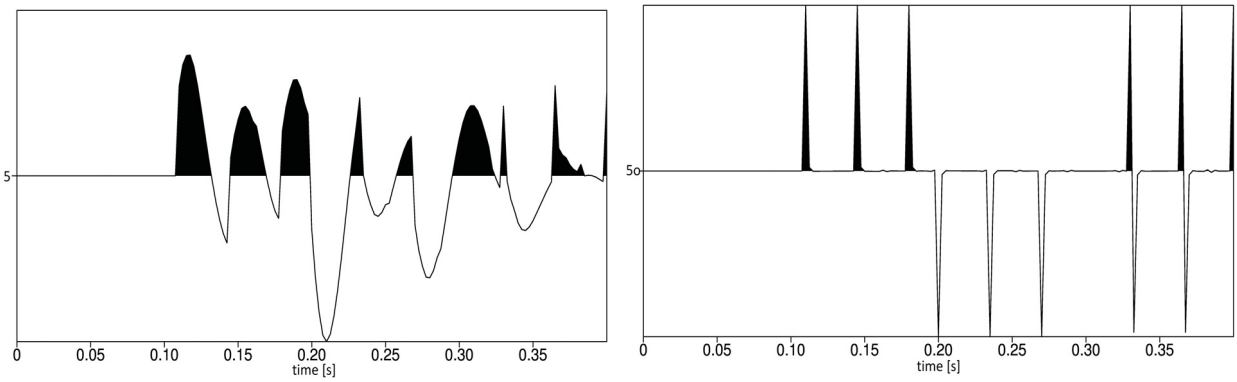

(a) (b)

Figure 3.12: (b) Resulting reflectivity series after deconvolving (a) seismogram 5 using generated shaping filter 3

Assuming that there are just impulses belonging to the source, seismogram 4 has to be considered. Seismogram 4 contains a wavelet that includes the signals of three shots and this would be an example of how the real data trace could look like, if the traces got stacked beforehand and thus the reflectivity function of the earth was reduced to the first arrival. Furthermore it is possible to create a filter out of seismogram 4 and it can be deconvolved so that the energy of the three impulses is compressed to an impulse at $t = 0$ s (Fig 3.13b). There are some small negative and positive spikes left, which indicate only $\frac{1}{5}$ or more of the height compared to the main peak, though.

3.5.2 Resume

ProMAX was not working properly for this third test and did not deliver some outputs that showed better results at all. In contrast, the shaping filter worked quite well for all different tests and they demonstrated what is possible using different inputs.

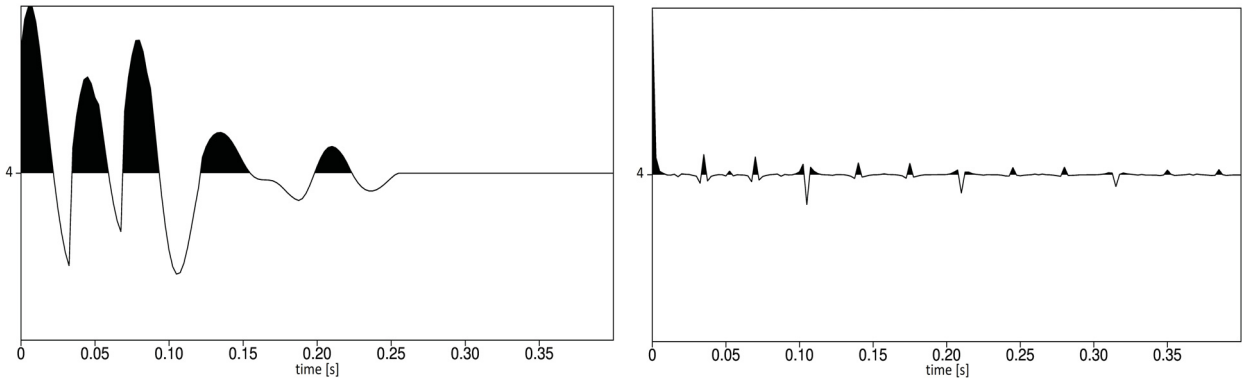

(a) (b)

Figure 3.13: (a) Seismogram 4 is used to create a filter, which can be convolved with the input seismogram to create (b) the zero-lag spike output

Therefore this method is used for the real data set in the next chapters. Beforehand it has to be mentioned again that it is necessary to create a filter out of a stacked section. This stacked section should comprise a wavelet containing impulses belonging to the source. The signals of this wavelet should be compressed to one single spike as tested in the first test where a simple minimum-phase wavelet was deconvolved or in the third test where the wavelet containing three impulses was used as input. This method will be tested first on the real data of shotpoint 22 and will be explained in chapter 5.

Chapter 4

Data collection

4.1 Introduction to SLIM

The master thesis is part of the *SLIM* project, a project that aims to find a **s**ustainable **l**ow **i**mpact **m**ining solution based on rock-mass fragmentation using blasting models, airborne particulate matter, vibration affections and nitrate leaching mitigation actions (*https://www.slim-project.eu/, retrieved August 19, 2018*). The geophysics part includes finding a solution to minimise the vibrations during rock blasting in quarries and open pit mines located in areas next to dense settlement. Vibration minimisation is a widely discussed topic and there are several influences which have to be considered. A wave interference model should be introduced whereby waveform modelling is combined with electronic delay detonators and at the end ground vibration amplitudes at critical frequencies should be diminished. To obtain such a model, P- and S-wave velocity models have to be generated beforehand. Therefore P- and S-waves have to be separated first which leads to the first goal of this work (see *Tauchner C. (2018) Seismic Tomography of Mt. Erzberg*).
The Montanuniversitaet Leoben and 12 other contributors participate in the project. Tests have been and will be performed at two mines in Spain and in the Mt. Erzberg mine in Eisenerz. The *SLIM* project is funded by the European Union's Horizon 2020 research and innovation programme and started in 2016 (*https://www.slim-project.eu/, retrieved August 19, 2018*).

4.2 Test site Mt. Erzberg

The measurements took place at Mt. Erzberg mine in November 2016.
Mt. Erzberg, which is located in Eisenerz, is an active mine, where the VA Erzberg GmbH started to mine Siderite ore in 1988. A total amount of 12 Mio t per year is produced. Geologically the area belongs to the Upper East-Alpine and is located in the "Noric nappe". The profile (Fig 4.1) shows that volcanic rocks, so-called Porphyroids (green), are found in

the lying position. The Werfen Formation (pink), characterised by Clayshales, Sandstones and Breccias, is located in the hanging wall. In between is the the actual core of the deposit, built up of Siderites in alternating sequence with Ankerites (orange and yellow) (*http://www.vaerzberg.at/, retrieved August 19, 2018*). The P-wave velocity for Siderite, Limestone and the Werfen formation is around 2-6 km/s. The Porphyroid exhibits a P-wave velocity around 4 km/s.

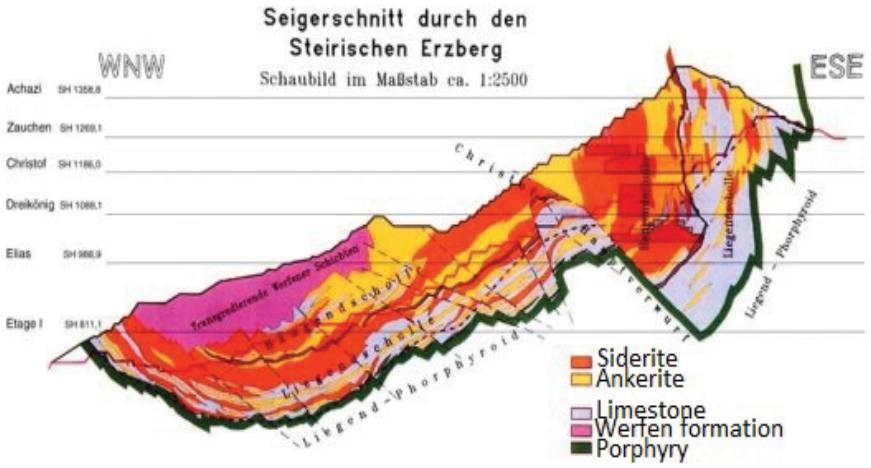

Figure 4.1: Cross section through Mt. Erzberg (*http://www.vaerzberg.at/, retrieved August 19, 2018*)

The tomography experiment lasted for three weeks and during this time a team of four to six people installed and dismounted 124 3-component geophones in and around the Mt. Erzberg mine.

The installation of the geophones took place between 9th and 11th November 2016 and the array encompassed an area of 2x2 km (Fig 4.2). The utilised 3-component geophones (PE-6/B) are composed of one SM-6/U-B 4.5Hz vertical geophone and two SM-6/H-B 4.5Hz horizontal geophones. Information concerning further parameters are listed in table 4.1. The geophones are constructed by SENSOR Nederland and were borrowed for our measurements from the GFZ Potsdam. Each geophone was connected to one data cube and one 12 V battery. The utilised DATA-CUBE3 package was constructed at the GFZ Potsdam and borrowed there as well (*https://www.gfz-potsdam.de, retrieved October 1, 2018*). Further information can be found in table 4.1 too. The gain value of 8 implies that recording took place when signals indicated impulses of at least 0.51 V and this means that with a signal input range of 0.51 V and a resolution of 24 Bit, the smallest detectable voltage change (LSB - least significant bit) is 30.5 nV (*https://www.sensoren.info/LSB, retrieved October 1, 2018*).

On the 11th November test explosions were carried out to test the optimal amount of

Table 4.1: Parameters concerning utilised geophones and data cubes

Geophone PE-6/B	**DATA-CUBE3**
3D Geophone: 236 units and 4.5 Hz	*CUBE3*: 359 units
sensor: 3-component geophone with 5 m lead-in cable	*gain*: 8
generator constant: 28.8 Vs/m	*LSB*: 30.5 nV
response: ground velocity from 4.5 Hz to $>$ 150 Hz	*sensitivity*: 3,2787$*10^7$ [counts/Volt]
damping: 0.56	*clip*: 0.51 V

charge for the seismic shots. It turned out that a charge of 500 g of explosives would produce far too weak signals and therefore the charge was increased to 2.3 kg. For each of the 21 seismic blasts, 3-5 boreholes were drilled, which were filled with a total of 2.3 kg of explosives. For the production blasts, which are normally carried out once a week in the quarry, 4000-10000 kg of explosives were used. The production blasts were performed via the NONEL blasting system. Nonel is based on a non-electric ignition system and each borehole is connected through a shock tube, which transfers the detonation impulse to the detonators and connectors. As connectors in-hole delay devices were used, which means that delay detonators were placed in the borehole. Detonating cords made sure that the detonators were initiated at the same time, indicating a marginal delay time (*https://www.oricaminingservices.com/uploads/Germany/NobelHefte2003.pdf, retrieved August 19, 2018*). Different amounts of boreholes, either in one or two rows, were drilled and for each production shot various amounts of explosives were used. Detonation of each borehole took place in intervals between 30 and 50 ms. A list of detailed information can be found in appendix B.

The recorded data exhibits signals from 21 small scale seismic blasts and 10 production blasts, but the work is focusing on the vertical component of the data collected through the production blasts. A total amount of 10 data sets were produced, starting with SYBO298, which is referred to shotpoint (SP) number 22. As visible in appendix B SYBO298 comprised 11 boreholes arranged in a row at a distance of 6 m. A total of 4430 kg of explosives were used and the delay time between each detonation is referred to 33 ms. ETM3371, or SP 27, comprised five boreholes and PALM385, which is ascribed to SP 28, indicated 9 boreholes. In Figure 4.3 the arrangement of the boreholes of the three named shotpoints is shown. This three SPs are chosen to be further investigated and the results are discussed in chapter 5. The final results for the other shotpoints are displayed in appendix D.

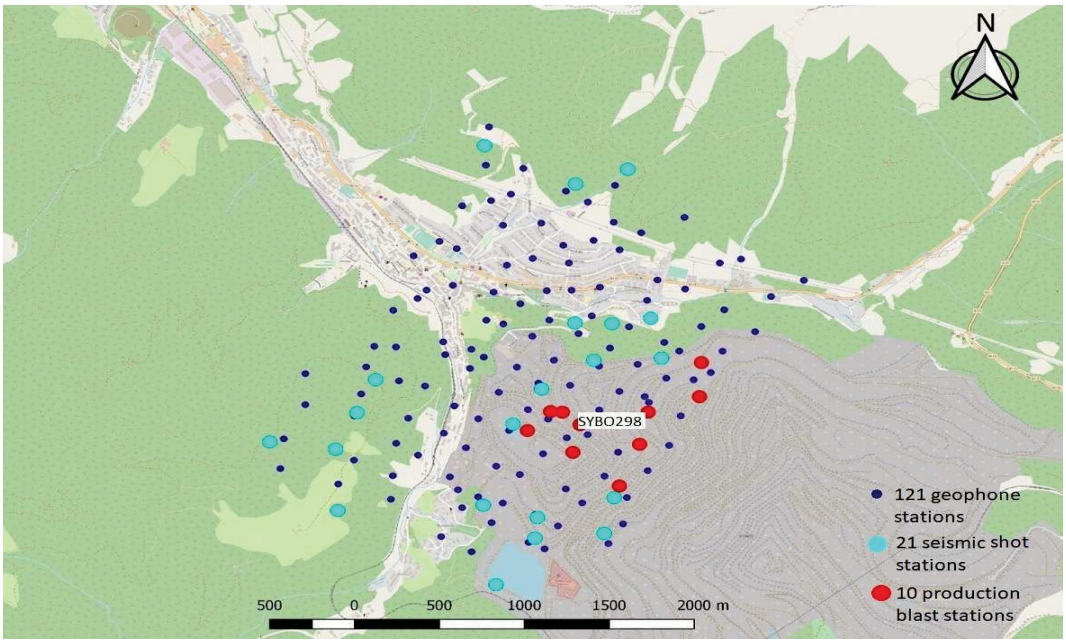

Figure 4.2: Seismic array of Mt. Erzberg mine and Eisenerz using 124 geophones (blue dots) and 31 operation areas for blasting work (turquoise and red dots)

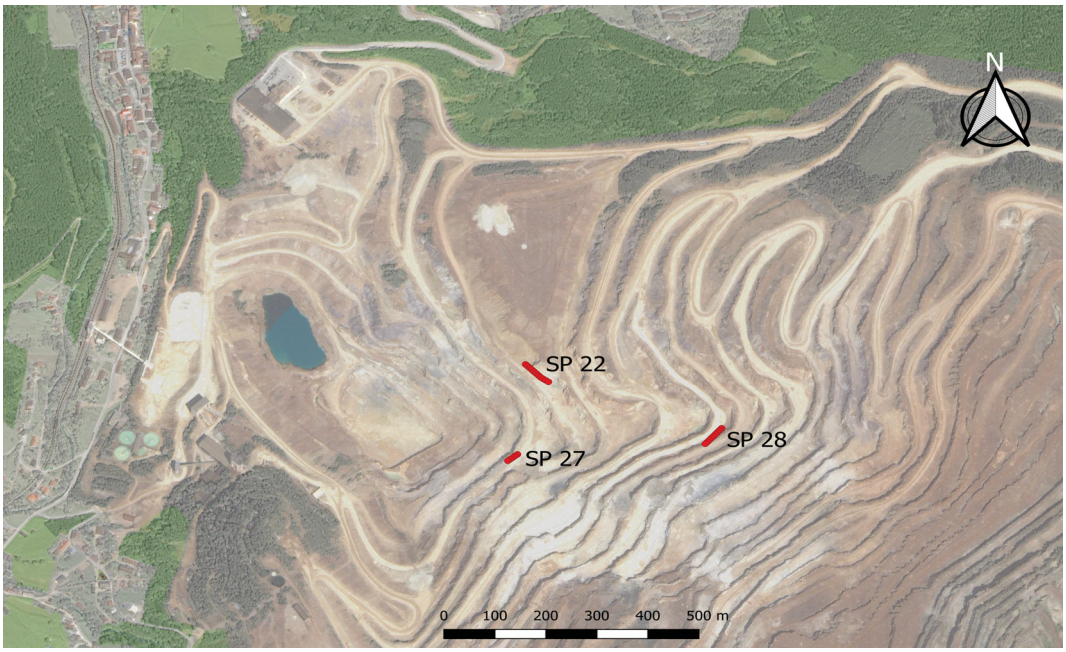

Figure 4.3: Borehole configuration for SP 22 (SYBO298), SP 27 (ETM3371) and SP 28 (PALM385)

Chapter 5

Applying the Wiener Shaping Filter method on real data

5.1 Data set of shotpoint 22

The methods performed with the synthetic dataset were tested first hand on one data set. Shotpoint 22 was selected for this purpose. The shot gather visible in Figure 5.1 shows 121 traces, ordered by offset, containing signals from the z component (vertical direction). 1601 samples with a sample interval of 2.5 ms can be found. The corresponding amplitude spectrum is shown in appendix C. The seismogram should probably show P-waves and S-waves but only the P-wave arrival of the first shot could be picked so far. The red rectangle shows the duration of the blasting sequence and in this ∼330 ms the 11 signals from the direct wave should be visible, but neither this signals nor other phases can be identified. Furthermore the traces start at 0.6 s, because the trigger unit was placed before the first delay detonator of the first borehole and a delay of 0.617 s between the first trigger and the delay detonator was measured. The delay times vary between 0.617 and 1.020 s and therefore at least 0.6 s had to be cut off to pick the P-wave onset of the first shot more precisely. This kind of delay times are only valid for signals recorded through production shots, because of the utilised detonation system.

Pseudo LMO correction

Perfoming a deconvolution at this stage was not an option, because it was not possible to generate a filter out of the seismic section. To generate an appropriate filter, the following procedure was chosen: the shot gather was corrected from the pseudo linear moveout (LMO) and a stacked section was created. Pseudo in this case, because the picked traveltimes were used and they are scattering around the linear. After executing a pseudo LMO correction primary onsets should be horizontally aligned in x-direction. The picked traveltimes were corrected with 0.6 s, because the traces start at 0.6 s as explained beforehand. For example for trace number 1 a traveltime of 0.101 s was picked, 0.6 s were added and

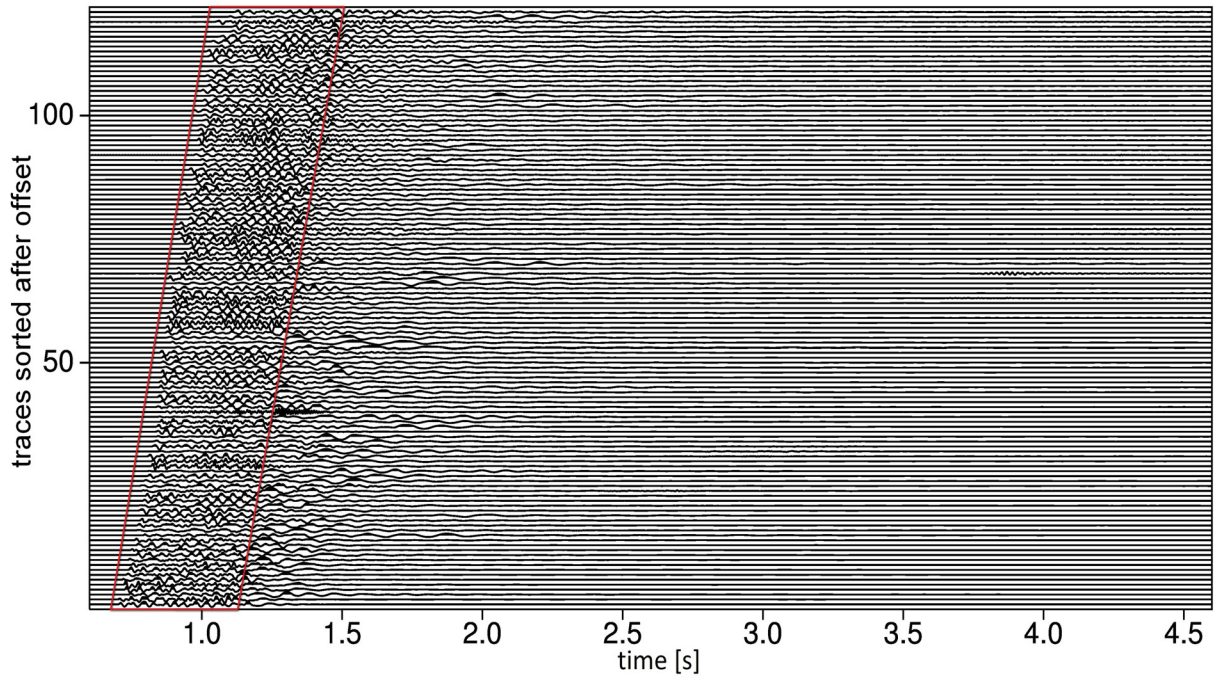

Figure 5.1: Shotpoint 22 vertical component, whereby the red rectangle indicates the 400 ms time slot after the first arrival

resulted in a new time of 0.701 s. Each trace was resampled to t=0 s and corrected using the new calculated time. The first 400 ms of the pseudo LMO corrected section is shown in Figure 5.2. High and low amplitudes are vertically aligned for each trace and 11 stripes are visible now which mark the 11 shot signals. This 11 signals are labelled with the numbers 1 through 11.
The first 3 signals and number 6, 7, 8 and 9 are better visible than 4, 5, 10 and 11. They exhibit stronger amplitudes, especially 6, 7, 8 and 9 indicating higher amplitudes with increasing offsets. Probably the surface waves mask the signals at the beginning, but this is reviewed later on. Further assumptions concerning the delay times between the individual shots can be proposed. The impulses do not arrive at intervals of 33 ms, but rather between 30 and 50 ms, because the first arrival of the last signal can be found at $t = 0.38$ s and not at $t = 0.33$ s as supposed.

Stacking

In the next step, the newly created section was stacked. The traces were summed over the offset axis and the output, a single stacked trace, is given in Figure 5.3, respectively. Through the pseudo LMO correction and stacking, the reflectivity function of the earth is reduced to the first-arrival, since the earth's impulse response is different for each receiver. The obtained mastertrace, called mastertrace 22, reveals 11 high-amplitude lobes, whereby 10 and 11 are joined.

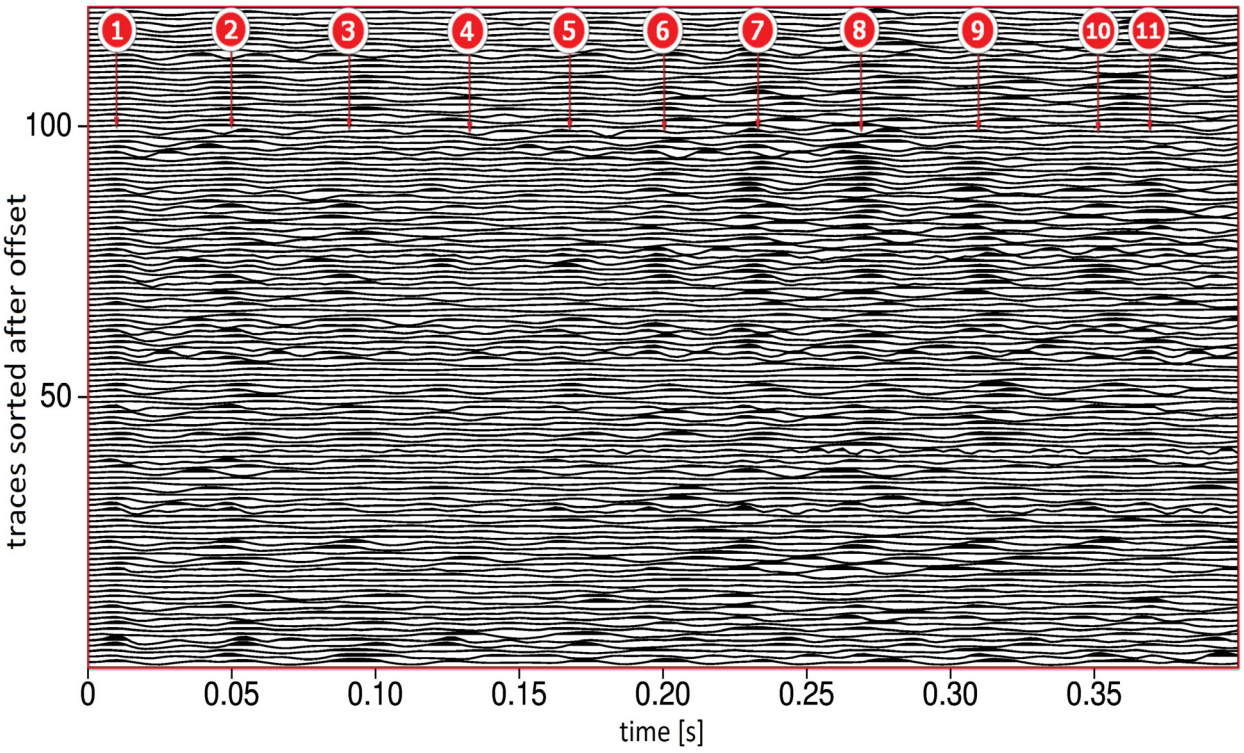

Figure 5.2: Pseudo LMO corrected traces with signals aligned vertically close up showing 11 stripes in the first 400 ms which are marked by the red arrows

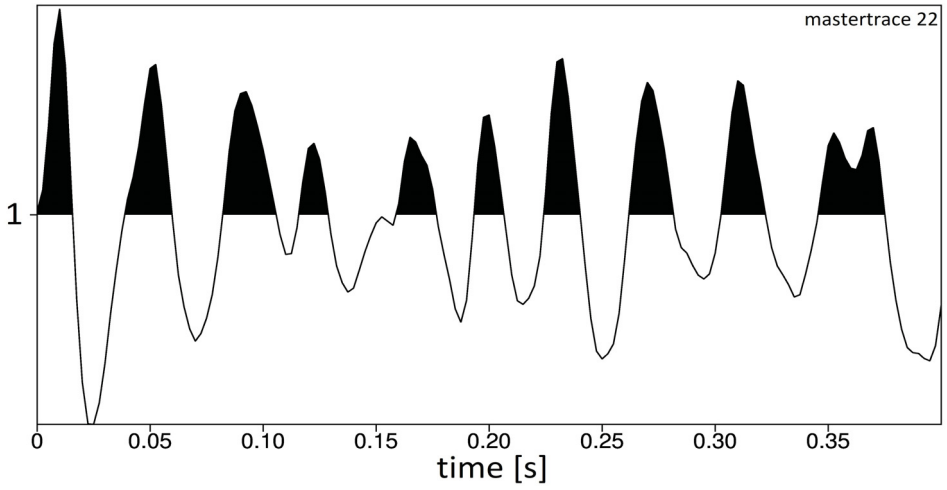

Figure 5.3: LMO corrected traces stacked to mastertrace 22

One reason could be that the delay time between shot 10 and 11 was really short and the result is more clearly visible in the stacked section now. It is important to emphasise, that the mastertrace represents the wavelet of 11 shot-impulses and that the earth's impulse response is proposed to be eliminated.

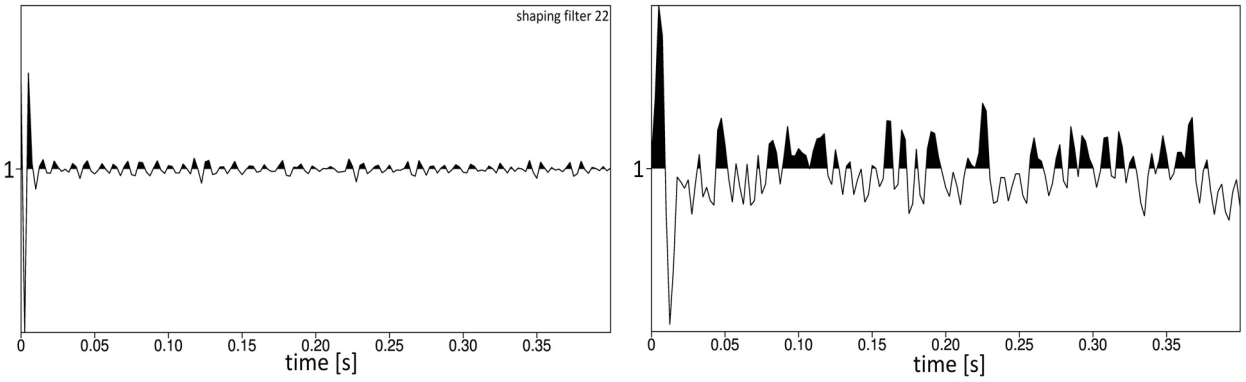

(a) (b)

Figure 5.4: Mastertrace 22 was used to generate (a) filter 22, which was used to create (b) the deconvolved trace showing spike-like pulse at the beginning of the trace

Furthermore it has to be stated that it is possible to create a filter operator (Fig 5.4a) like in the test of synthetic seismogram 4 (Fig 3.13). The filter can be used for convolving it with the mastertrace to obtain a deconvolved output. The deconvolved trace, displayed in Figure 5.4b, shows that the energy of the 11 shots is gathered to nearly one spike at the onset of the trace. Granted, it is not a zero-lag spike and there are several low-amplitude spikes left, yet the fact remains that the energy can be compressed to a spike-like pulse, which has a much higher amplitude than incoming spikes afterwards.
Hence, the consideration followed that the filter and thus the deconvolved output could be improved. That is why for the next mastertrace, depicted in Figure 5.5, the first 56 traces were rejected before the stacking procedure to exclude the surface waves. Only 65 traces were used for stacking. The resulting trace does not differ much from the former in the first instance. The deconvolved output has not improved either, so the surface waves do not enhance or worsen the output and therefore all traces can be kept.

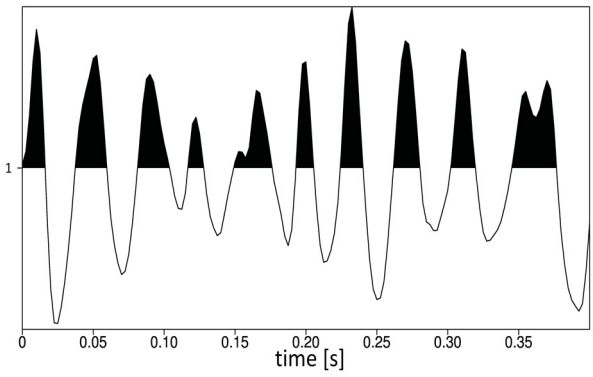

Figure 5.5: Mastertrace, whereby 65 traces, neglecting the first 56 ones because of surface waves, were stacked

5.1.1 Crosscorrelation

To improve the pseudo LMO corrected section a crosscorrelation is performed. With the support of crosscorrelation it is possible to determine the times at which the traces show maximum similarity. These times can be used as correction values for the picked traveltimes. This means that the new determined value is either added or subtracted from the traveltime.
The first step encompassed correlating mastertrace 22 (Fig 5.3) with the pseudo LMO corrected section (Fig 5.2). The crosscorrelated output is given in Figure 5.6. In SU it is possible to determine maximum amplitude values at a certain time with the command *sumax*. The crossplot in 5.6 shows that the depicted maximum values are fluctuating around 0, except for a few outliers. The crosscorrelated plot (Fig 5.6) indicates that only the last 20 are deviating more and in the crossplot an increase in time is visible, but the values are still close to zero. As already mentioned, the values can be used for correcting the traveltimes and accordingly also the sequence of the maximum amplitudes. Comparing the amplitudes in the marked area of Figure 5.6 and the ones of Figure 5.7, the amplitudes now show a perfect alignment.

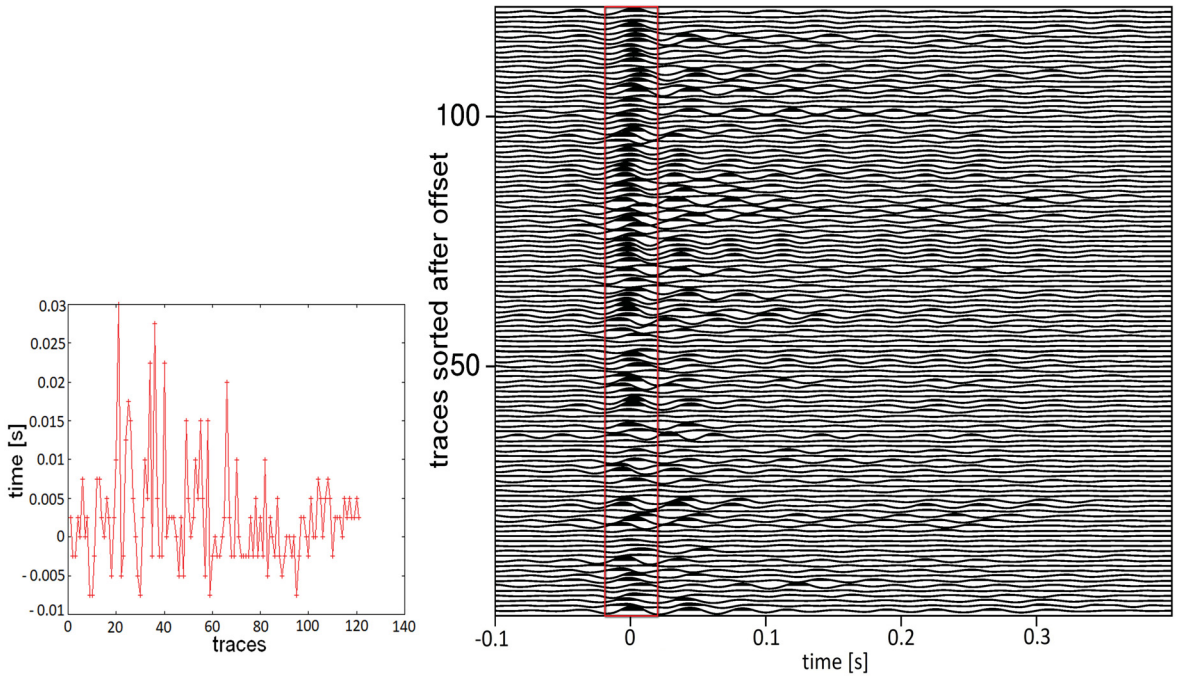

Figure 5.6: Crossplot of time indicating maximum amplitude values (y-axis) vs. traces (x-axis) on the left handside and crosscorrelated output on the right handside

After correcting the crosscorrelated section, the traveltimes from the pseudo LMO corrected section were corrected as well. Each shot is clearly aligned now and the stripes are much stronger (Fig 5.8). Stacking this section should normally improve the mastertrace and thus the filter and the deconvolved trace. The stacked section (mastertrace 22.1) shows

again 11 lobes whereby number 10 and 11 are better distinguishable from each other (Fig 5.9). The first peak looks smaller compared to mastertrace 22. Moreover it has another shape and the maximum is further away from t=0 s. Peaks 7, 8 and 9 have improved and are strong and clear now. As beforehand with mastertrace 22 a filter and a deconvolved trace is generated. Looking at the deconvolved trace, a smaller spike at t=0 s before the start of the actual, larger one can be found and it is encircled in Figure 5.10. As tested with the synthetic data, it seems that trying to create a zero-lag spike can not work properly because the wavelet is not perfectly minimum-phase as the onset of maximum energy is not at the start of the trace. Of course that is also not the case for mastertrace 22, but examining the trace in detail it is indicating that it is onsetting 2 samples earlier and milliseconds shifts are essential for this investigation.

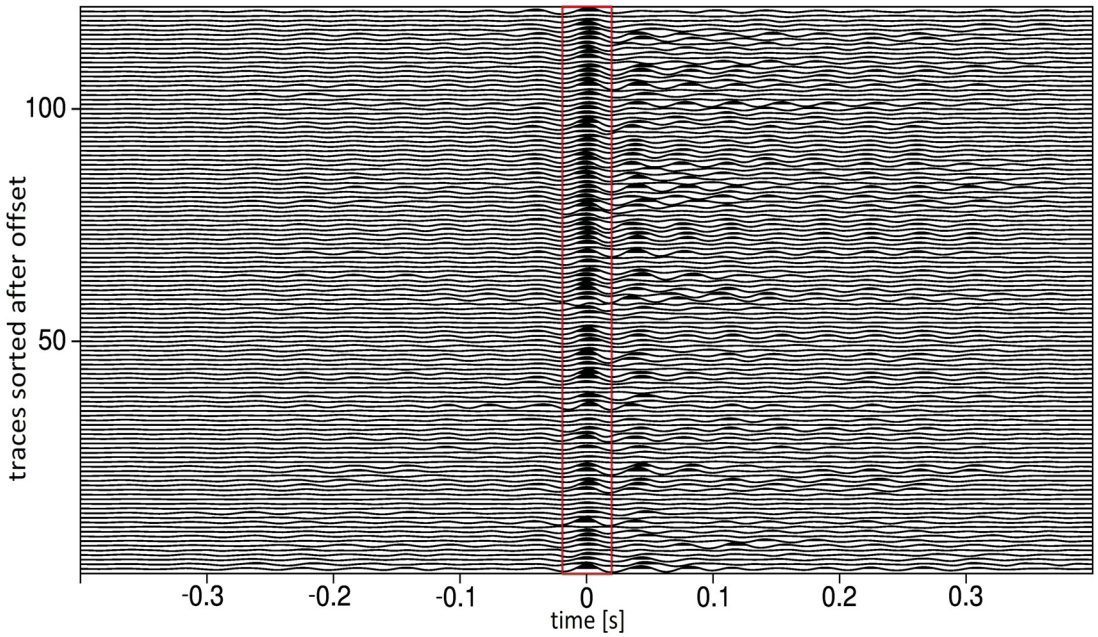

Figure 5.7: Crosscorrelated output after correcting the traveltimes

The deconvolved output looks also more noisy and more high-amplitude spikes are following after the large one. Therefore mastertrace 22.1 was shifted 6 ms backwards in time so that the maximum peak is nearly at t=0 s. The final mastertrace and the filter generated from it are displayed in Figure 5.11a and 5.11b and ascribed as mastertrace 22.2. It was just a very narrow shift, but the deconvolved trace tends to look much better too (Fig 5.11c). This time a definite zero-lag spike was created, there are still following spikes left, but they are clearly smaller and smoother than the ones from the other two deconvolved mastertraces.

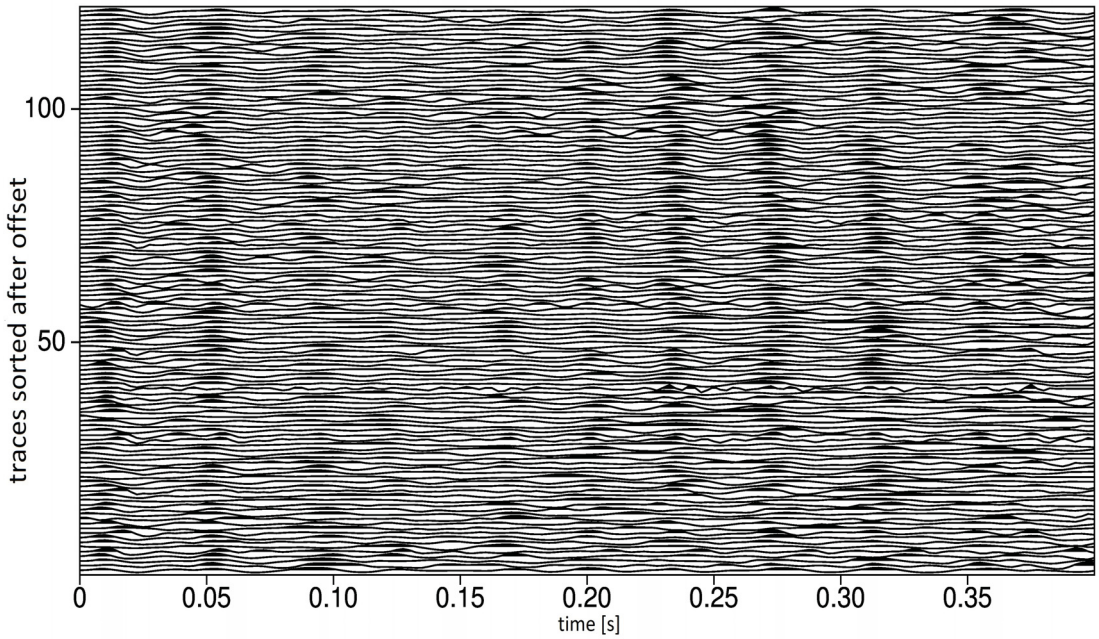

Figure 5.8: Pseudo LMO corrected section after correcting the traveltimes

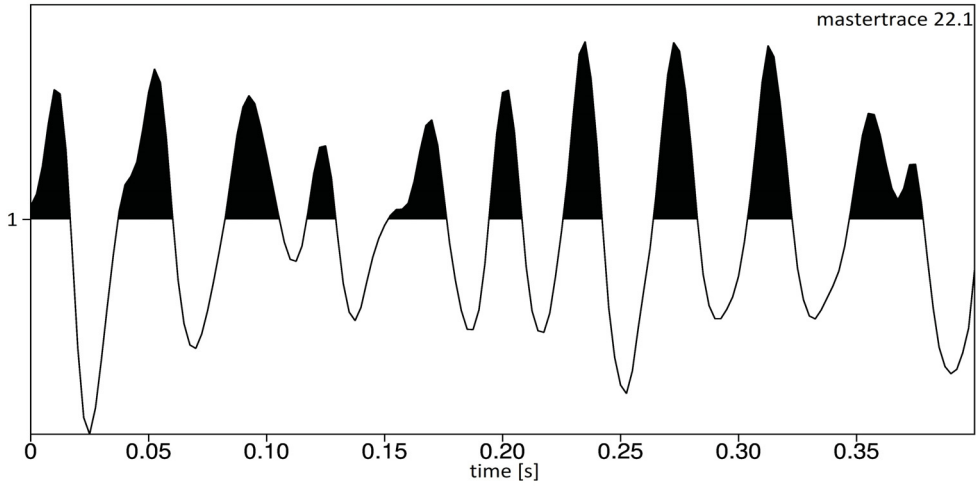

Figure 5.9: Pseudo LMO corrected section after correcting the traveltimes, stacked to mastertrace 22.1

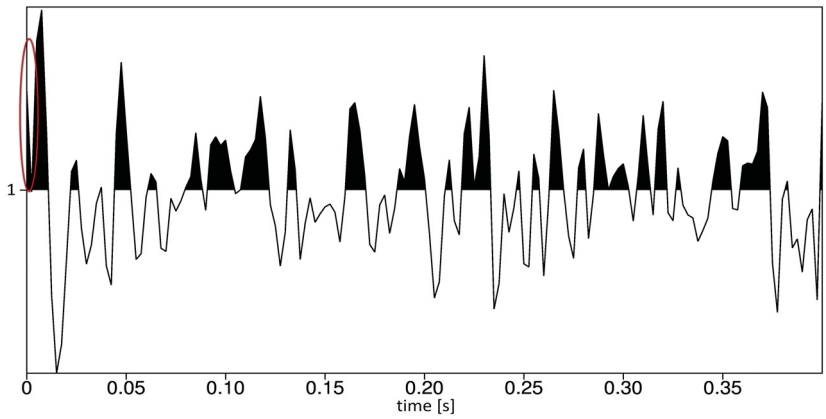

Figure 5.10: Mastertrace 22.1 was convolved with appropriate filter to create deconvolved trace showing two spike-like pulses at the beginning of the trace whereby the first one is encircled in red

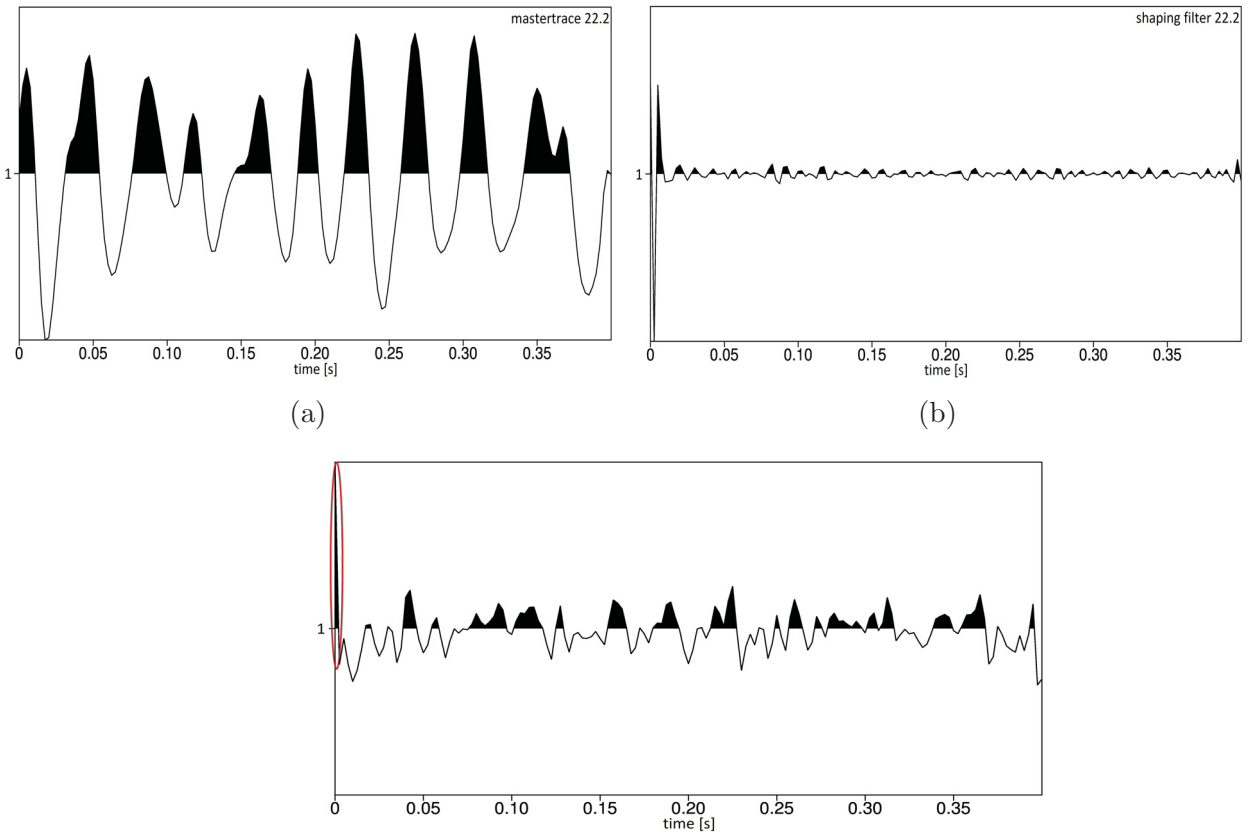

Figure 5.11: (a) Time corrected mastertrace 22.2 was convolved with (b) filter 22.2 to create (c) the deconvolved trace showing a zero-lag spike (red circle)

5.1.2 Deconvolution of the entire section

Since the deconvolution of the stacked traces has worked very well, the deconvolution is now being tried out on the entire shot gather. On the one hand the time corrected section displayed in Figure 5.8 is deconvolved and on the other hand all traces are shifted by 6 ms and then they are deconvolved using the appropriate filters 22.1 and 22.2. Shaping filter 22.1 is not presented here, because the appearance is only slightly different to filter 22. All three filters differ in the height of the peaks, but the shape is more or less the same. Following that Figure 5.12 is the result obtained through convolving the time shifted section with shaping filter 22.2 (Fig 5.11b).
Both deconvolved sections indicated an amplitude alignment at t=0 s and a second one at t=0.4 s, but the first band is stronger visible in Figure 5.12. That is why the focus moves to the deconvolved section with the little time shift and the output of the convolution of Figure 5.8 with filter 22.1 is not shown. Looking at the section showing the whole trace length of 4 s, it seems that more signals of higher frequencies are still present (Fig 5.13).

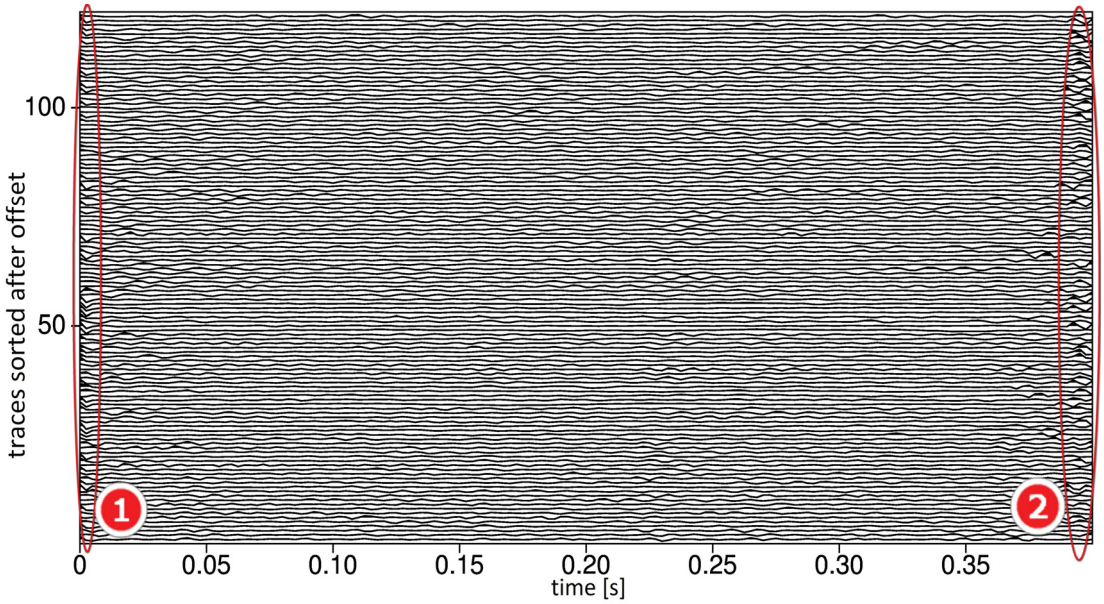

Figure 5.12: Deconvolved section where traveltimes have been corrected first and then a time shift of 6 ms have been performed, showing first 400 ms

There is one band at approximately t=0.25 s (number 3 encircled in red), which can be remnant signals from shot 8, and the strong one at t=0.4 s (number 2 encircled in red), which definitely does not belong to the signals from the shot sequence. It could be a reverberation of the 11 blasts that are more prominent now. To get rid of high frequencies, a low-pass filter was applied. Frequency filtering in time domain is possible with the *sufilter* command in SU. Based on the amplitude spectrum of the stacked section (app C), a cut-off frequency of 50 Hz was selected. Directly below the second amplitude-alignment from

Figure 5.13, which were thought to be reverberations, low-frequented, long-wave signals become visible which probably represent down-falling rocks caused by the detonations (Fig 5.14).
Furthermore, a signal is recognisable which could present the signal of the S-wave. It is highlighted in blue in Figure 5.14. However, the signal can only be traced up to approximately 0.5 s and whether it starts at 0 can not be seen here. One reason for this could be surface waves, which superimpose the signal in this area and therefore it can not be traced further, but it is more likely that there is just a weak S-wave signal due to geology. Last but not least the original section (Fig 5.1) was deconvolved too, using filter 22.1. Looking at the not LMO corrected, deconvolved section, which is also already low-pass filtered, the same low-frequency signals can be found (Fig 5.15). If there is a S-wave signal can not be seen really clearly, but it is unlikely that the S-wave is ending at approximately $t = 1.8$ s and being so much steeper than the P-wave.

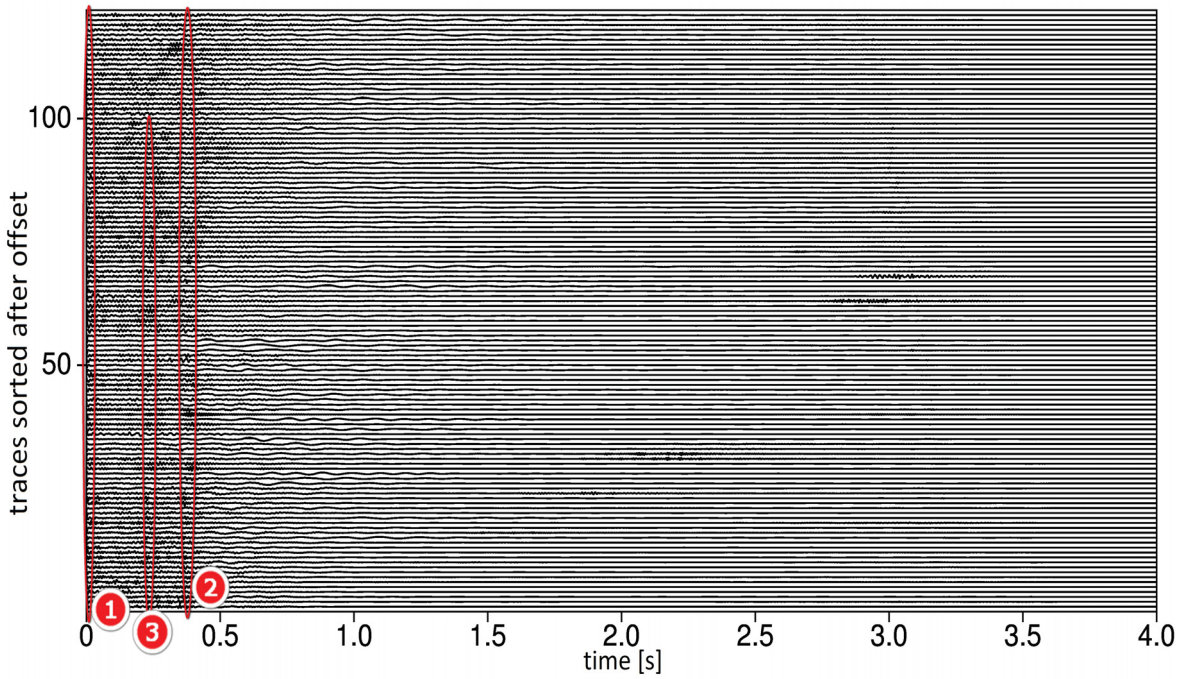

Figure 5.13: Deconvolved section where traveltimes have been corrected first and then a time shift of 6 ms have been performed, showing whole trace length of 4 s. Red circles mark the still present high-frequency signals

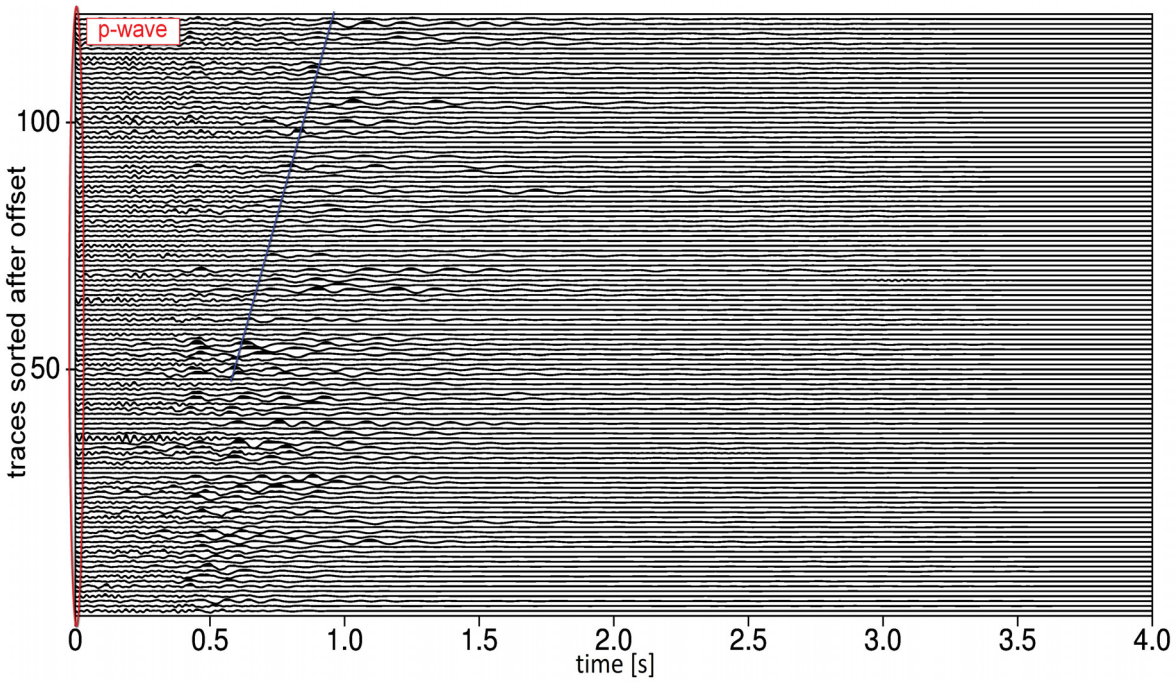

Figure 5.14: Deconvolved section where traveltimes have been corrected first and then a time shift of 6 ms have been performed and a low-pass filter is used to remove high-frequency signals

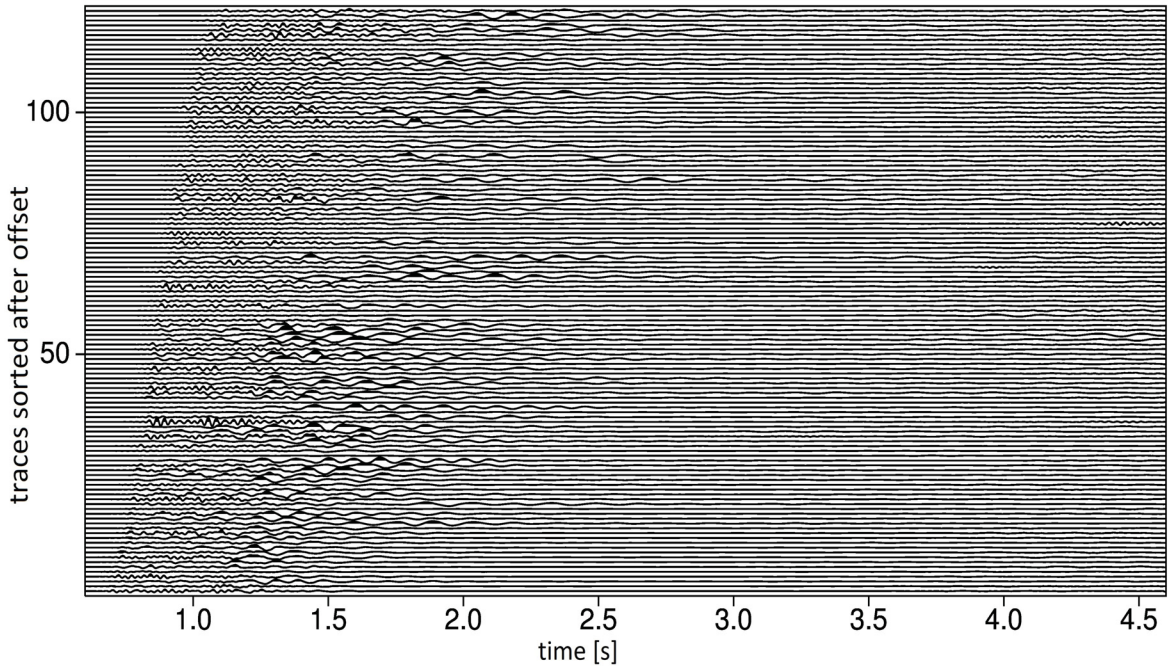

Figure 5.15: Deconvolved original section where a low-pass filter is used to remove high-frequency signals

5.2 Data set of shotpoint 27

In order to compare the results SP 27 was considered next. The whole processing steps were already shown with SP 22, that is why in the following figures only the original seismic section and important results are presented. In Figure 5.16 the vertical component is shown and the red rectangle indicates the shot sequence of ∼200 ms. This time 123 traces can be found, but the sample interval stayed the same. The amplitude spectrum is given in appendix C.

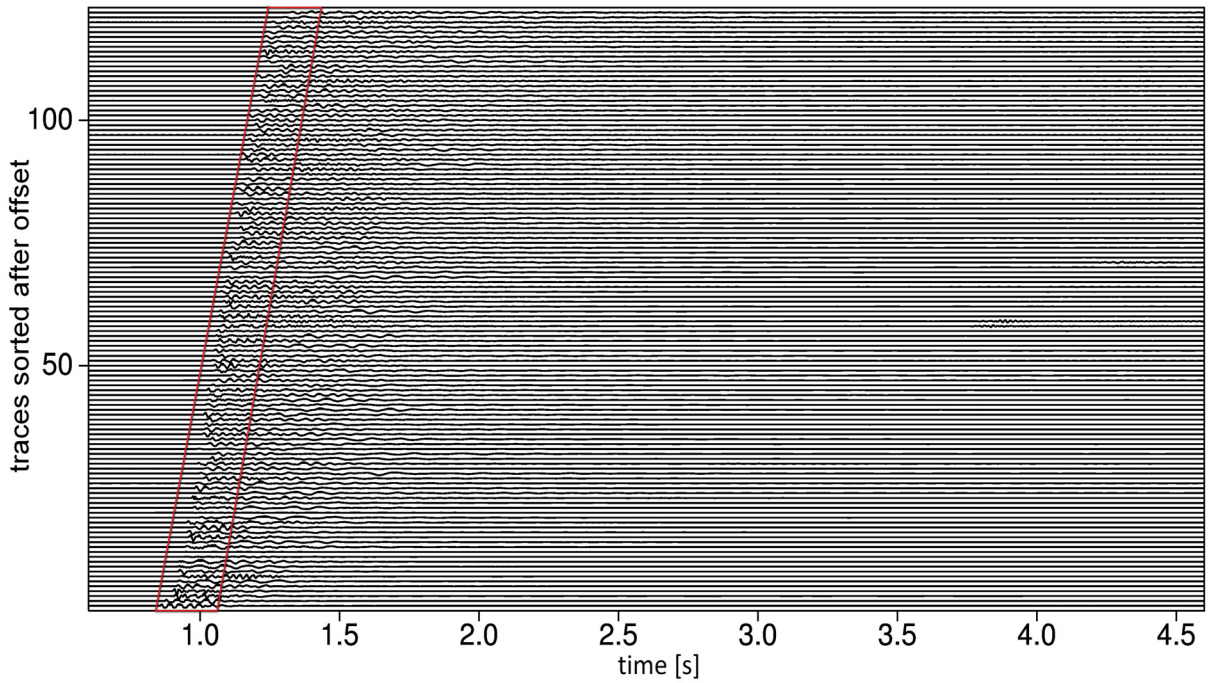

Figure 5.16: Shotpoint 27 vertical component, whereby the red rectangle indicates the 200 ms time slot after the first arrival

SP 27 comprised five boreholes and therefore the stacked mastertrace shows a wavelet containing five shot signals. The final mastertrace 27.2 in Figure 5.17a is already time shifted using 15 ms. The wavelet shows five strong signals and the deconvolved output has further improved, compared to the one from SP 22. The output shows a zero-lag spike whereby only one small negative peak is following and afterwards it stays pretty smooth.

5.2.1 Deconvolution of the entire section

As already described beforehand for deconvolving the entire pseudo LMO corrected and crosscorrelated section, which was shifted 15 ms backwards, shaping filter 27.2 was used. For deconvolving the original section filter 27.1 was utilised. The deconvolved outputs can be found in Figures 5.18 and 5.19. Figure 5.18 indicates that the whole energy is

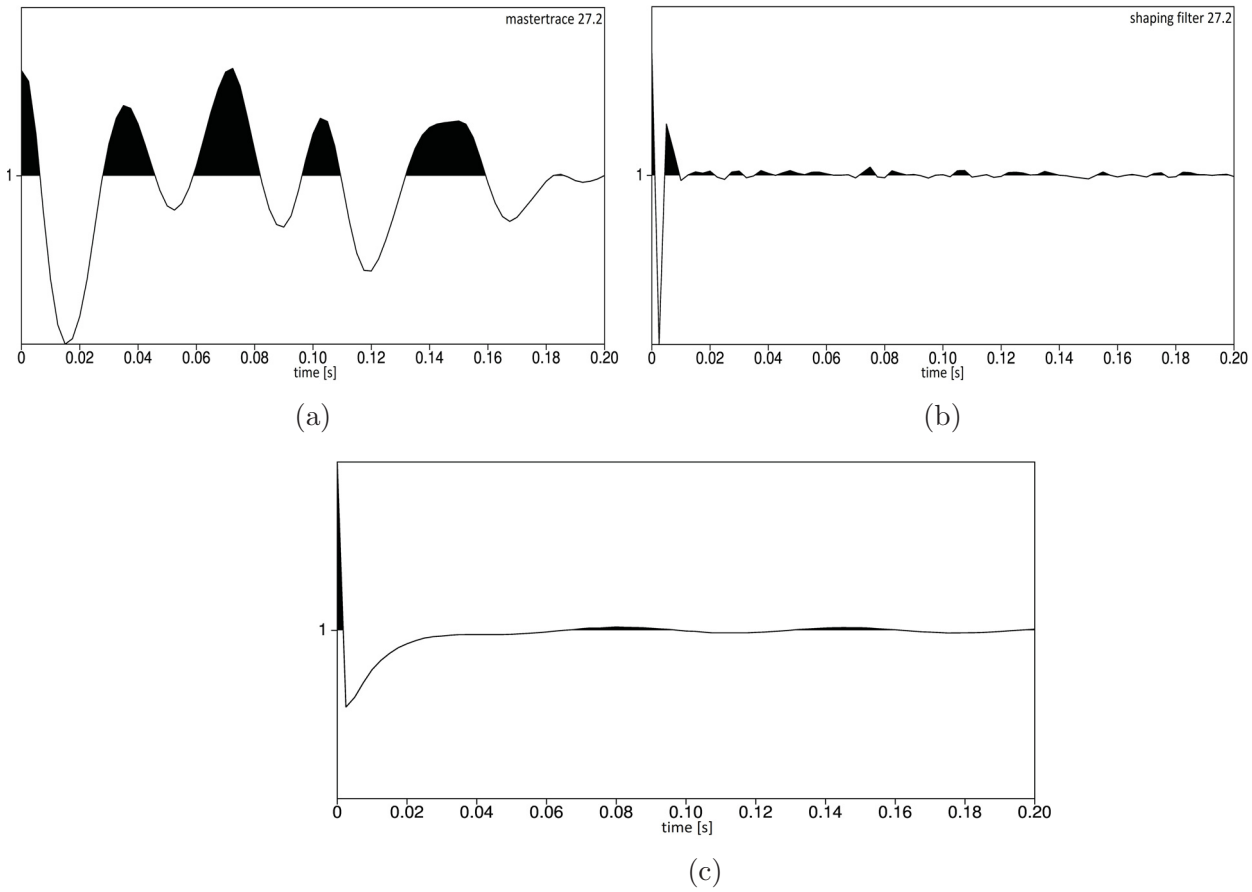

Figure 5.17: (a) Time corrected mastertrace 27.2 was convolved with (b) filter 27.2 to create (c) the deconvolved trace showing a zero-lag spike

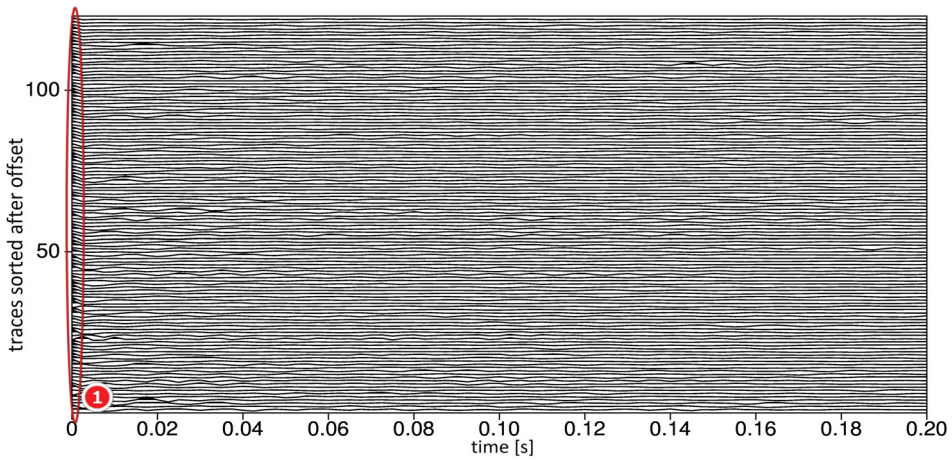

Figure 5.18: Deconvolved section where traveltimes have been corrected first and then a time shift of 15 ms have been performed, showing first 200 ms

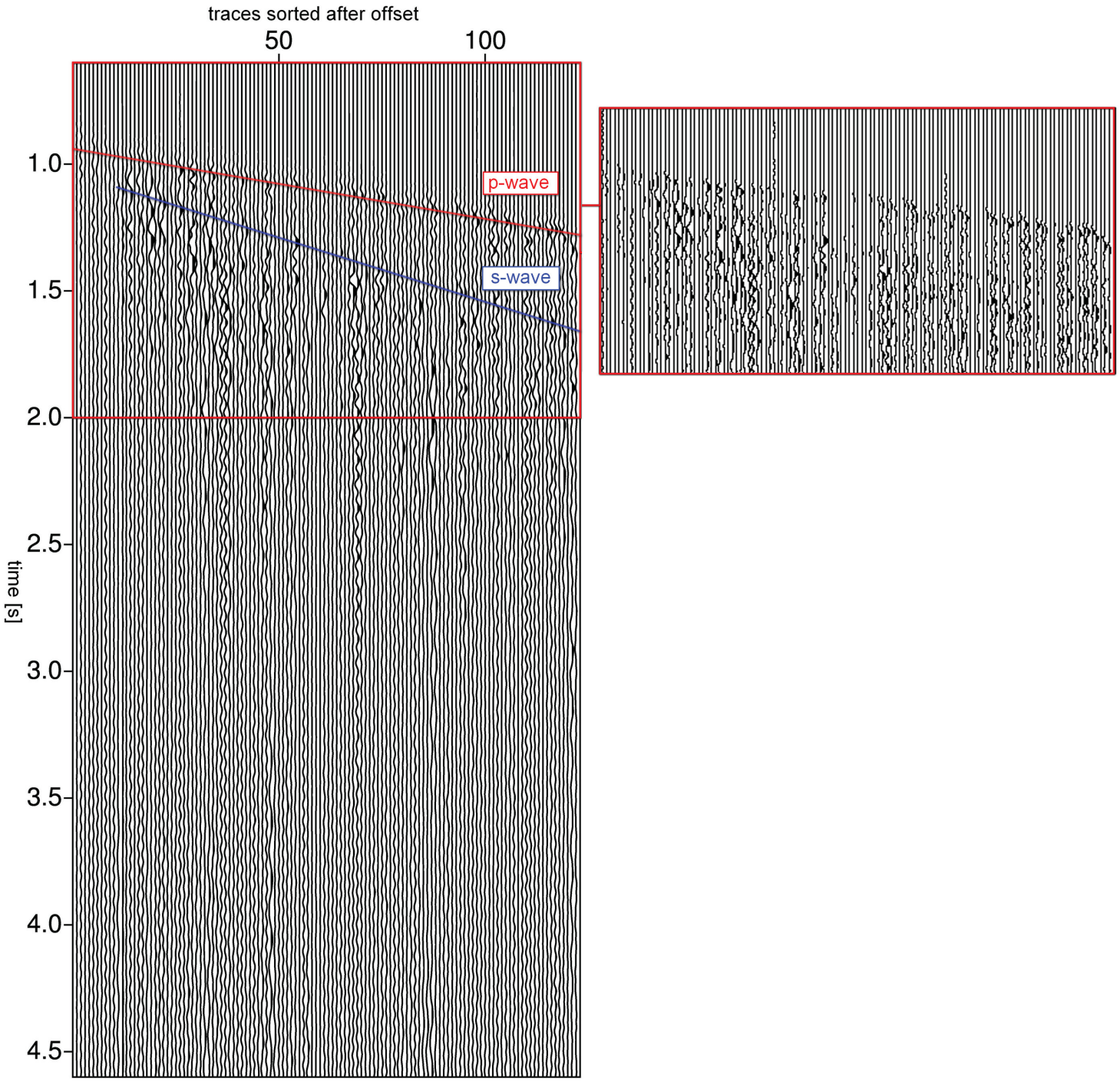

Figure 5.19: Deconvolved original section where a low-pass filter is used to remove high frequency signals

compressed at the beginning (number 1 encircled in red). There are no high frequency signals left. The latter is already low-pass filtered, whereby a cut-off frequency of 30 Hz

was selected (app C). This time a vertical illustration was chosen to better identify the P- and S-wave, because S-wave signals are clearly visible now (Fig 5.19). For better distinction the red highlighted box on the right handside is used, where only the first 2 s are displayed again. Focusing on this part, the S-wave is even better visible and it is indicating a velocity of ∼2000 m/s, whereby the P-wave velocity is around 3850 m/s. Using following relation: $v_s = \frac{v_p}{1.73} = 2220 m/s$ as reference, the estimated velocity would fit quite well.

5.3 Data set of shotpoint 28

As final example SP 28 was selected, because this shotpoint contained also less than 12 boreholes. The blasting sequence should last approximately 380 ms since 9 boreholes were detonated in an interval of 42 ms. The red rectangle highlights this sequence again. This time the shot gather indicates 122 traces containing signals from the vertical component. The appropriate amplitude spectrum can be found in appendix C.

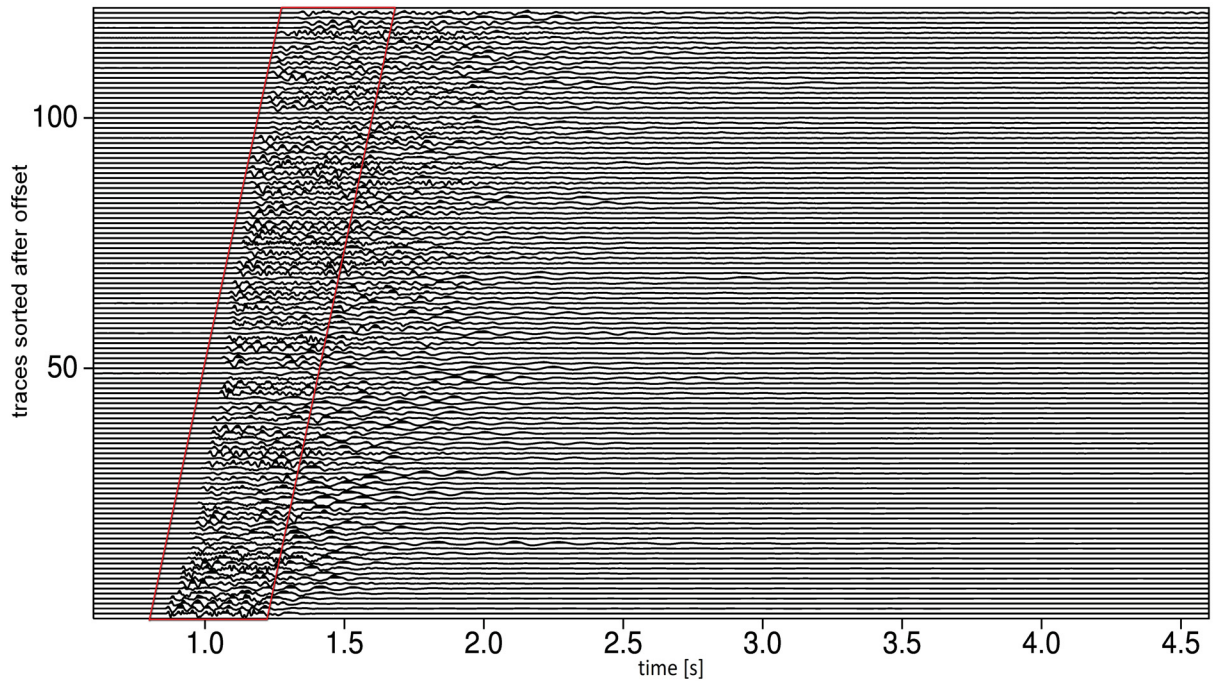

Figure 5.20: Shotpoint 28 vertical component, whereby the red rectangle indicates the 400 ms time slot after the first arrival

In the final mastertrace 28.2 (Fig 5.21a), whereby a time shift of 10 ms was applied, the shot signals can not be seen that clear as in mastertraces 22.2 and 27.2. The first four signals are clear and strong, but it can not be identified if the small lobe at $t = 0.17$ s should depict the fifth signal or if rather the lobe at $t = 0.23$ s should be considered (encircled in red in Fig 5.21a). This could be because signals are interfering. The deconvolved output however

shows a zero-lag spike again (Fig 5.21c). Not as smooth as the output of mastertrace 27.2 but also not as noisy as SP 22.

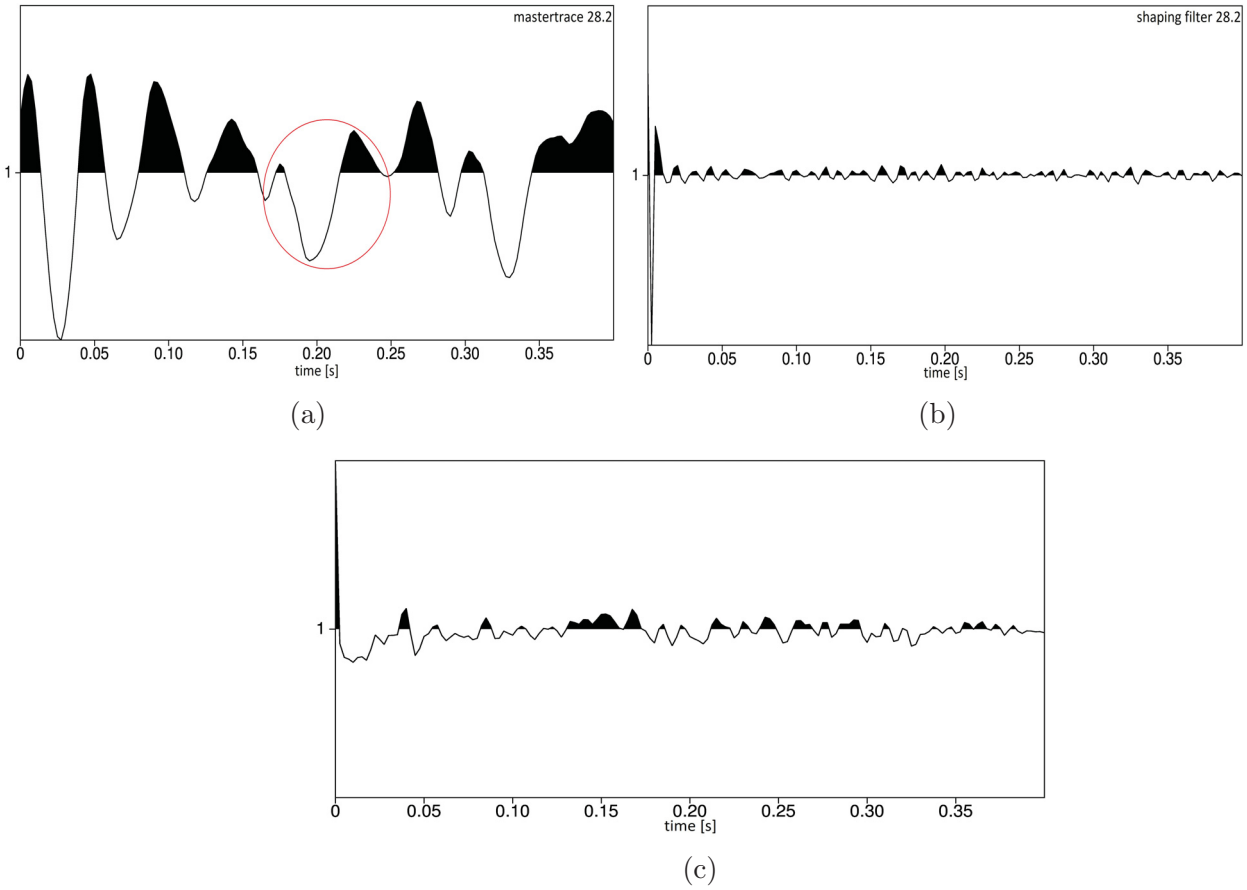

Figure 5.21: (a) Time corrected mastertrace 28.2 was convolved with (b) filter 28.2 to create (c) the deconvolved trace showing a zero-lag spike

5.3.1 Deconvolution of the entire section

For deconvolving the processed and time shifted section shaping filter 28.2 was used and for the unprocessed original section shaping filter 28.1 was considered. Figure 5.22 depicts the first output and it can be said that the energy is compressed at the beginning, but the band is not that significant as for SP 27 or SP 22. The second output (Fig 5.23) is already low-pass filtered and frequencies above 40 Hz are excluded, based on the amplitude spectrum of the stacked section shown in appendix C. The final output does not show the smallest hint for a S-wave, although a filter was applied and a cut-off frequency of 40 Hz was considered to produce the best result. The result does not show a S-wave which could be due to the geological conditions in this area.

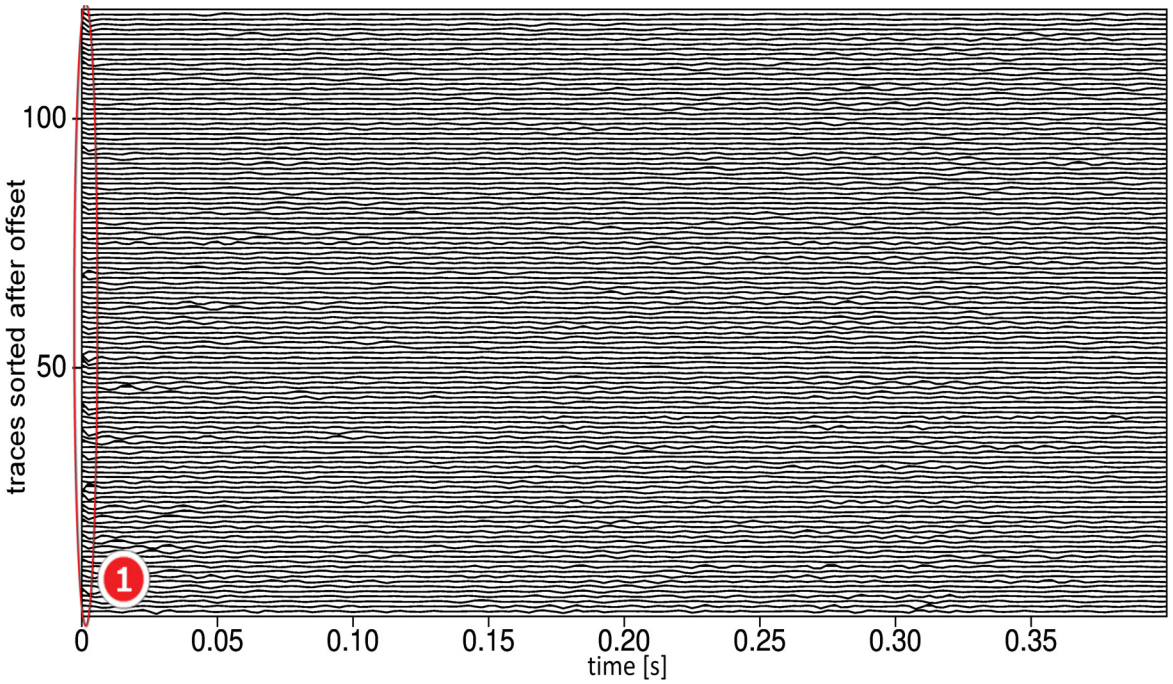

Figure 5.22: Deconvolved section where traveltimes have been corrected first and then a time shift of 15 ms have been performed, showing first 400 ms

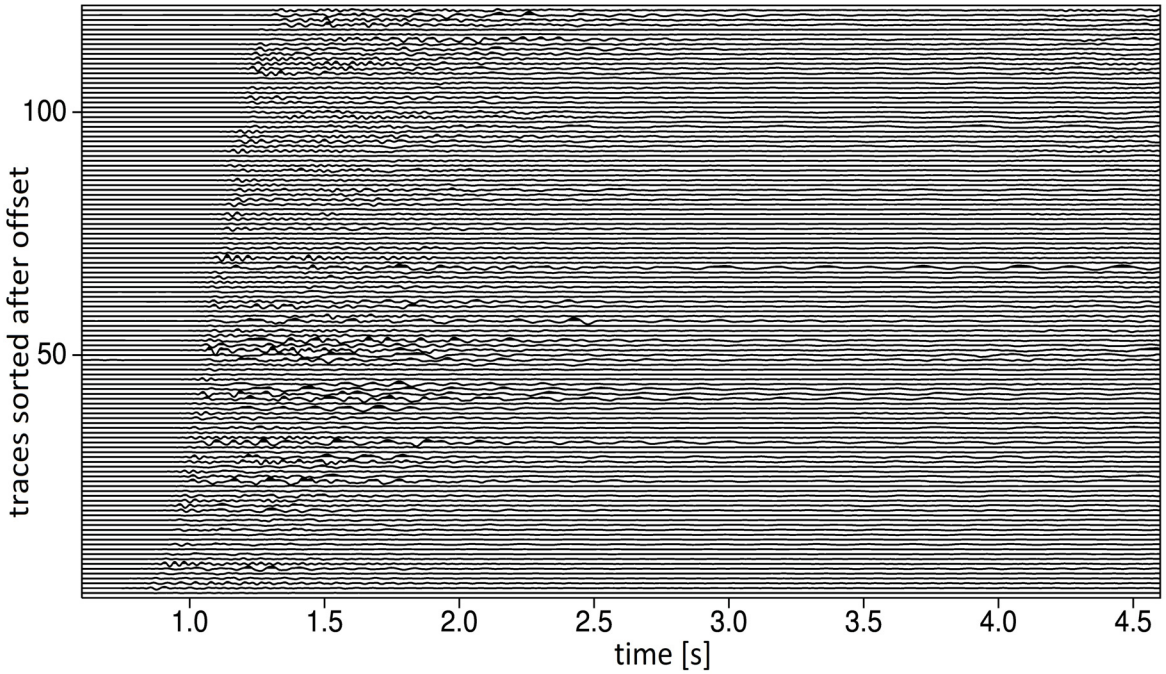

Figure 5.23: Deconvolved original section where a low-pass filter is used to remove high frequency signals

5.4 QC of the results

The goal to compress the various amount of shot signals to one could be using the Wiener Shaping Filter method. At the end results were obtained, where a zero-lag spike with some sidelobes were produced and to some point the shaping filter worked on the whole section as well. Deconvolving finally the original section, where no pseudo LMO or traveltime correction has been performed, leads to an output shown for example in Figure 5.19, which would be the result of SP 27. The section is already low-pass filtered as well and for this SP the S-wave signals could be found. Both, S- and P-wave, are highlighted in blue and red and in the red box, on the right handside, they can be even better identified.

In the case of SP 22 the S-wave could only be assumed. There is a slightly black stripe at the beginning of the traces indicating the P-wave (Fig 5.14). Signals which can be thought to be S-wave signals are again highlighted in blue, but they can not be traced further then shown in the figure and they are probably too weak. Since one also does not see any onset at t=0 s, the assumption of the S-wave is very vague and further investigations would have to be carried out to determine the trend of the S-wave really clearly. Therefore no final conclusion is drawn.

Finding the S-wave in any of the other datasets was not possible, although the same processing methods were performed. The S-Waves are probably too weak in this seismic sections because of the hard rocks in this area or further processing methods have to be carried out to emphasise the S-waves in these seismograms as well.

Chapter 6

Determining the source wavelet of one single shot

6.1 Theoretical background and synthetic data

For further modelling reasons the wavelet shape, when firing only a single borehole, should be established. Therefore a deconvolution in time domain has to be performed, which correspond to a division of the amplitude spectra in frequency domain. To stabilise the results the water-level deconvolution should be considered, whereby gaps in the amplitude spectrum of the deconvolved output are filled to a small level w:

$$h(t) *^{-1} f(t) = g(t) \quad \overrightarrow{FT} \quad \frac{H(w)F^*(w)}{max[F(w)F^*(w), w]} = G_w(w) \tag{6.1}$$

where

$h(t, w)$ = recorded signal

$f(t, w)$ = source signal

$g(t, w)$ = impulse response

So far, the Wiener shaping filter was used to remove the source signal and compress the impulse responses to a spike. Now the source wants to be known and the spikes should be removed from the wavelet indicating the various amounts of shots, which is shown with equation 6.2.

$$h(t) *^{-1} g(t) = f(t) \quad \overrightarrow{FT} \quad \frac{H(w)G^*(w)}{max[G(w)G^*(w), w]} = F_w(w) \tag{6.2}$$

where

$h(t, w)$ = mastertrace (in this case)

$f(t, w)$ = source signal

$g(t, w)$ = impulse response (spike series of 11 shots)

Normally a Fourier transformation of the time domain data would be performed to fulfil a division of the amplitude spectra. SU, however, provides a command called *sucddecon*, with which it is possible to perform a complex division in the frequency domain although the input is in time domain. As input the stacked mastertrace h(t) and an impulse response sequence g(t), simulating the 11 shots (considering SP 22), are required. The inputs are transformed to frequency domain to compute the output and the output is then backtransformed to time domain. The routine is demonstrated with equation 6.3. To stabilise the output a white noise factor is added, which is the same principal as described above with the water level. The standard white noise factor (pnoise) value is 0.001 but it can be further increased (see *Stockwell J. (2008) Complete Listing of CWP Free Program Self-Documentations*).

$$\frac{H(w) * \quad complex \quad conjugate[G(w)]}{|G(w)|^2 + (pnoise * mean \quad of \quad G(w) \quad power \quad spectrum} = F(w) \quad \overrightarrow{FT} \quad f(t) \qquad (6.3)$$

where

$h(t, w)$ = mastertrace (in this case)

$f(t, w)$ = source signal

$g(t, w)$ = impulse response (spike series of 11 shots)

The procedure is shown with synthetic data first, whereby a synthetic generated 11-shot sequence (Fig 6.1a) is convolved with source wavelet 3 (Fig 6.1b) to generate a wavelet containing 11 signals (Fig 6.1c). As described beforehand the wavelet and the impulse series are used as input to deconvolve the wavelet and obtain the source signal. The output is shown in Figure 6.2 and it is marked with number 3 because the original used wavelet was minimum-phase wavelet 3. The output indicates an anticausal and causal part, but the energy is concentrated in the center of the trace and the wavelet is exactly reproduced, comparing the red highlighted box with Figure 6.1b.

In the case of the real data the exact sequence of the shots is unknown, therefore different spike sequences were generated to test which one would fit best. The four, in my opinion, most likely are shown in Figure 6.3. Beside the synthetic impulse series *a* three others were created, designated *b*, *c* and *d*. The spacing between each impulse is based on real mastertrace 22.1. For impulse series *a* the times of the onsetting of each lobe were measured and for *b* the impulses were shifted in milliseconds range to test the impact on the output. For impulse series *c* and *d* the times of the maximum of each lobe were measured and for *d* the first spike was shifted to $t = 0.01$ s. The height of each spike fits also to the height of the lobes of mastertrace 22.1. This impulse series are tested in the next section with the real data, using mastertrace 22.1.

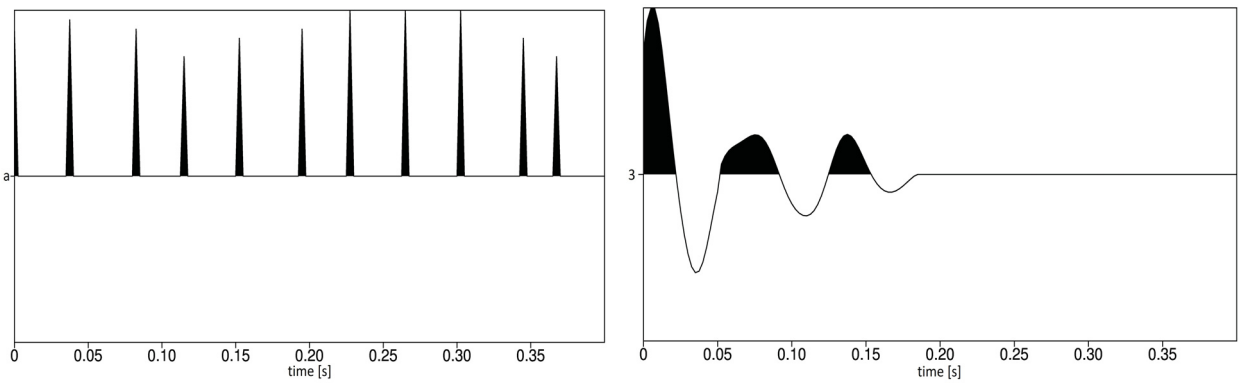

(a)

(b)

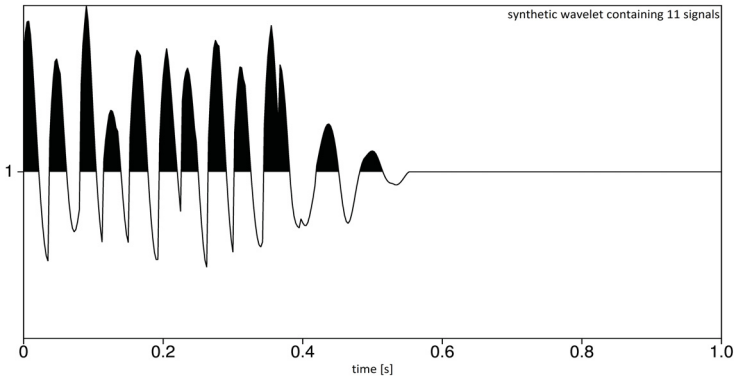

(c)

Figure 6.1: (a) Synthetic generated impulse series a was convolved with (b) minimum-phase wavelet 3 to produce (c) synthetic wavelet which contains the signals from 11 detonations

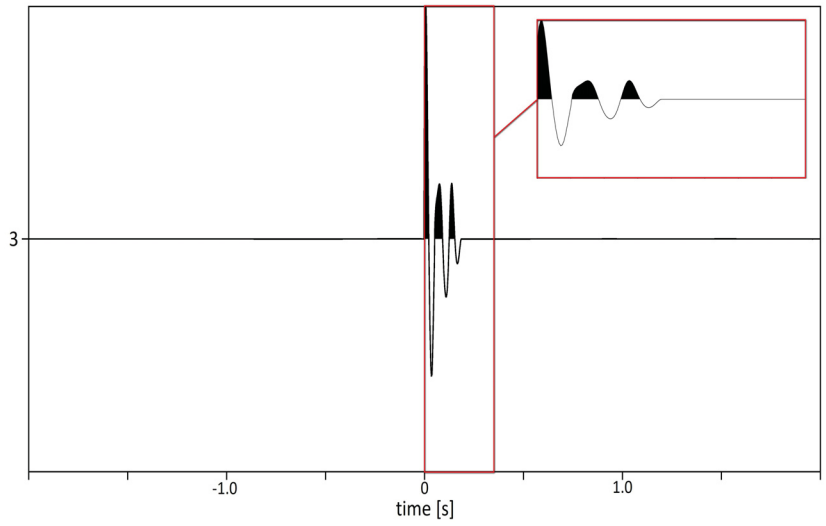

Figure 6.2: Output from the deconvolution of the synthetic mastertrace

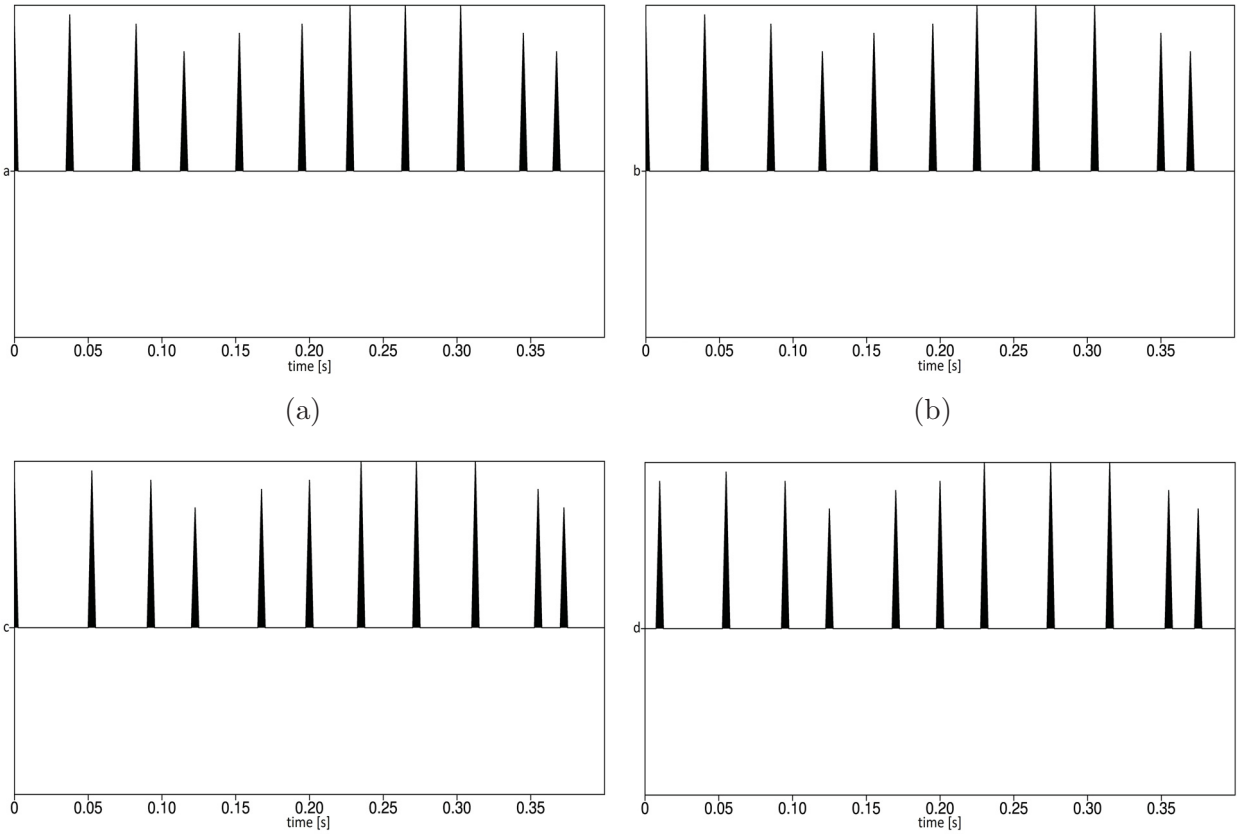

(a) (b)

(c) (d)

Figure 6.3: 5 impulse series responses showing different spacings

6.2 Deconvolving the wavelet of SP 22

For SP 22, mastertrace 22.1 (Fig 6.4a) was deconvolved with impulse series a (Fig 6.4b) to produce a wavelet representing the signal from one shot (Fig 6.4c). The supposed source signal of one single shot now shows an extremely long signal, with a lot of noise and artefacts in the anticausal part. There is a narrow, high-amplitude onset at t=0 s, which indicates the form of a minimum-phase wavelet, but the signals present along the whole trace are erroneous. The output gets a little bit smoother when increasing the amount of the white noise factor. Therefore different values are tested and finally 0.5 is chosen, because beyond this value the output did not change much anymore. The anticausal part now indicates less noise signals (Fig 6.4d), but the shape of the source wavelet can not be seen either. Comparing the synthetic wavelet output with the real one, the length of the source wavelet can be approximated. In the synthetics the wavelet is made up of three lobes, which last for ∼0.2 s (Fig 6.2), but the reverberations, which are visible in the real trace as low-frequent signals, are missing in the synthetics.

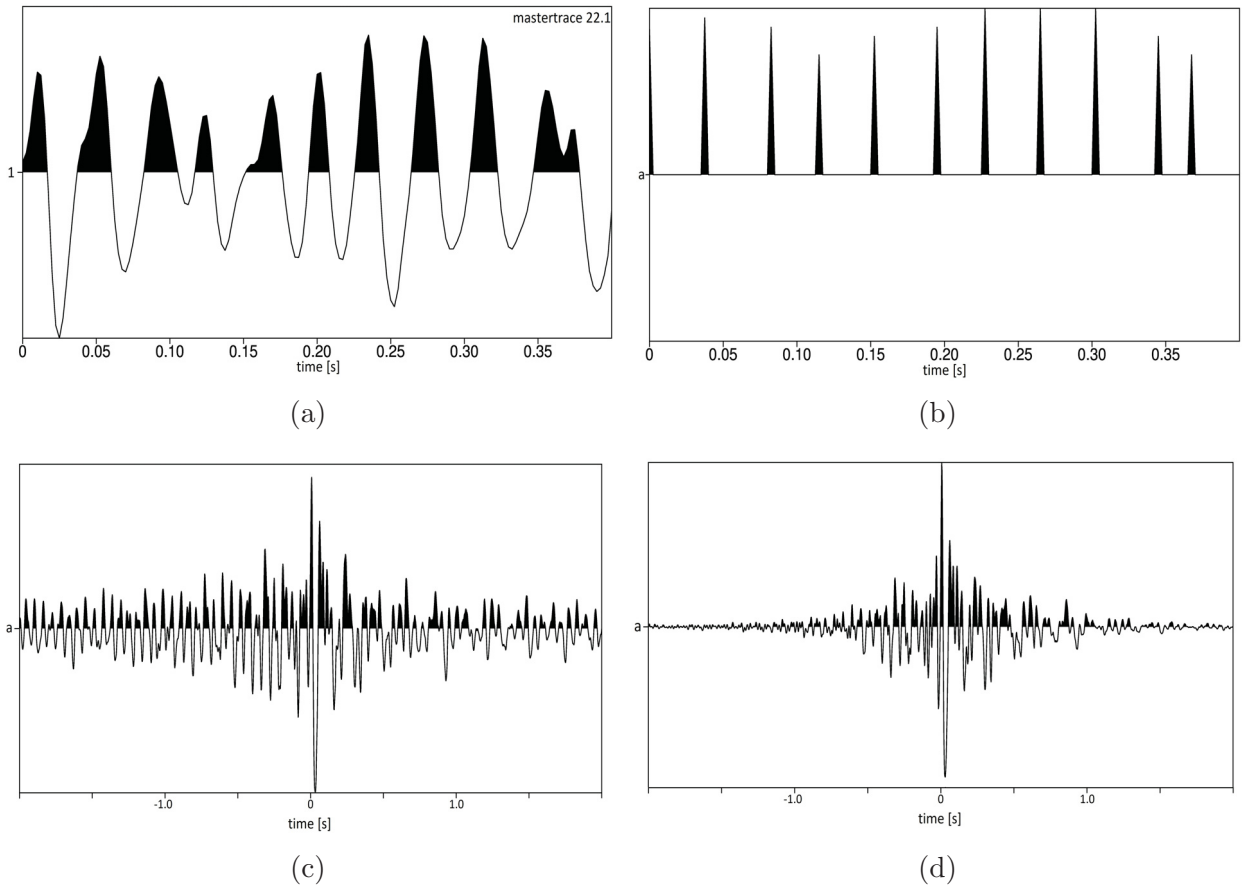

Figure 6.4: (a) Mastertrace 22.1 was deconvolved with (b) impulse response a to generate (c) the source signal representing one shot and (d) source signal when pnoise is increased

Nevertheless, it can be estimated that the length of the main wave-train amounts to +/-

400 ms in the case of the real output and there should be no signals in the anticausal part. Therefore the following figures are displaying the first 1000 ms of the deconvolved outputs to focus on this 400 ms. The results of a, b, c and d are shown in Figure 6.5, which were obtained using an increased pnoise value of 0.5.

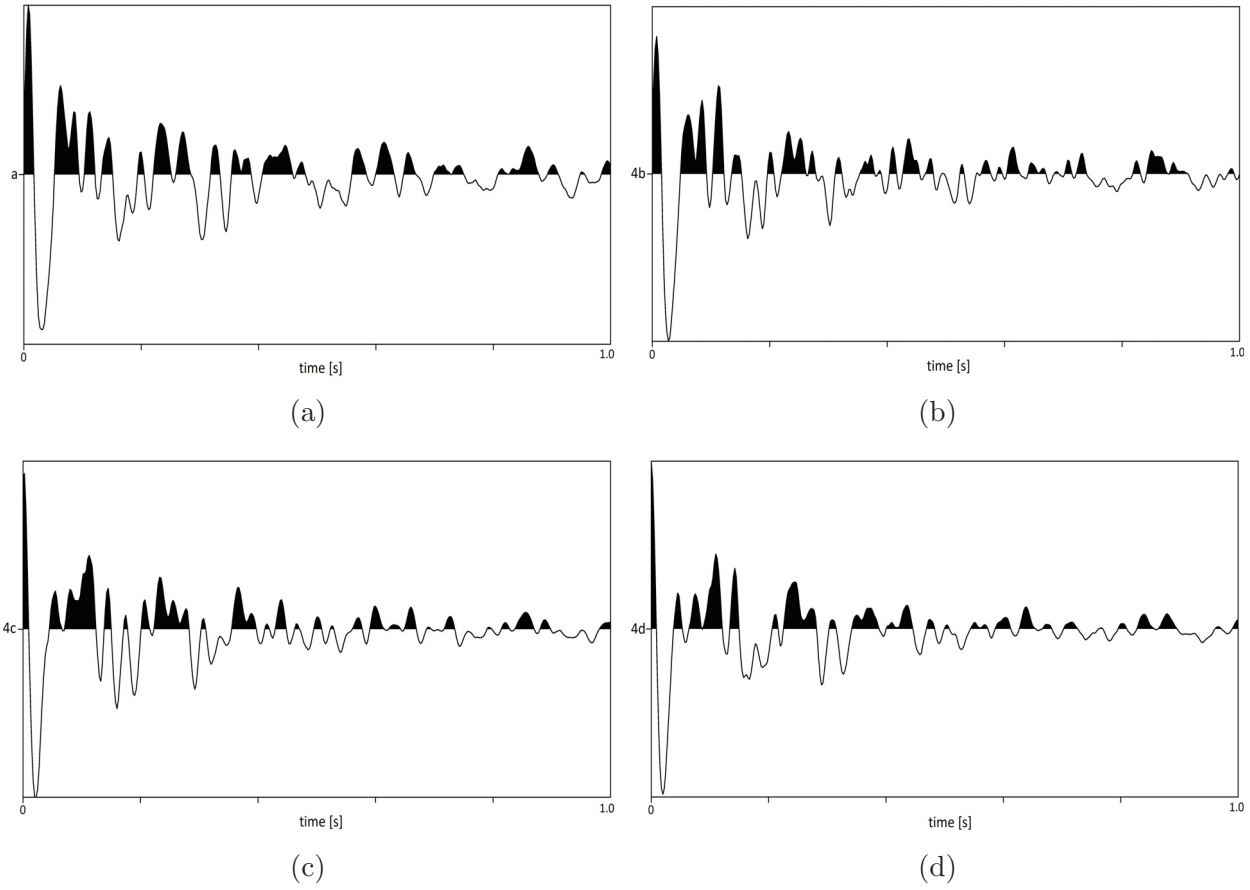

Figure 6.5: Real mastertrace was deconvolved using on the one hand (a) impulse response series a (b) impulse series b and on the other hand (c) impulse response series c and (d) d. Additionally an amount of 0.5 white noise factor was added

Impulse series b creates an output which can be compared to the one from a, but in a the amplitudes following after the main peaks are broader and the same shape is more or less repeated (Fig 6.5a and Fig 6.5b). With c and d, deconvolved outputs are created which show more narrow high-amplitude signals over the whole trace length, but looking at the first 1 s the main peak at the beginning is not so clearly visible (Fig 6.5c and 6.5d). All in all there is a slightly difference in the sidelobes in all four outputs, but the most striking ones are visible in the first $\sim$400 ms.

Since the deconvolution did not work so smoothly as for the synthetics, one can only look for the reason or reasons for failure. Several factors could play a role, but the most

important factor is the arrangement of the spike sequence in the first instance and the exact sequence is unknown. To prove where the artefacts may come from and why an exceptionally long signal is produced, the deconvolution is tested on the synthetic trace, but simulating the real situation and using a wrong impulse series this time.

Comparing wrong synthetic output with real output

The synthetic mastertrace shown in Figure 6.1c is deconvolved with impulse series b and c from Figure 6.3. The outputs are displayed in Figure 6.6.

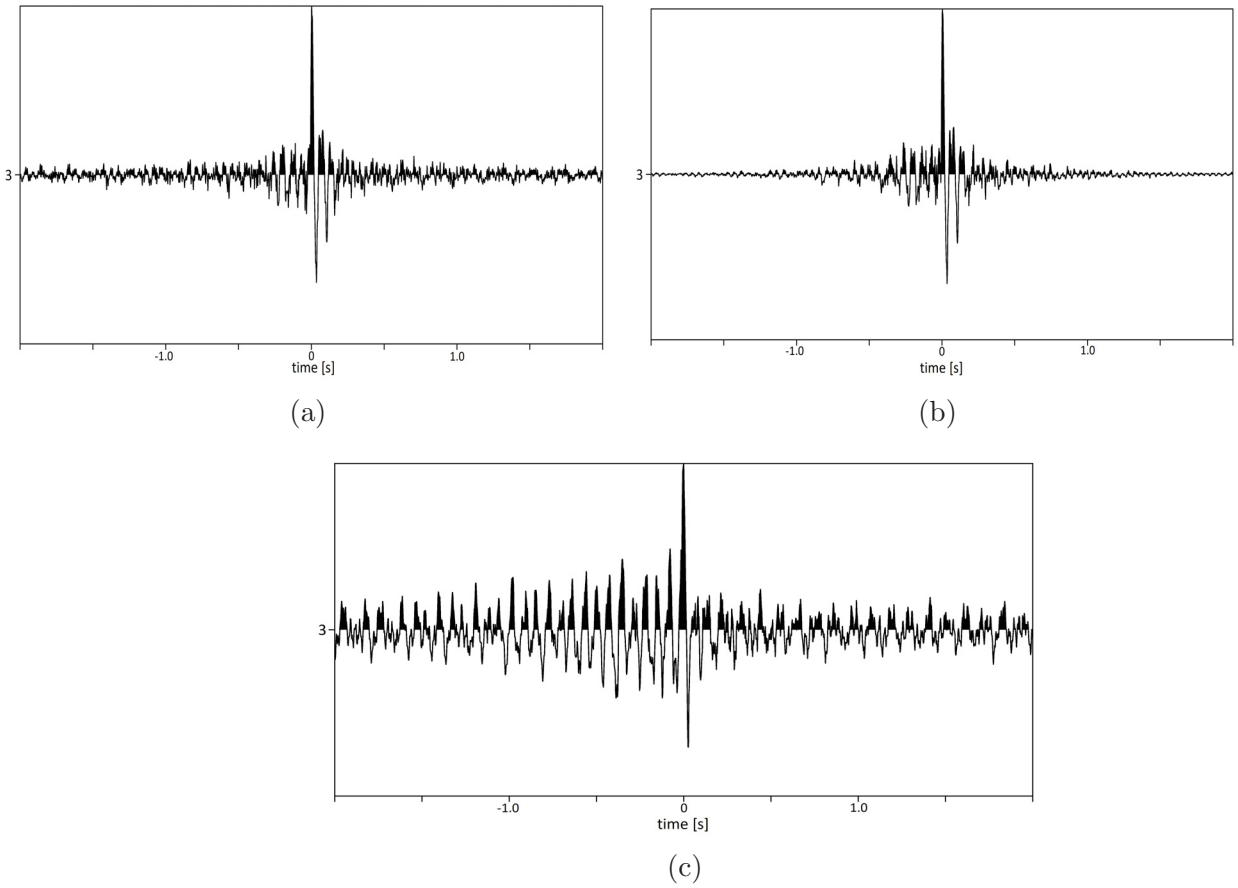

Figure 6.6: Synthetic mastertrace was deconvolved using on the one hand (a) impulse response series *b*, (b) add some pnoise amount of 0.5 and on the other hand (c) impulse response series *c*

The deconvolution with wrong impulse series shows the same artefacts now. Wrong signals in the anticausal part are produced as well. Deconvolving with impulse series *c* produces even more noise (Fig 6.6c) than using *b*. Impulse series *b* is pretty similar to *a*, which was used first, and therefore it looks smoother (Fig 6.6a). Using an increased pnoise value minimises the noise here too, but the source signal can not be identified neither (Fig 6.6b).

Comparing output of Figure 6.6b (considering only the first s) with the output of Figure 6.5a, the shape of the wavelet can be reconstructed in the case of the synthetic one, because the minimum-phase wavelet is already known (Fig 6.7b). Displaying the wrong output with the minimum-phase source wavelet in one figure shows that the real shape would be hard to recognise if the original shape would not be known, though. The two peaks which are following after the main peak are normally constituting the second lobe and the same can be recognised for the third lobe. The width is also not correctly.

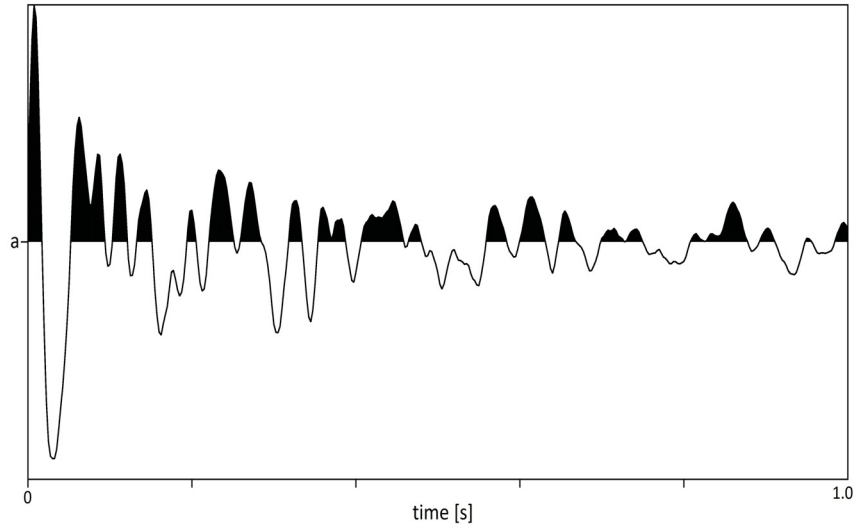

(a)

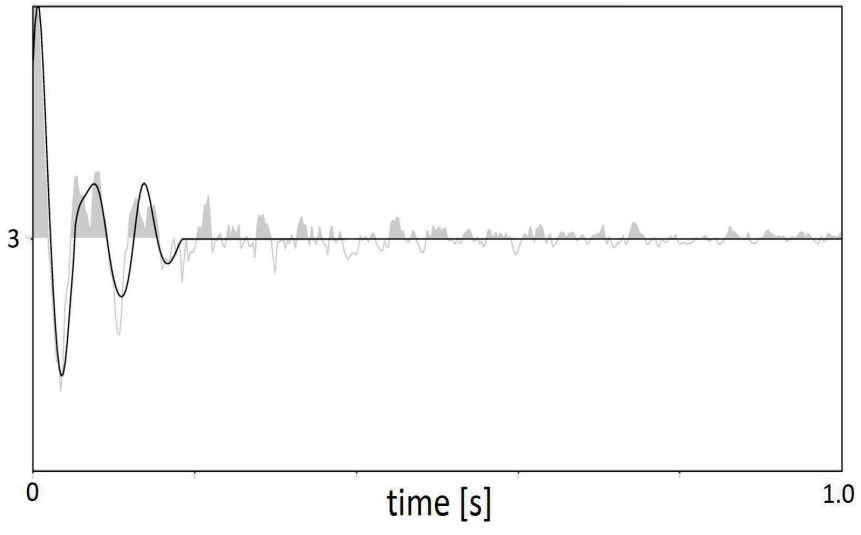

(b)

Figure 6.7: Deconvolved traces using (a) the real mastertrace 22 and deconvolve it with impulse series a and (b) the synthetic one which is deconvolved using spike series c (grey), whereby the original wavelet shape is drawn in black

Therefore the shape of the real deconvolved source (Fig 6.7a) is hardly to identify and it could only be assumed following the principal of reconstructing the synthetic minimum-phase source wavelet. After the first peak, which occurs at t=0 s in all four plots, the two adjacent peaks could be compressed to one positive lobe, two negative and positive lobes follow alternately and afterwards the two connected lobes could be combined to one negative lobe. The five low-amplitude lobes are finishing the wavelet and shortly after, it is getting more noisy. It could be imagined to look something like that, but that is only a probability. The width of the lobes is presumably also not correct.

6.3 QC of the results

Before finishing this chapter, an overview of the obtained results will be done. In first instance it has to be mentioned that the goal of deconvolving mastertrace 22.1 to obtain the source wavelet of one single shot could not be fulfilled. Performing a deconvolution of such complex data is complicated and more time would probably have to be invested to find the correct impulse series. Furthermore even if the correct sequence is known, it could be that each source signal is different, because of the various amounts of explosives used for the detonations. This would impede deconvolution even more. The source wavelet could only be approximated to last for ∼400 ms, because the first 0.4 s in all four results look similar in some ways. The shape could of course vary in multiple ways, because through deconvolving with a wrong impulse series it is distorted and more low frequency signals are preserved. The wrong synthetic source wavelet can be easily related to the original source wavelet, because the latter is known. In my case the real source wavelet shape is not known in the slightest and therefore no further conclusions can be drawn from the results.

Chapter 7

Conclusion and outlook

7.1 Conclusion

In this thesis, different deconvolution methods were tested to deconvolve seismic sections, which contain signals from production shots performed in the Mt. Erzberg mine. As already discussed in sections 3.3 through 3.5, ProMAX was tested using synthetic data, but the results were not that satisfying that is why the focus moved to the Wiener Shaping Filter method in Seismic Unix.
According to the outcome obtained with the Wiener Shaping Filter method, it can be said that generally encouraging results were achieved. Even if the goals could only be partially fulfilled, it was proved that the methods on the synthetic data work perfectly, but that there is still some potential for improvement on the real data. There are several factors which influence the real data and for fulfilling a properly deconvolution more technical constraints would certainly be a step forward. In the case of deconvolving the stacked mastertraces the amount of boreholes were influencing the output much, because the deconvolution worked best on data from SP 27, where only five shot signals were recorded. When deconvolving the whole original seismic section geology influences the presence of S-wave signals, as results from SP 28 showed. The result of the deconvolved mastertrace of SP 28 is even better than the one from SP 22, but in the final result of the deconvolved seismic section there is no hint for a S-wave signal.
Moreover, deconvolving the mastertrace to receive a source signal could not work properly, perhaps because the exact delay time between each detonation is unknown and the exact impulse sequence plays a major role when using it as input parameter. Furthermore even when the exact impulse series is known it seems that the source wavelet is not equal for each shot as the amount of explosives vary strongly. These factors would make the deconvolution much more complicated again. It can be said that, if the exact firing sequence would have been known and more data concerning the amount of explosives for each drillhole would have been available, performing a deconvolution would be more successful.

7.2 Outlook

Deconvolving data recorded through production blasts is a topic which can be expanded and experiments could still be carried out.
All of this mentioned above points to the fact that for further tests in future less detonations should be performed and more details concerning detonation parameters would be beneficial. For finding the source wavelet of one single shot, a test shot, comprising only one borehole, could be performed whereby the delay time between each detonation would be triggered precisely. Furthermore the results of the near-field vibration investigations of single blasts could be considered.
Another idea for finding the real impulse sequence could be building an algorithm in form of Marcov-chains to test various sequences of impulse responses. As seen in section 6.2 every millisecond shift can improve or degrade the results. Therefore different possibilities could be tried out and if the best possibility is found, it could be definitely said whether the source signals vary strongly among each other.

Bibliography

[Claerbout, 1985] Claerbout, J. F. (1985). *Fundamentals of geophysical data processing*. McGraw-Hill Book Co. 6

[Fuchs and Mueller, 1971] Fuchs, K. and Mueller, G. (1971). Computation of synthetic seismograms with reflectivity method and comparison with observations. *Geophys. J. R. astr. SOC.* 14

[John W. Stockwell and Cohen, 2008] John W. Stockwell, J. and Cohen, J. K. (2008). The new su users manual. *Colorado School of mines*. 11

[Kuepper, 1958] Kuepper, F. J. (1958). Theoretische untersuchung ueber die mehrfachaufstellung von geophonen. *Geophysical Prospection*. 14

[Mueller, 1970] Mueller, G. (1970). Exact ray theory and its application to reflection of elastic waves from vertically inhomogeneous media. *Geophys. J. R. astr. SOC.* 14

[Robinson, 1966] Robinson, E. A. (1966). Multichannel z-transforms and minimum delay. *Geophysics*. 13

[Robinson and Treitel, 1980] Robinson, E. A. and Treitel, S. (1980). *Geophysical signal analysis*. Prentice-Hall Book Co. 7

[Sunjay, 2010] Sunjay (2010). Wavelet transforms: Time-frequency presentation. *Geo Canada*. 13

[Yilmaz, 1987] Yilmaz, O. (1987). *Seismic data analysis: processing, inversion and interpretation of seismic data (Volume 1)*. Investigations in Geophysics. Society of Exploration Geophysicists. 3, 4, 5, 6, 8, 9, 10, 12, 13, 18

Appendix A

Workflow of synthetic data generation

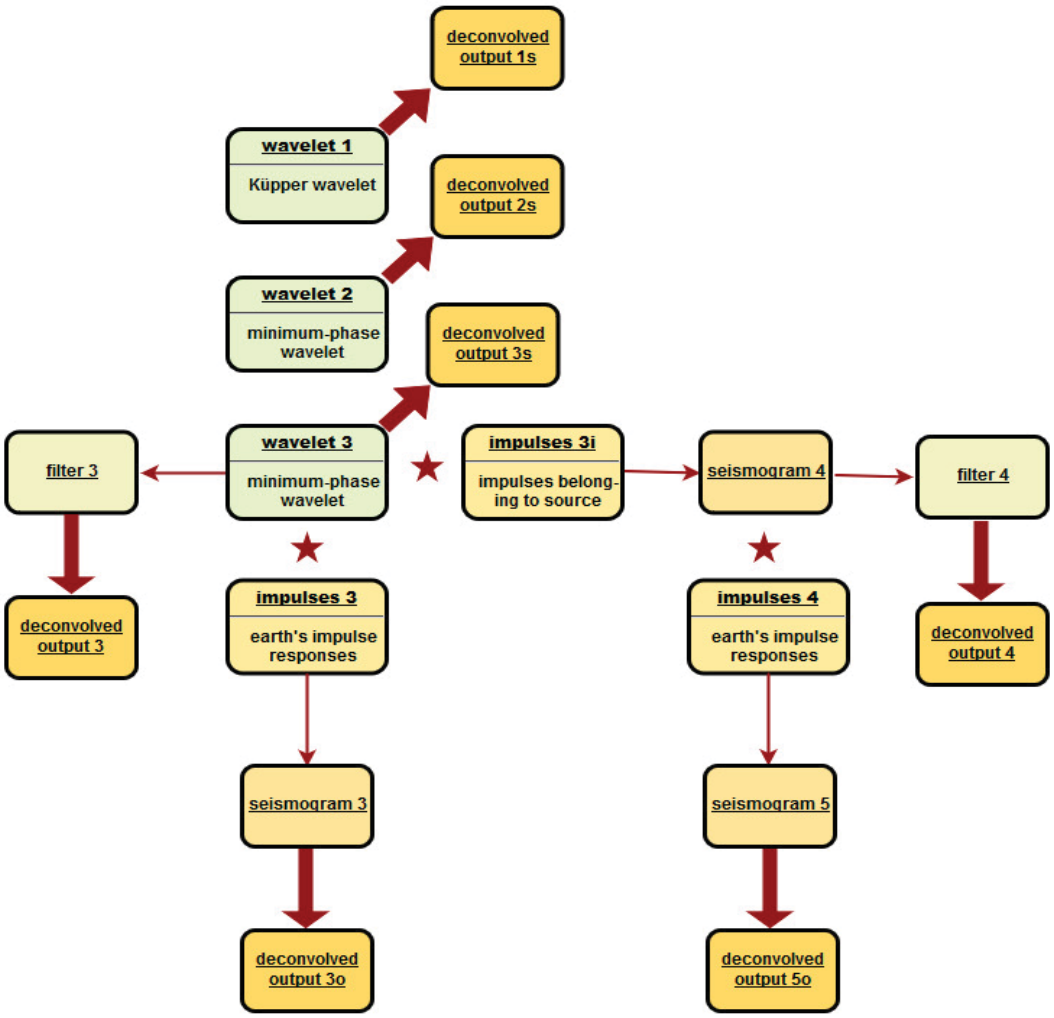

Appendix B

Shotlist

Productionshots					
Name	Amount of boreholes	Rows	Distance [m]	Amount of explosives [kg]	Delay time [ms]
SP 22: SYBO298	11	1	6	4430	33
SP 23: SCHI38H	18	1	6	5150	42
SP 24: ETM3374	16	2	6	6265	33
SP 25: WEGS523	28	2	6	6930	42
SP 26: SCHI453	19	1	6	6450	42
SP 27: ETM3371	5	1	6	2085	33
SP 28: PALM385	9	1	6	4200	42
SP 29: JUDA472	18	3	6	2280	42
SP 30: ETM530	17	1	6	4925	33
SP 31: SYBO297	12	1	6	4535	33
Seismicshots					
Name	Amount of boreholes	Rows	Distance [m]	Amount of explosives [kg]	Delay time [ms]
SP 1 - 21	3 to 5 (depending on underground)	no rows, various arrangement but close together	neglectable	2.3	0

Appendix C

Amplitude spectra of

Shotpoint 22

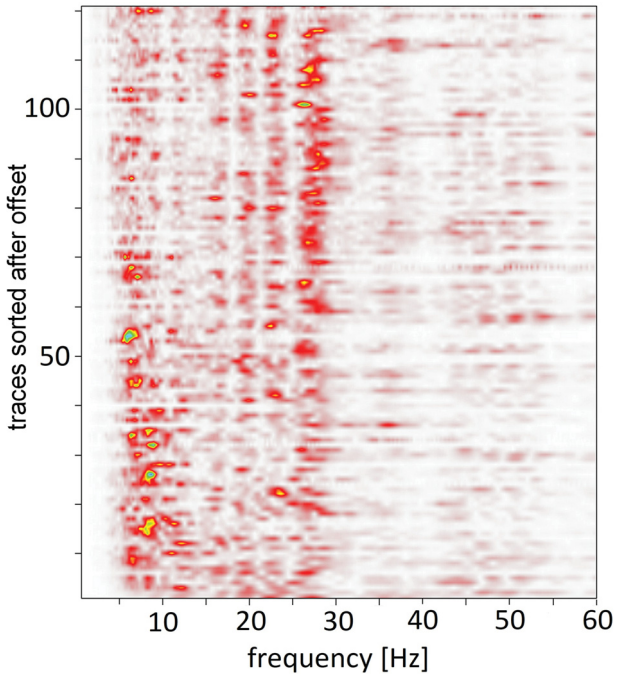

(a)

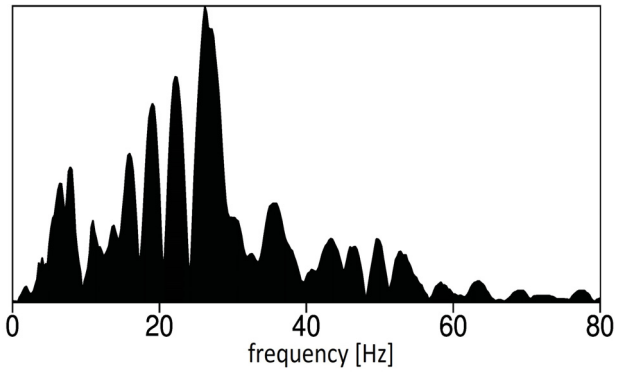

(b)

Figure C.1: (a) Amplitude spectrum of whole section and (b) amplitude spectrum of stacked mastertrace 22

Shotpoint 27

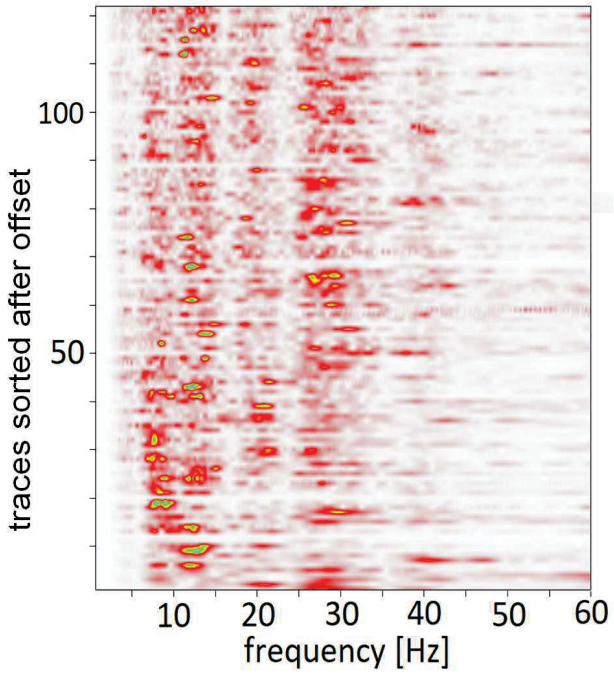

(a)

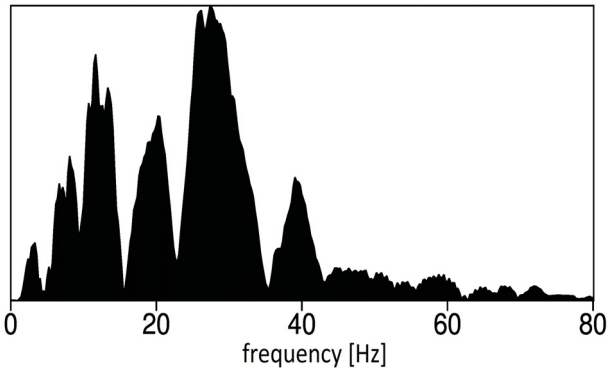

(b)

Figure C.2: (a) Amplitude spectrum of whole section and (b) amplitude spectrum of stacked mastertrace 27

Shotpoint 28

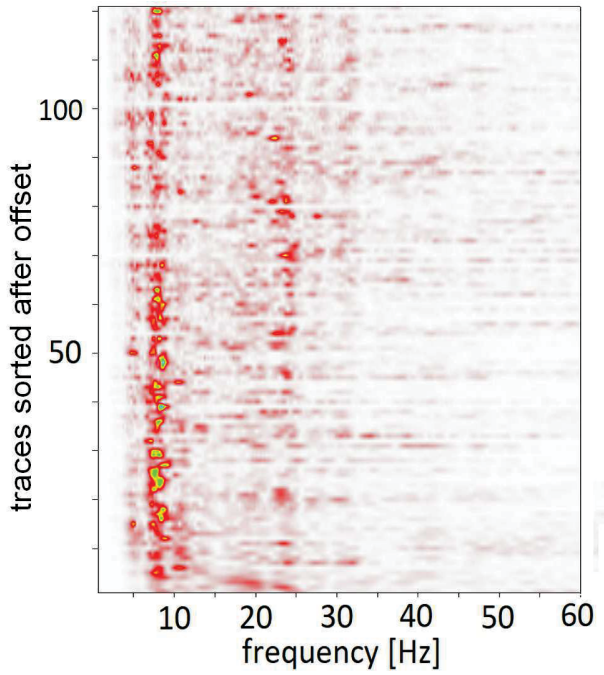

(a)

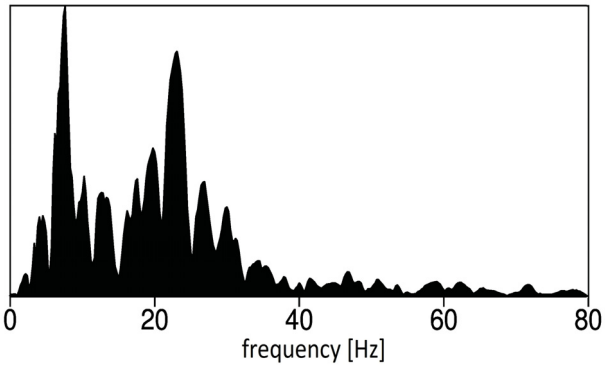

(b)

Figure C.3: (a) Amplitude spectrum of whole section and (b) amplitude spectrum of stacked mastertrace 28

Appendix D

Results of all shotpoints

Shotpoint 22

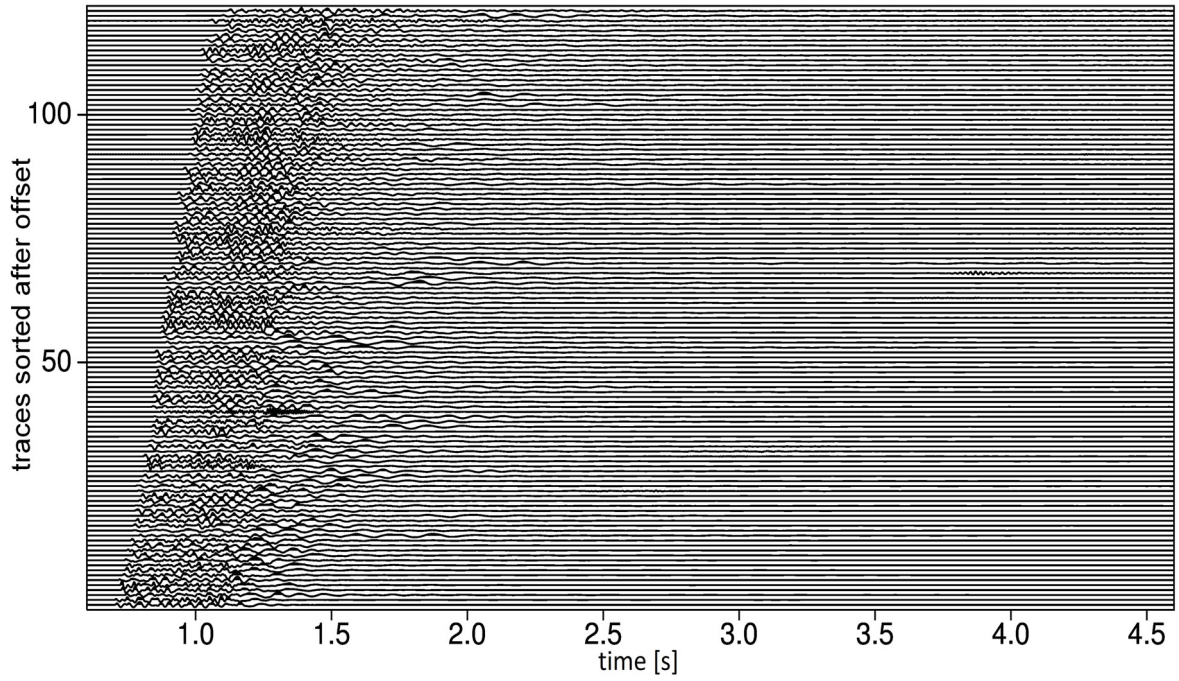

Figure D.1: Original seismogram (vertical component)

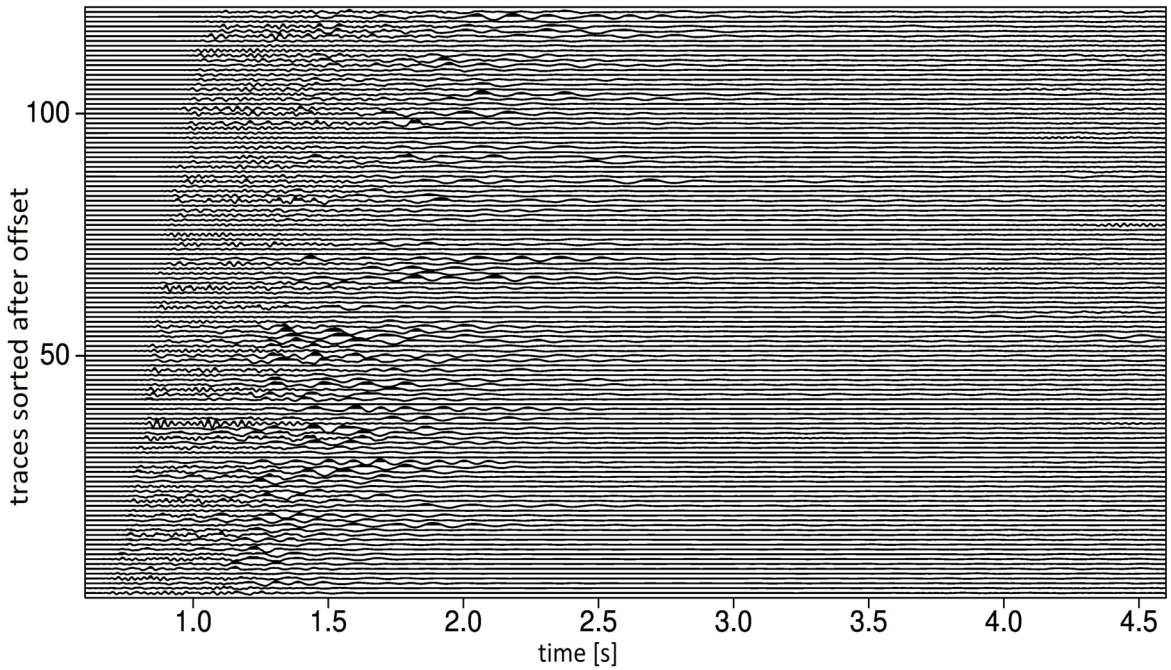

Figure D.2: Deconvolved original section where a low-pass filter is used to remove high-frequency signals

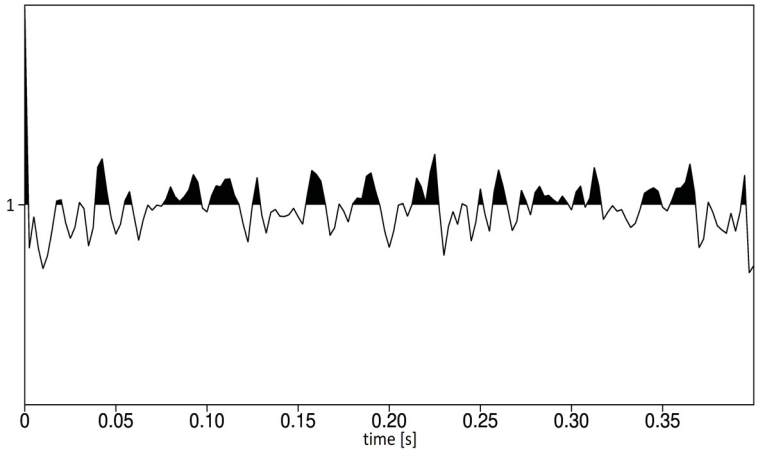

Figure D.3: Deconvolved mastertrace

Shotpoint 23

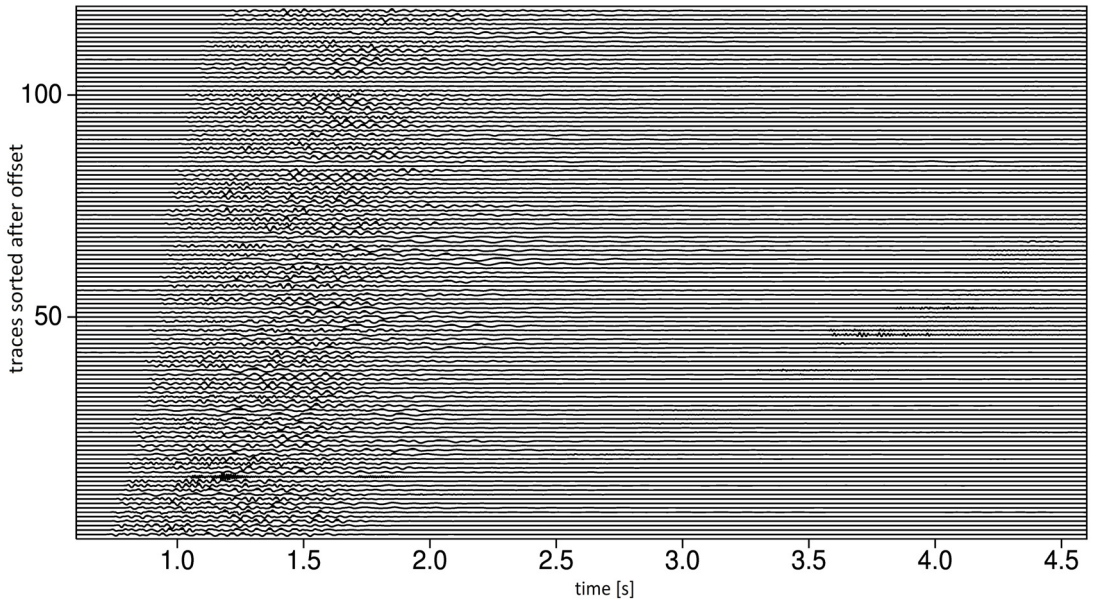

Figure D.4: Original seismogram (vertical component)

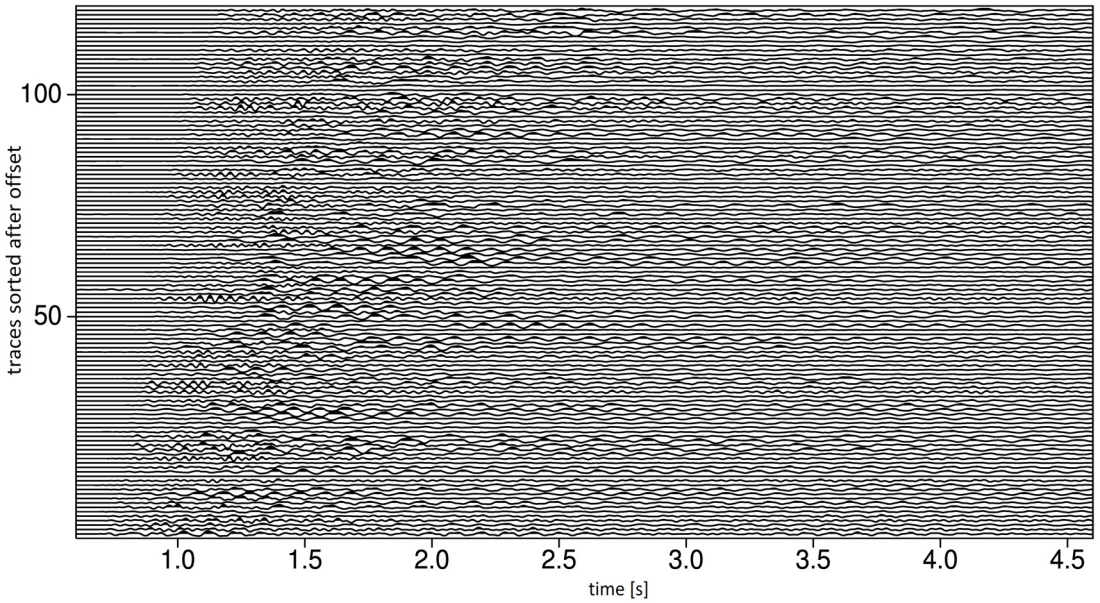

Figure D.5: Deconvolved original section where a low-pass filter is used to remove high-frequency signals

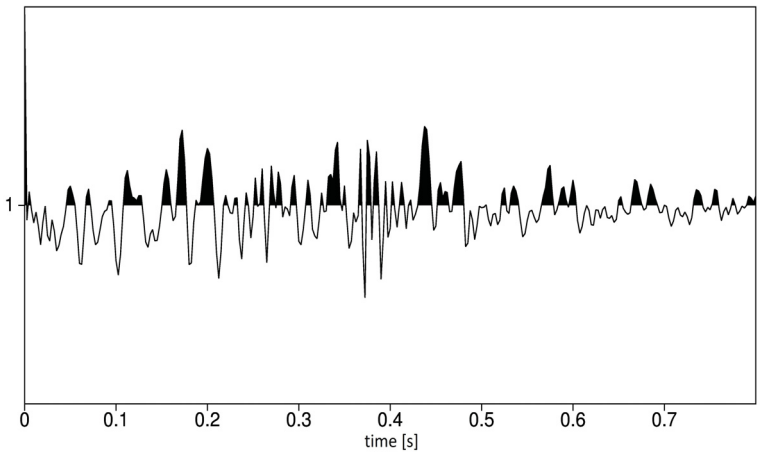

Figure D.6: Deconvolved mastertrace

Shotpoint 24

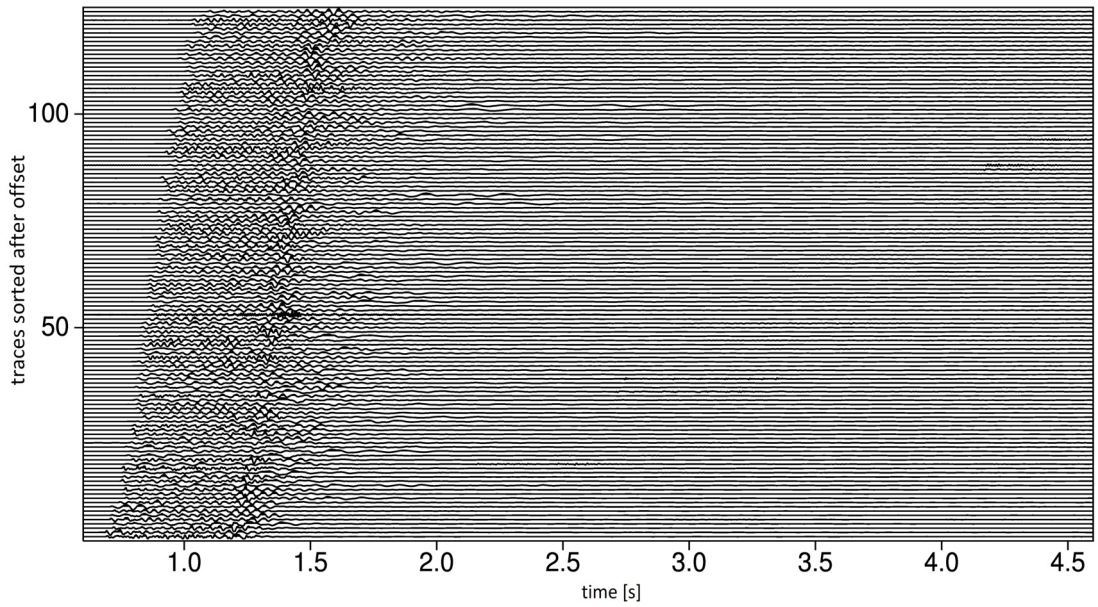

Figure D.7: Original seismogram (vertical component)

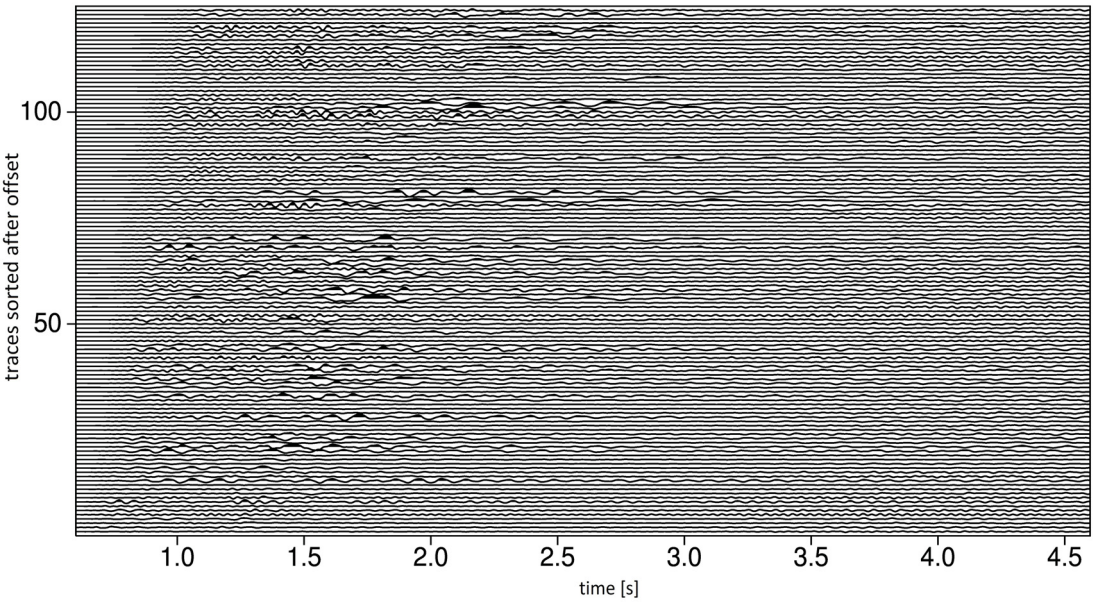

Figure D.8: Deconvolved original section where a low-pass filter is used to remove high-frequency signals

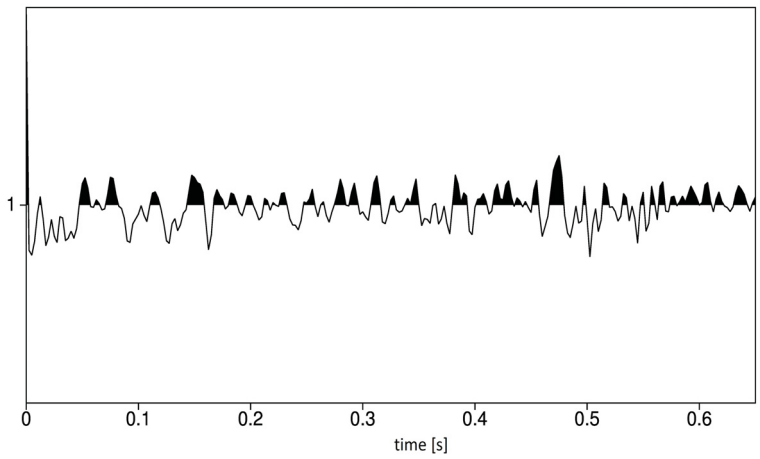

Figure D.9: Deconvolved mastertrace

Shotpoint 25

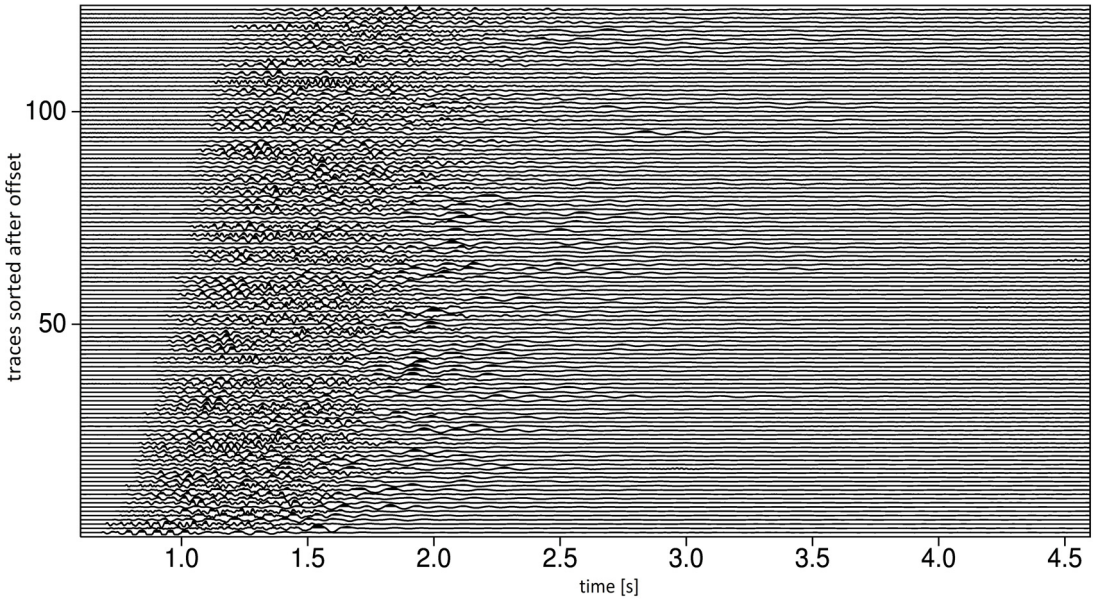

Figure D.10: Original seismogram (vertical component)

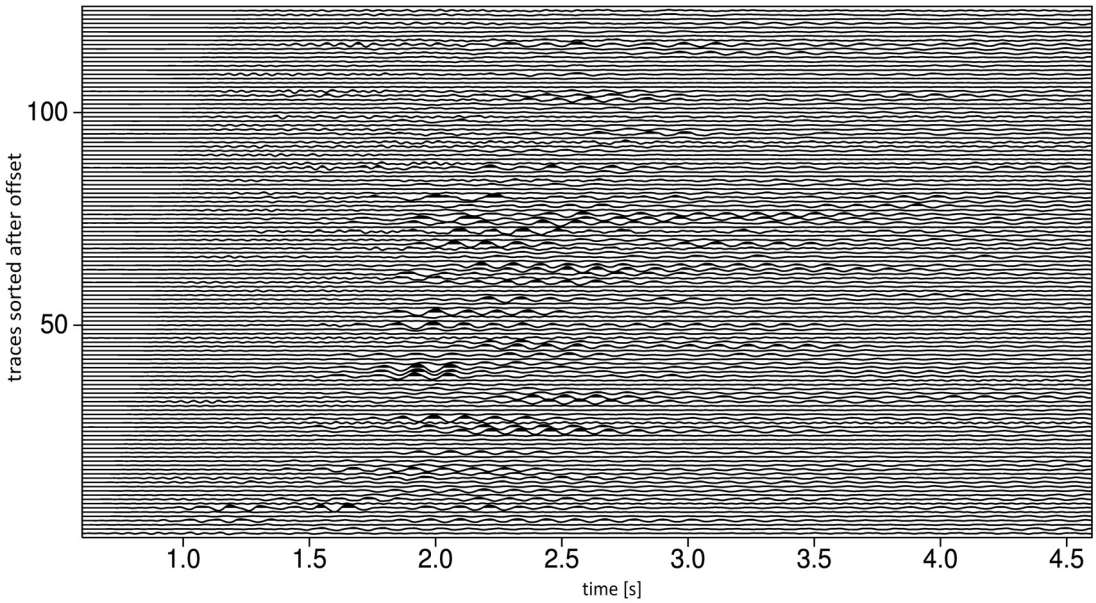

Figure D.11: Deconvolved original section where a low-pass filter is used to remove high-frequency signals

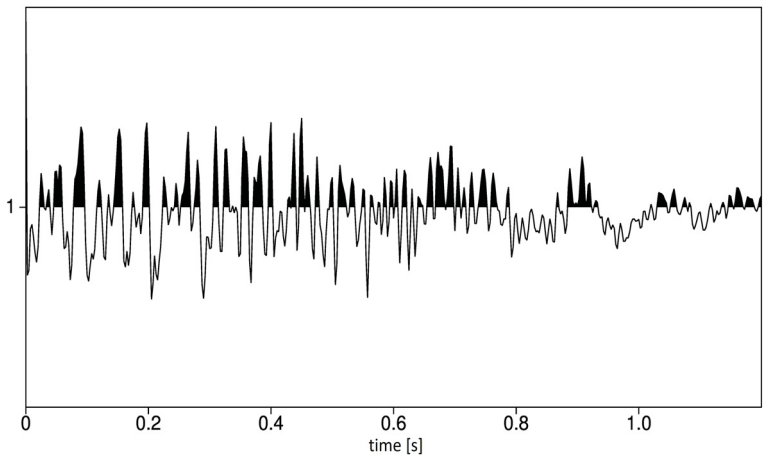

Figure D.12: Deconvolved mastertrace

Shotpoint 26

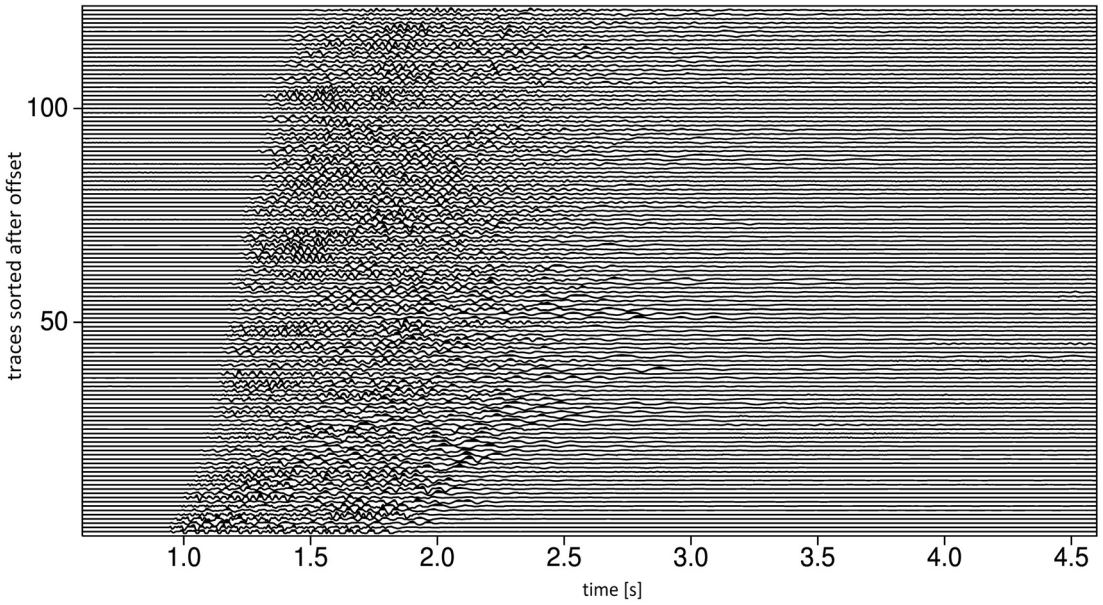

Figure D.13: Original seismogram (vertical component)

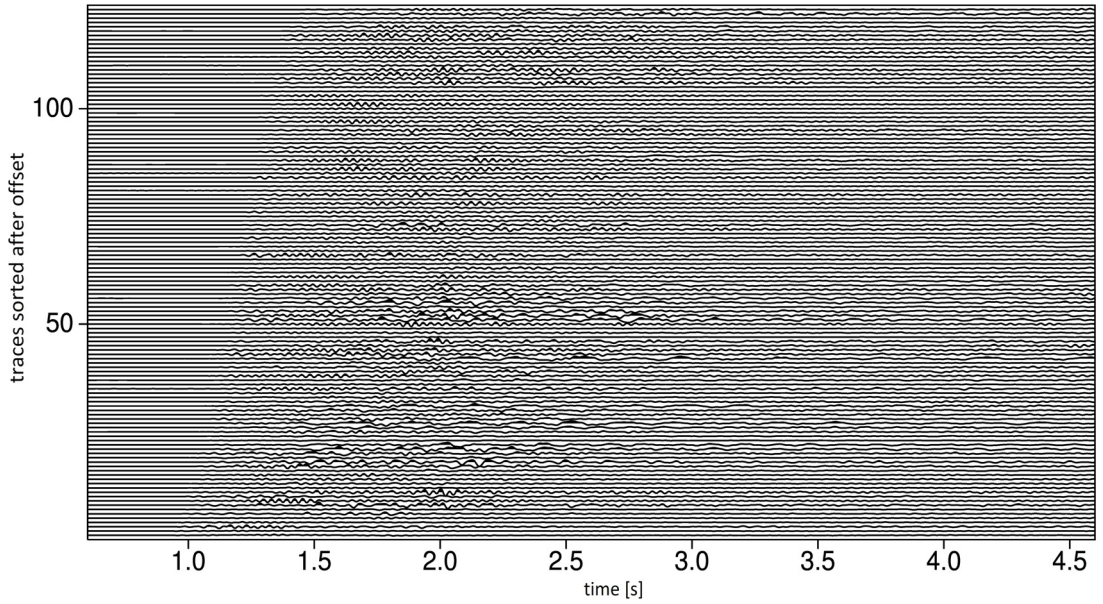

Figure D.14: Deconvolved original section where a low-pass filter is used to remove high-frequency signals

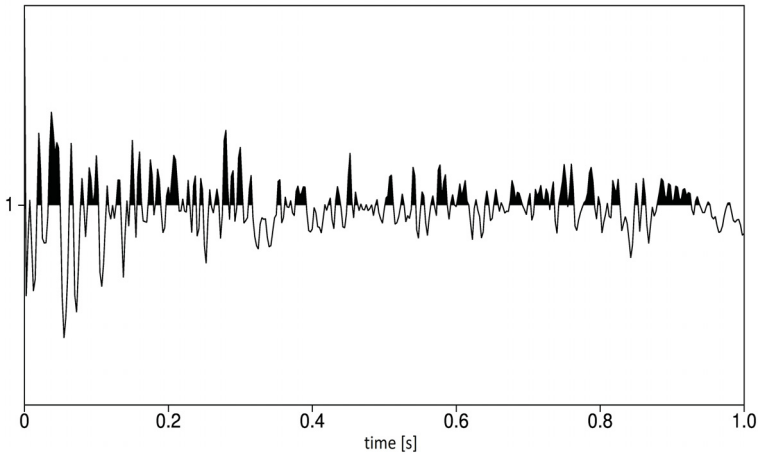

Figure D.15: Deconvolved mastertrace

Shotpoint 27

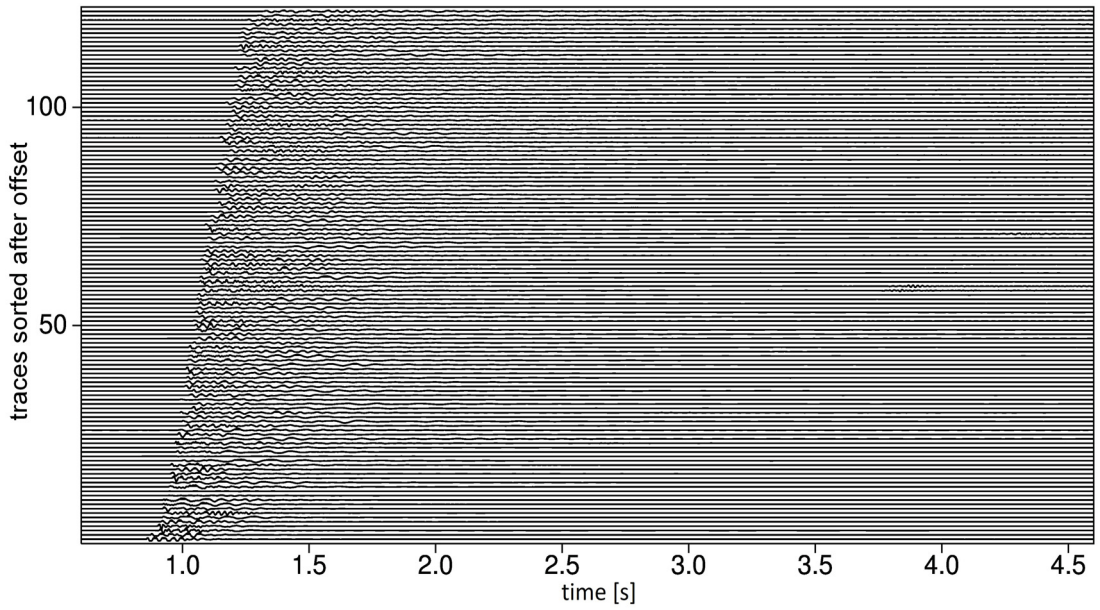

Figure D.16: Original seismogram (vertical component)

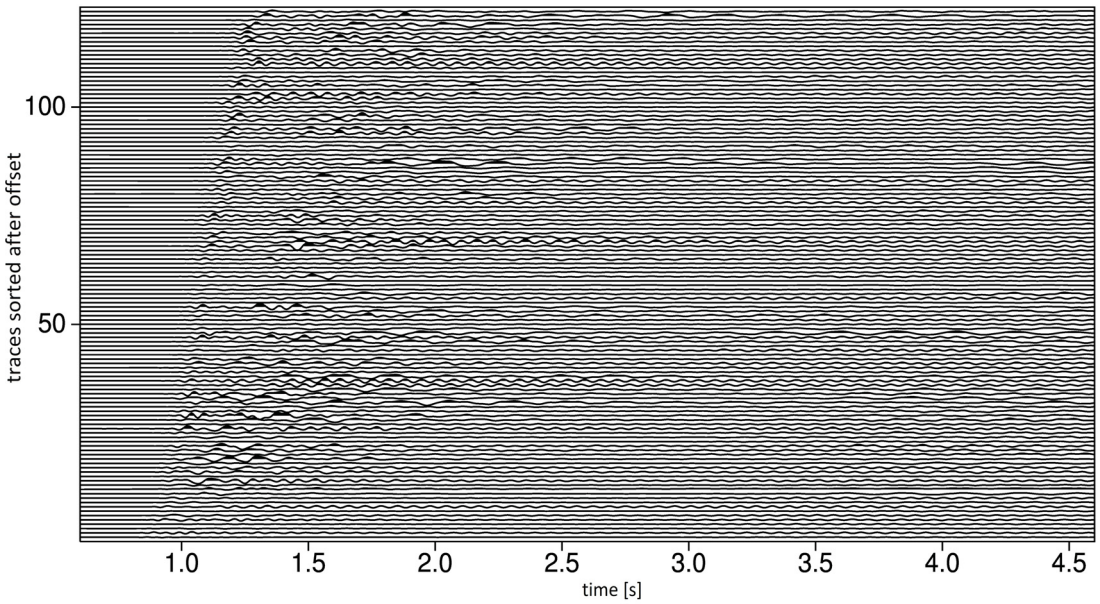

Figure D.17: Deconvolved original section where a low-pass filter is used to remove high-frequency signals

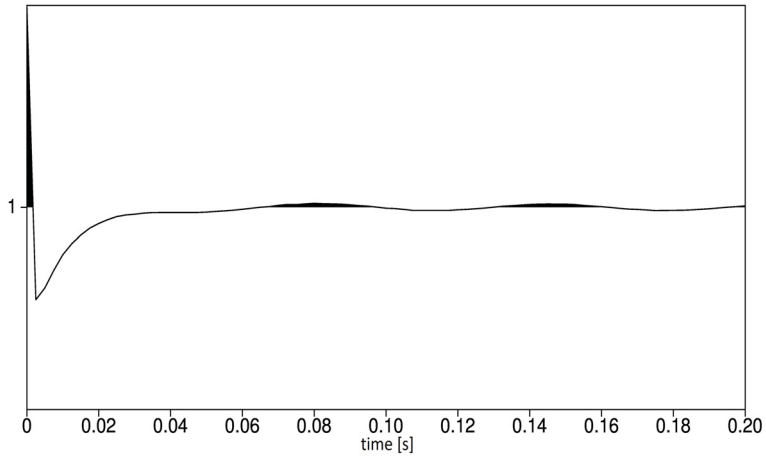

Figure D.18: Deconvolved mastertrace

Shotpoint 28

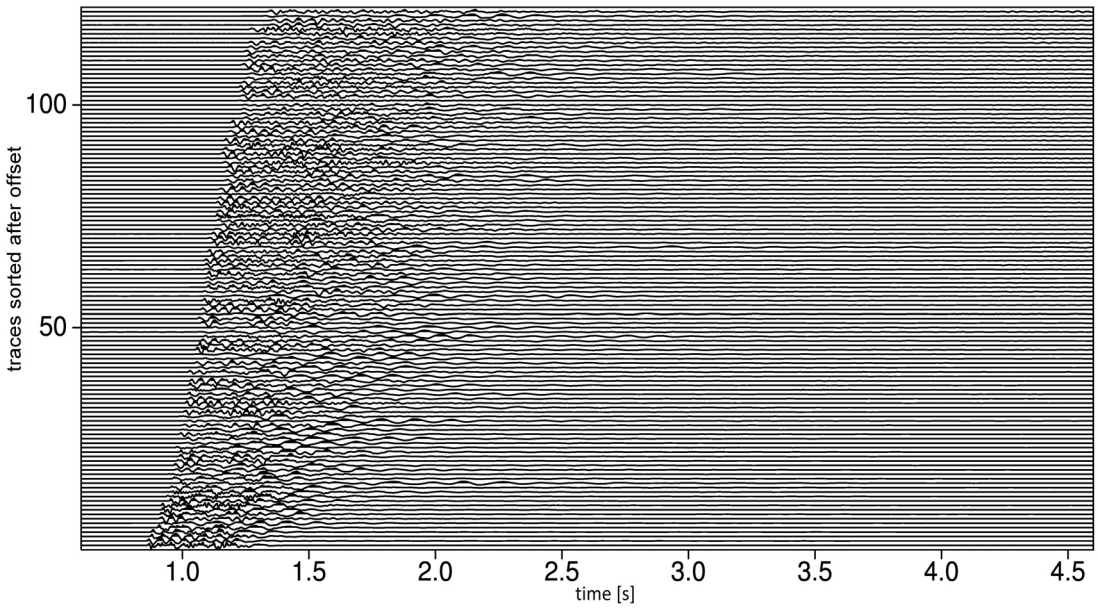

Figure D.19: Original seismogram (vertical component)

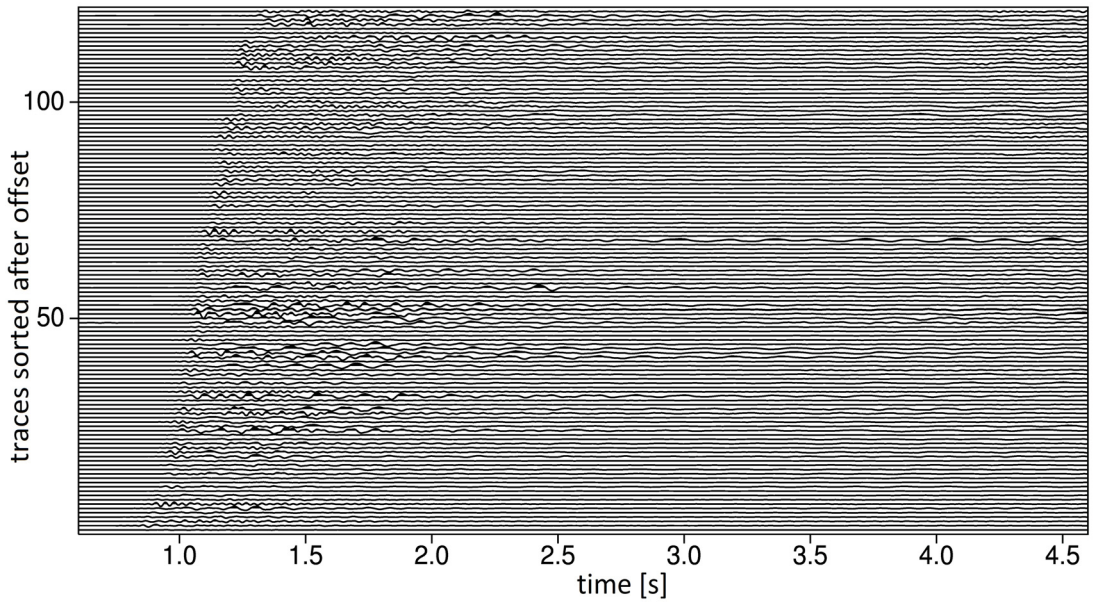

Figure D.20: Deconvolved original section where a low-pass filter is used to remove high-frequency signals

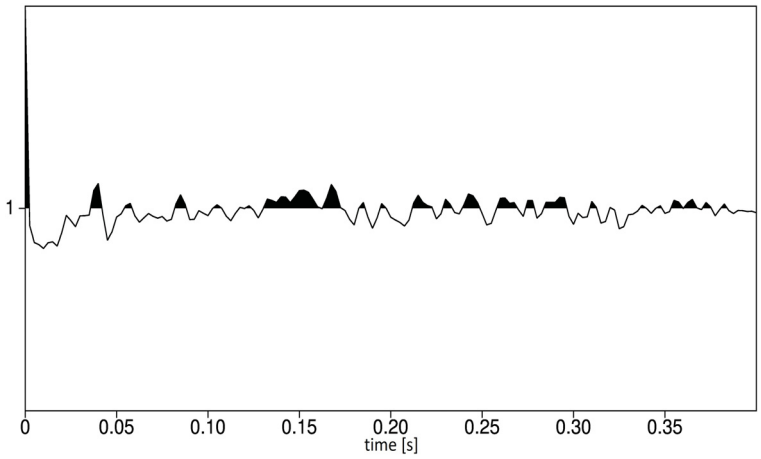

Figure D.21: Deconvolved mastertrace

Shotpoint 29

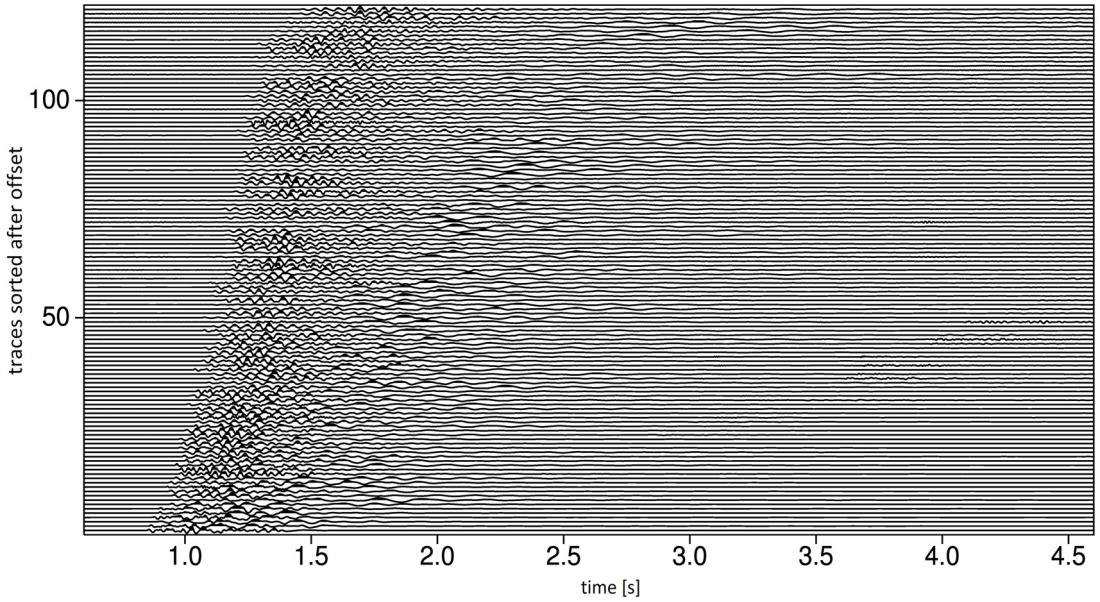

Figure D.22: Original seismogram (vertical component)

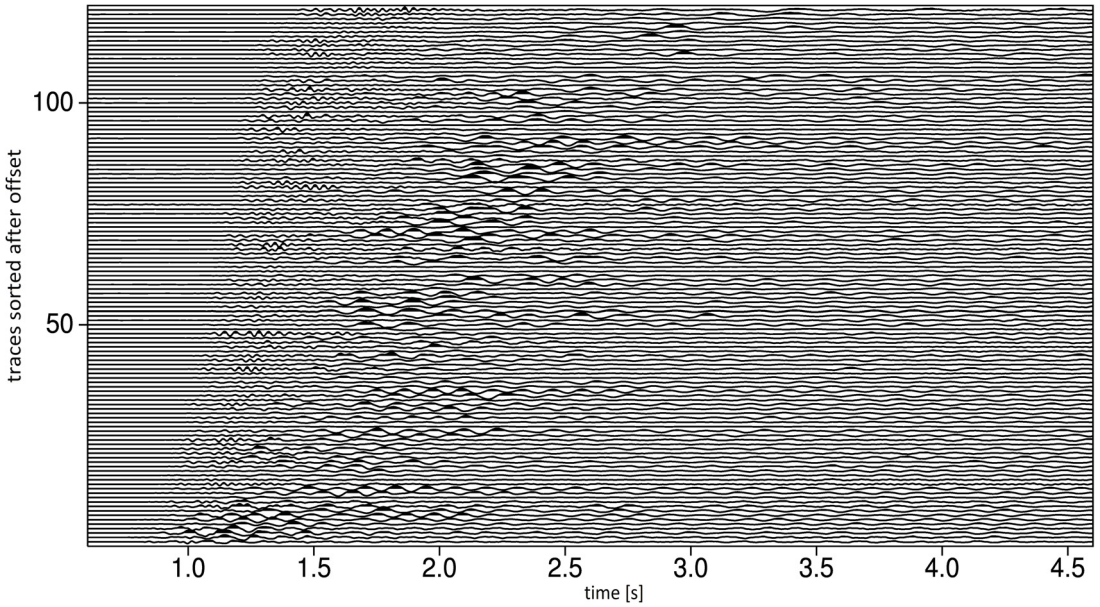

Figure D.23: Deconvolved original section where a low-pass filter is used to remove high-frequency signals

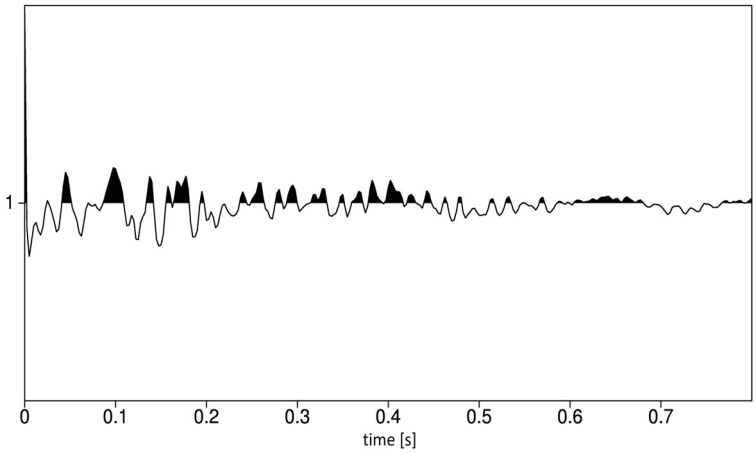

Figure D.24: Deconvolved mastertrace

Shotpoint 30

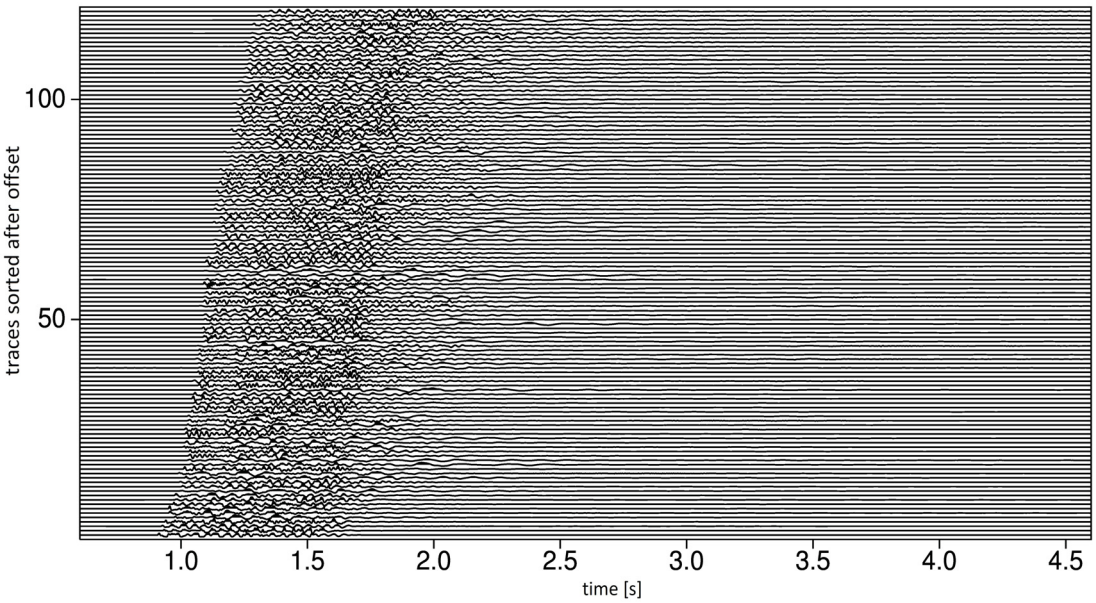

Figure D.25: Original seismogram (vertical component)

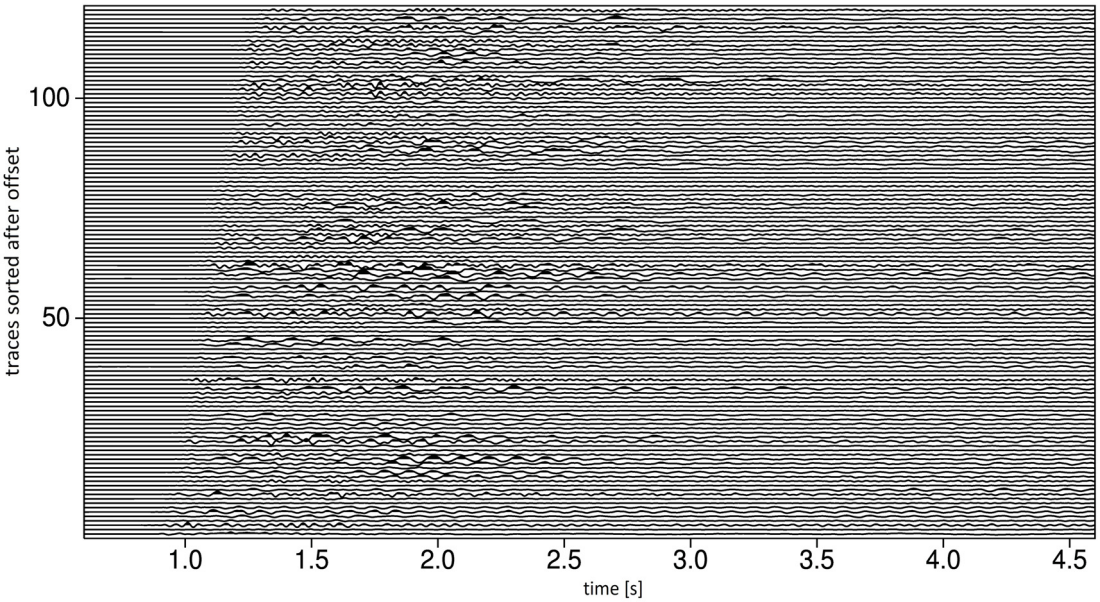

Figure D.26: Deconvolved original section where a low-pass filter is used to remove high-frequency signals

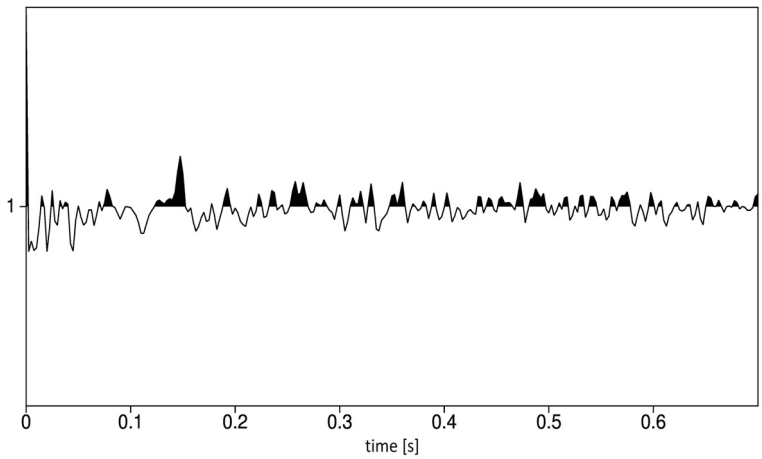

Figure D.27: Deconvolved mastertrace

Shotpoint 31

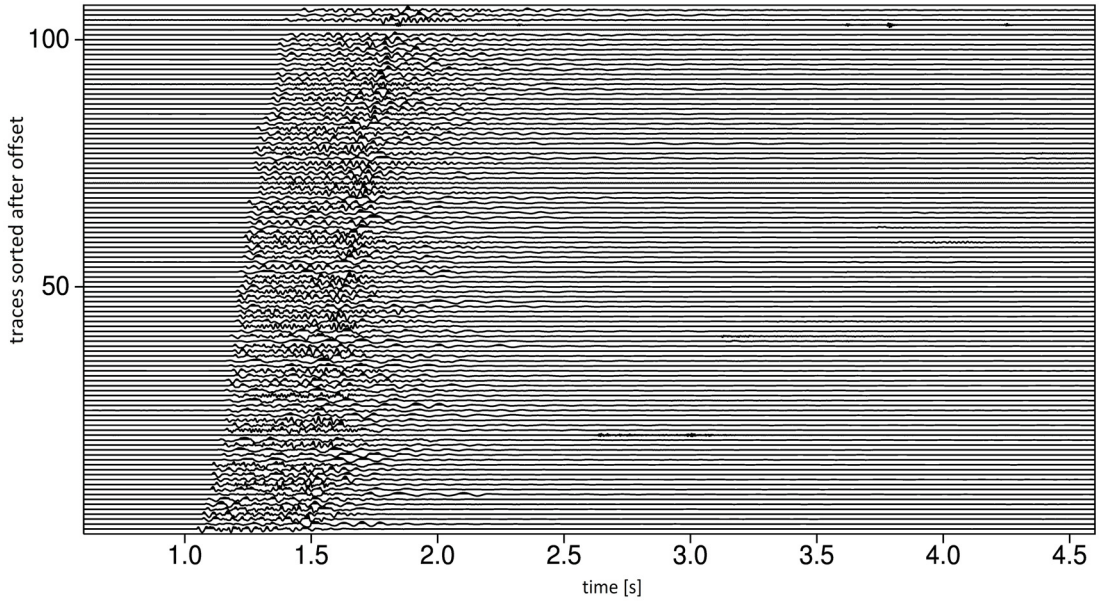

Figure D.28: Original seismogram (vertical component)

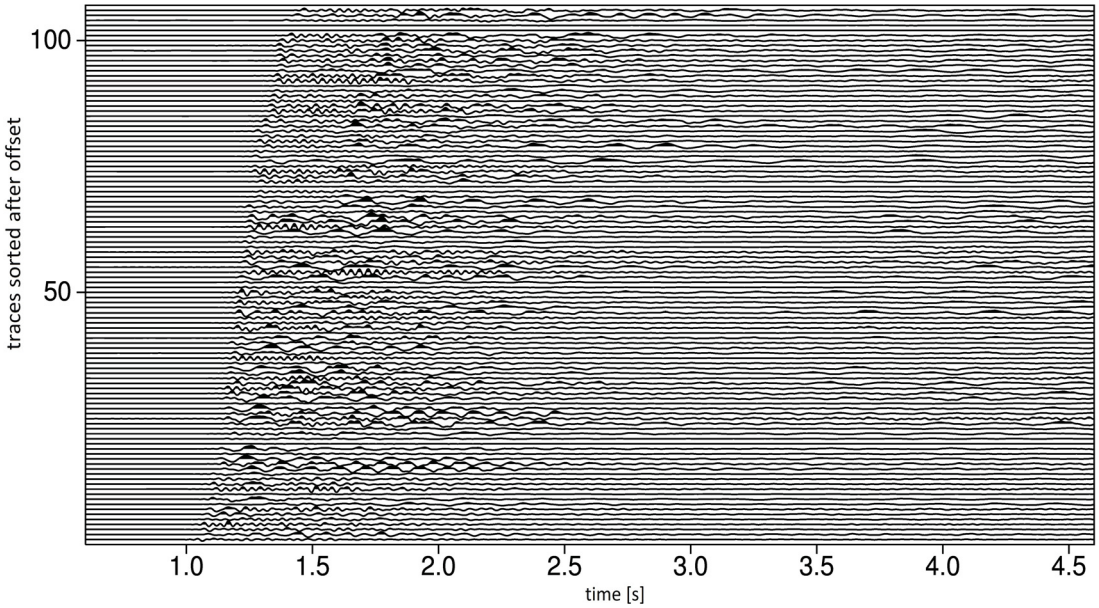

Figure D.29: Deconvolved original section where a low-pass filter is used to remove high-frequency signals

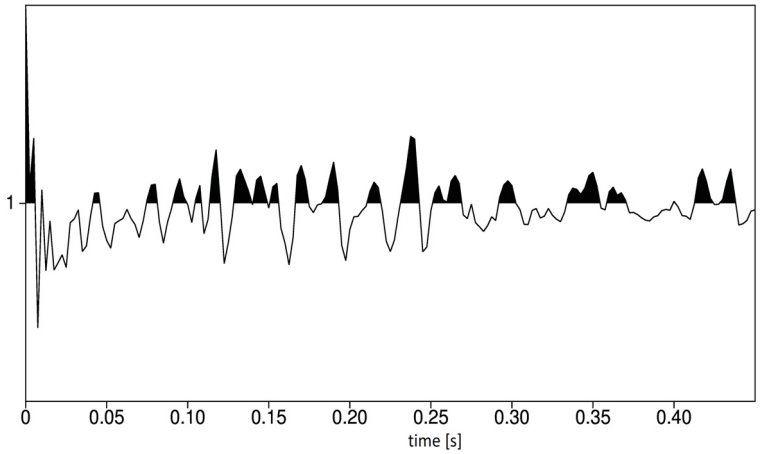

Figure D.30: Deconvolved mastertrace